Bachelor Thesis

Stable isotope dynamics in a seasonally changing snow cover on Samoylov Island, Northern Siberia

Bachelor Earth Science
University of Potsdam
Institute of Earth and Environmental Science

Potsdam, 18th of September 2014

Supervisors:
Dr. Hanno Meyer
Prof. Dr. Hans-Wolfgang Hubberten

Erik Böhm
Student Nr: 755378
erboehm@uni-potsdam.de

Table of Contents

Index of Figures

Index of Tables

List of abbreviations

AL	Active layer
a.s.l.	Above sea level
CAF	Cellulose Acetat Filter
d-excess	Deuterium xcess
FCC	Frost-crack crystal
FCD	Frost-crack depth hoar
FCI	Frost-crack ice
FCS	Frost-crack snow
FCW	Frost-crack water
GMWL	Global Meteoric Water Line
HDW2	Mixed standard water from the Potsdam region
IRMS	isotope ratio mass spectrometer
K	equilibrium constant
KARA	Kara Sea Water
LD13	Lena Delta 2013
MAAT	mean annual temperature
min.	Minimum
max.	Maximum
NGT	North Greenland Traverse
R	Ratio
SEZ	Severnaja Zemlja water
SLAP	Standard Light Antarctic Precipitation
SP	Snow profile
T_{annual}	mean annual temperature
VSMOW	Vienna Standard Mean Ocean Water
α	Fractionation factor
δ	Delta value
1σ	Standard deviation

Abstract

While climate change takes place world-wide, the Artic regions are very sensitive to these changes while influencing the biodiversity of the whole world. Therefore, climate archives are considered to better understand the climate of the past.

In permafrost regions, covering about 24% of the northern hemisphere land surface, established climate archives such as ice caps, deep lake sediments or tree rings are rarely found. On the other hand, the ground ice contained in permafrost soils is expected to provide paleoclimatic information. Ice wedges, vertically-foliated or –banded wedge-shaped ice bodies, are considered the most appropriate type of ground ice for climate reconstructions. They form mainly by the penetration and refreezing of snow melt water in open frost cracks in early spring, resulting in annual layers which are expected to contain the temperature signal of the year of their formation. To understand the paleoclimatic signal preserved in the climate archive "ice wedge", it is necessary to identify its source. For this purpose, a study on the spatial and temporal variability of the thickness and the isotopic composition of a snow cover during spring was carried out at Samoylov Island within the Lena Delta. Snow samples were collected at different geomorphologic units of different ice-wedge polygons and at a snow field and their isotopic composition has been correlated with weather data from Samoylov Island in order to identify annual cycles and predominant alteration processes.

It was difficult to characterize an annual cycle while it was possible to identify a late warm phase in late autumn and a late cold phase in early spring. It was observed that that the snow cover and its isotopic composition undergo changes over time due to sublimation, evaporation and wind drift processes. Percolating rain water highly reduced the thickness of the snow cover but had no significant influence on its isotopic composition, while the collection of initial-snow-melt-runoff water leads to a higher concentration of lighter isotopes in the polygon centers. It has been shown that the climate signal preserved in ice wedges is derived from early spring temperatures, as its isotopic composition best corresponds with that of snow from the bottom of the snow cover, depth hoar and ice out of snow melt water developing in the troughs above frost cracks, while showing an influence of moisture of precipitation of the previous summer period.

Zusammenfassung

Während sich weltweit das Klima ändert, sind die arktischen Regionen besonders sensibel für diese Änderungen und beeinflussen die Biodiversität auf der ganzen Welt. Aus diesem Grund werden sogenannte Klimaarchive betrachtet, um das Klima der Vergangenheit besser zu verstehen und Rückschlüsse für derzeitige Klimaänderungen schließen zu können.

In Permafrostregionen, welche etwa 24% der Landoberfläche der nördlichen Hemisphäre bedecken, sind etablierte Klimaarchive wie Eiskappen, Sedimente aus tiefen Seen oder Baumringe nur spärlich zu finden. Andererseits wird angenommen, dass das Grundeis welches in Permafrostböden enthalten ist, paleoklimatische Informationen enthält. Eiskeile, vertikal gebänderte, keilförmige Eiskörper, werden als der für Klimarekonstruktionen geeignetste Grundeistyp angesehen. Sie bilden sich hauptsächlich durch das Eindringen und Wiedergefrieren von Schneeschmelzwasser in Frostspalten im frühen Frühling, wodurch jährliche Schichten entstehen. Von diesen Schichten wird erwartet dass sie das Temperatursignal aus dem Jahr erhalten, in dem sie gebildet worden. Um das im Klimaarchiv „Eiskeil“ enthaltene Paleoclimasignal zu verstehen ist es wichtig seine Quelle zu identifizieren. Um dies herauszufinden wurde während des Frühlings auf der Insel Samoylov im Lena Delta eine Studie über die räumliche und zeitliche Variabilität der Mächtigkeit der Schneedecke und ihrer isotopischen Zusammensetzung vorgenommen. Es wurden Schneeproben von den verschiedenen geomorphologischen Einheiten von unterschiedlichen Eiskeilpolygonen und in einem Schneefeld genommen und ihre isotopische Zusammensetzung mit Wetterdaten von der Insel Samoylov korreliert, um Jahreszyklen und vorherrschende Alterierungsprozesse zu identifizieren. Obwohl es möglich war eine späte Warmphase im späten Herbst und eine Kaltphase im frühen Frühling zu identifizieren, war es schwierig einen Jahreszyklus zu erkennen. Es wurde beobachtet, dass die Schneedecke und ihre isotopische Zusammensetzung über die Zeit Veränderungen durch Sublimation, Evaporation und Windumverlagerung unterworfen ist. Perkolierendes Regenwasser reduzierte zwar stark die Schneedecke, hatte aber keinen signifikanten Einfluss auf die isotpoische Zusammensetzung, während sich in den das in den Polygonzentren sammelnde erste Schneeschmelzwasser hier zu einer erhöhten Konzentration an leichteren Isotopen führte. Es wurde gezeigt, dass das in den Eiskeilen erhaltene Klimasignal von den Frühfrühlingstemperaturen abgeleitet werden kann, da ihre isotopische Zusammensetzung am besten zu denen des Schnees am Grund der Schneedecke, und denen des sich in den Trögen über den Frostspalten bildenden Tiefenreifs und Eises aus Schmelzwasser passt, während sie einen Einfluss von Feuchtigkeit von Niederschlägen aus dem vorangegangenen Sommer zeigen.

1. Introduction

Climate change takes place world-wide as increasing temperatures, melting glaciers, reduced sea ice, thawing permafrost and rising sea levels indicate (ACIA, 2004). In the Arctic regions, which are very sensitive to global warming (Costard et al., 2007), temperatures increase by twice the rate than the rest of the world (ACIA, 2004). The impacts of climate change in the Arctic will have implications for the biodiversity around the world (ACIA, 2004) .

To assess the recent climate changes, it is necessary to understand the climate processes which took place in the past. Because meteorological observations only go back to the 20th, in some cases into the 19th, century, paleoclimatic archives are needed for the climate reconstruction, such as ice cores, lake sediments or tree rings (Opel et al., 2010).

In permafrost regions, governing about 24% of the northern hemisphere (Zhang et al., 1999), such archives are less available (Opel et al., 2010). Permafrost is defined as soil or bed rock that remain frozen for at least two consecutive years (van Everdingen, ed. 1998 revised 2005) and mostly contains ground ice (Zhang et al., 1999).

Ground ice is defined as all type of ice contained in frozen ground (van Everdingen, ed. 1998 revised 2005) and able to provide paleoclimatic informations (Meyer et al., 2002a). Ground ice includes ice wedges, which are wedge-shaped ice bodies consisting of foliated or vertically banded ice (French, 2007) and are considered to be the most appropriate type of ground ice for paleoclimate reconstruction (Vaikmäe, 1989; Vasil'chuk, 1991).

Ice cores preserve the variations in stable water isotope composition of precipitation (Clark and Fritz, 1997), which are widely used for paleoclimate studies, especially for paleotemperature reconstruction and identification of moisture sources (Merlivat and Jouzel, 1979), due to their dependence on condensation temperatures (Dansgaard, 1964).

As ice wedges form through the penetration and refreezing of snow melt water they also can be used for paleoclimate reconstruction. Mackay (1983), Vaikmäe (1989) and Vasil'chuk (1991) consider oxygen isotope variations in ice wedges as an indicator for winter temperature changes. Nikolayev and Mikhalev (1995), Meyer et al. (2002a; 2010) and Opel et al. (2010) show that climate reconstruction with ice wedges is possible on different time scales. As the main source for the formation of ice wedges is snow melt water, the development of the isotopic composition in the snow cover from precipitation until snow melt has to be characterized in order to understand the paleoclimatic signal preserved in the paleoclimatic archive "ice wedge". For this aim, about 250 snow samples were taken on different sites at Samoylov Island during the Lena Delta 2013 campaign (LD13). Samoylov Island is located in the zone of continuous permafrost within the Lena Delta (Boike et al., 2013), which is a key region for the

understanding of permafrost related processes and dynamics in the Siberian Arctic (Hubberten et al., 2006).

In order to characterize spatial and temporal trends in the isotopic composition of a seasonal snow cover and the dominant processes during its alteration, depth profiles were sampled along transects through ice-wedge polygons and in a snow field and analyzed in their isotopic composition. For this purpose the spring period (2013) was selected. In spring, the snow cover undergoes major changes through e.g. melting, percolation, wind drift and sublimation processes. Hence it is assumed that these processes are responsible for generating the isotope signal ($\delta^{18}O$) which is transferred to the ice wedges later on.

Therefore the modification of the snow cover and its isotopic composition in spring is the subject of this bachelor thesis to better understand the climate signal preserved in ice wedges.

2. Study area and study objects

2.1. Study area

The study site on Samoylov Island is one of 1.500 islands of the Lena river delta, which is with an delta area of 32104km² and an catchment area of 2430000 km² the largest in the Arctic and one of the largest in whole Eurasia (Costard et al., 2007; Gordeev and Shevchenko, 1995). The total length of the Lena River exceeds 4400 km (Costard et al., 2007). The Lena is divided in four major delta branches, namely the Trofimovskaya branch, which is the largest followed by the Bykovskaya branch towards the southeast, the Tumatskaya branch to the north and the Olenyokskaya branch to the south (Fig. 2-1 A, B) (Schwamborn et al., 2002).

Grigoriev (1993) identified three main geomorphological units (river terraces) within the Lena Delta. The first terrace is with a maximum age of 8000 yr. the youngest one (Schwamborn et al., 2002). It covers the main part of the eastern sector of the delta between the branches Tumatskaya and Bykovskaya and includes polygonal tundra, large thermokarst lakes and active floodplains and is therefore assumed to represent the “active” part of the delta (Akhmadeeva et al., 1999; Schwamborn et al., 2002). A fluvial facies built up since the Mid-Holocene changing from organic-rich sands at the bottom to silty-sandy peats at the surface and is characteristic for this terrace (Schwamborn et al., 2002). The second terrace covers most of the northwestern part of the delta and is characterized by organic-poor fine sands with Late Pleistocene (14.5–10.9 ka BP) to Early Holocene age (6.4 ka BP) and a low ice content but contains a net of narrow-standing ice veins (Schwamborn et al., 2002). The third terrace is observed in parts along the Olenyokskaya and the Bykovskaya branch and is characterized by sandy deposits and

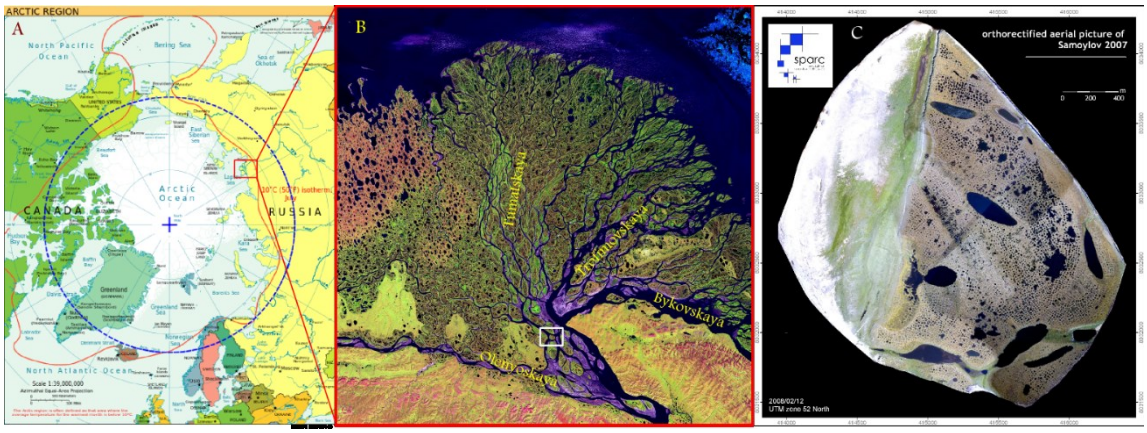

Fig. 2-1 Investigation Area A - Location of the Lena River Delta within the Artic regions, B – Map of the Lena River Delta with the four main branches and the location of Samoylov Island (white square) (Satellite image provided by Landsat 2000), C- Samoylov Island (Boike et al., 2012)

represents a fluvial stage of the Lena River for the period of 88-43ka BP, overlain by late Pleistocene ice- and organic-rich silty sands, the so called Ice Complex, formed between 43 and 14ka BP (Schwamborn et al., 2002).

Samoylov Island is located at N72°22', E126°30' on the first river terrace at the Olenyokskaya branch (Fig. 2-1 B) (Akhmadeeva et al., 1999; Grigoriev, 1993). For this south-central part of the Lena delta and the Late Holocene terrace, Samoylov Island is representative (Sachs et al., 2008; Akhmadeeva et al., 1999; Boike et al., 2013). Samoylov has an area of 12 km² and can be divided into two areas with different geomorphologic patterns (Fig. 2-1 C), an accumulation site in the western part of the island and an erosional site in the eastern part (Akhmadeeva et al., 1999; Hubberten et al., 2006). Fluvial and aeolian accumulation processes provide fine to medium sand to the west. At this part, three flood plains can be distinguished: a lower floodplain, a middle floodplain and a high flood plain (Hubberten et al., 2006; Meyer, 2003). The low and the middle flood plain are generally annually flooded by the Lena River but for different time spans, while the high flood plain is only reached by water during high floods (Meyer, 2003).

These three geomorphological units are separated from a fourth unit in the eastern part, the old river terrace which is part of the first Lena river terrace (Meyer, 2003). In this part recent erosion processes formed an abrasion coast with cliffs up to 8 m while different erosion resistances are responsible for the recent shoreline with overhangs and thermokarst (Akhmadeeva et al., 1999). The high flood plain and the first Lena river terrace are characterized by polygonal-patterned ground with ice-wedge growth (Meyer, 2003). Samoylov Island reaches a maximum elevation of 12 m a.s.l. (Akhmadeeva et al., 1999; Meyer, 2003). The entire delta is located in a zone of continuous permafrost, reaching a thickness of about 500 to 600 m (Romanovskii and Hubberten, 2001). Samoylov Island is, according the Köppen-Geiger classification, part of the

polar tundra climate zone (Boike et al., 2013). The Lena Delta has a dry continental arctic climate and is characterized by low precipitation and very low temperatures (Boike et al., 2008). The weather at Samoylov Island during spring, summer and autumn is characterized by the rapid change between the advection of arctic cold and moist air masses from the north and continental warm dry air masses from the south (Boike et al., 2008).

Usually rainfall occurs between the middle of May and the end of September. The summer rainfall annual mean from 1999 to 2011 was about 125mm. The snow season on Samoylov starts between the middle of September and the middle of October (Boike et al., 2013). The snow depth has a high spatial and temporal variability because strong winds redistribute the snow and snow-free surfaces in the polygonal rim and snow-filled polygon centers can be found at the same time (Boike et al., 2013). Between August 1998 and August 2002, the snow heights on Samoylov Island were measured on a polygon rim and after that moved into a polygon center, resulting in a measurement of greater thicknesses (Boike et al., 2013, Tab. 2-1). In spring 2008, a mean snow depth of about 17 cm on the polygon rims and of about 46 cm in the centers were measured during an examination of snow-physical characteristics of 216 sites (Boike et al., 2013). The snow mainly consists of very loose, large-grained depth hoar and hardened, sediment-rich layers. The snow melt starts usually in the second half of May and by early June the snow cover typically disappears. While rainfall contribute 70% of the mean annual precipitation of 190mm, snow fall events only contribute less than 30% (Hubberten et al., 2006; Boike et al., 2013).

Tab. 2-1 Dates and durations of snow covered periods for the years 1998-2011. Note that the snow sensor in 2002 was moved from polygon rim to polygon center (after Boike et al., 2013)

	1998	**1999**	**2000**	**2001**	**2002**	**2003**	**2004**	**2005**	**2006**	**2007**	**2008**	**2009**	**2010**	**2011**
Snow end date	n.d.	22 May	11 May	15 May	20 May	12 May	16 Jun	25 May	7 Jun	20 May	26 May	3 Jun	9 Jun	26 Apr
Snow start date	26 Oct	8 Oct	19 Oct	4 Oct	23 Oct	21 Oct	28 Sep	26 Sep	3 Oct	24 Oct	4 Oct	15 Oct	11 Oct	n.d.
Max. snow depth (cm)	n.d.	9	13	30	27	28	56	23	n.d.	44	36	42	32	27
Length of snow season (days)	n.d.	208	216	208	228	201	239	239	254	229	215	242	237	197
Length of snow-free season (days)	n.d.	139	161	142	156	162	104	124	118	157	131	134	124	n.d.

January and February are generally the coldest months with -30.1°C and -33.1°C, while July and August show the highest mean temperatures with +10.1°C and +8.5°C. The mean annual air temperature (MAAT) between 1998 and 2011 was -12.5°C (Boike et al., 2013).

Since 1993, Samoylov Island is the focus of multidisciplinary research including climate, land cover, ecology, hydrology, permafrost and limnology. For this purpose, a research base was

built in 1999 and enhanced in 2005. In 2012, a new and more modern station was build with the help of the Russian federation.

2.2. Study objects

2.2.1. Snow

Snow is defined as ice crystals in mainly hexagonal form precipitated from the atmosphere and often agglomerated into snowflakes (van Everdingen, ed. 1998, revised 2005).
Snowy precipitation, later referred as snow, is a type of solid precipitation, which is after shape, structure and formation divided into snow, sleet, ice grains and hail (Wilhelm, 1975).
The formation of solid precipitation, where water vapor in the atmosphere sublimates on ice nuclei or condensed water drops freeze, is therefore bound on temperatures below the freezing point. While the formation is related to temperatures below 0°C, snow fall is also observed at near surface temperatures over 0°C and higher temperatures during formation cause more snow fall because higher amounts of vapor are carried in the warmer air masses (Wilhelm, 1975).
Although all types of solid precipitation have a hexagonal crystal shape, their overall shape is dependent on air temperature and amount of moist available during formation (Wilhelm, 1975). The shapes can be subdivided into ten main types such as plate crystals, snow stars, pillars, needles, spatial dendrites, capped pillars, irregular aggregates, sleet, ice-grains and hail (Wilhelm, 1975).
The size of the snow crystals is also dependent on the temperature conditions. The density of the primary snow cover is dependent on the snow type, but after accumulation density differences within one layer of the snow cover are often eradicated fast through metamorphism processes which are strongly dependent on temperature, air moisture and wind speed (Wilhelm, 1975).
By the deposition of successive snow falls a snow cover stratified with many layers is formed, while each layer has its own physical properties due to the initial snow conditions at the time it is deposited at the surface of the previous layer and subsequent metamorphism depending on the load and arrangement of the ice particles within the layer and the varying field conditions (Singh et al., 2011). In general, changes in the snow cover are dependent upon the prevailing weather conditions such as temperature, precipitation, radiation and wind (Singh et al., 2011).
The metamorphism processes can either be divided into destructive and constructive, where primary crystal structures are degraded and new secondary structures are build up, or into pressure and thermal metamorphism (Singh et al., 2011; Wilhelm, 1975). Three types of

thermal metamorphism such as the equi-temperature metamorphism, the temperature-gradient and the melt-freeze metamorphism can be differentiated (Singh et al., 2011).

During the melt-freeze metamorphism, frequent melting and refreezing due to cyclic variations in the snow surface temperature as allowed at temperatures around the freezing point leads to a fast transformation of the hexagonal crystals into large poly-angular grains (Singh et al., 2011), also called firn grains (Wilhelm, 1975).

In cold regions the whole redistribution of water within the snow cover happens in the vapor phase, but the crystals are also transformed into grains by melt water, preferentially during the melting period in spring (Wilhelm, 1975). But the main transformation is performed due to the equi-temperature metamorphism, where the rounding of the grains and the redistribution of water happens due to vapor transfer taking place because the vapor pressure at the regions of the branches of the crystals of the fresh snow is higher than at its centers (Singh et al., 2011; Wilhelm, 1975).

At steep temperature gradients within the snow cover, the temperature-gradient metamorphism is predominant, a strong water vapor transport occurs and at the condensation and sublimation of the vapor, new hexagonal cup shaped crystals are formed within the snow cover, called depth hoar (Singh et al., 2011; Wilhelm, 1975). Vegetation has a strong influence on this type of metamorphosis, as it influences the soil temperature before the snow fall and so the snowpack temperature is graded between the soil and the upper snow surface (Singh et al., 2011).

The transformation of the crystal shape leads to a settlement of the snow cover and therefore to compaction (Wilhelm, 1975). As shown above, evaporation and condensation processes are highly involved at these settlement processes (Wilhelm, 1975). By the metamorphic modification of structure, texture and density of the snow, its mechanical properties change as well (Singh et al., 2011). The snow cover can then be divided into four types named new snow, fine grained snow, coarse grained snow and depth hoar (Wilhelm, 1975).

During dry periods, sublimation will cause mass loss at the surface of the snow cover, resulting in a further reduction of the snow-cover height (Stichler et al., 2001). Moser and Stichler (1974) showed, that the extent of sublimation also depends on the exposed surface area of the snow but not on its thickness, while being highly dependent on the temperature gradient between the surface and the deeper layers (Stichler et al., 2001).

2.2.2. Ice wedges

Ice wedges are wedge-shaped ice bodies which are composed of vertically-banded or -foliated ice and are formed when hoar frost develops in opened frost cracks in winter and the cracks in early spring are penetrated of water from melting snow (Fig. 2-2) (French, 2007).
Since glacier ice cores, which are widely used as archives for paleoclimatic reconstruction, are not available in most parts of the Eurasian Artic (Meyer et al., 2002b), other climatic archives such as ice wedges have to be considered. Because of the mean cold-season air temp near the ground surface and the $\delta^{18}O$ in recent ground ice are highly correlated and can be used for paleoclimatic reconstructions (Nikolayev and Mikhalev, 1995), ice wedges are considered to be reliable paleoclimatic archives.
They are widely distributed in non-glaciated high northern latitudes, in general indicative of periods of cold and stable climate conditions (Meyer et al., 2010) and as a strictly periglacial feature, they are indicative for permafrost conditions (Meyer et al., 2002a).
The favored environments for the formation of ice wedges are poorly-drained tundra lowlands that are underlain by continuous permafrost (French, 2007). In unconsolidated sediments they are best observed, but may also occur in bedrock or on slope terrain (French, 2007)
The frost cracks preferentially form between mid-January and mid-March and the cracking occurs in a zone of weakness that is preformed by the ice vein of the previous cracking event (Mackay, 1974). At Samoylov Island, the main season for frost cracking lies in December but last from mid-November till mid-February (Kleine, 2014).
After Péwé (1966), frost cracking occurs where mean annual temperature (MAAT) is -6°C or colder. Although (Mackay, 1993) identified a temperature drop over 4 days with a drop of 1.8°C/day as the best conditions for frost cracking, it is not simply related to the rapid drop in air temperature, since the best correlation between cracking and air temperature drop occur at sites with a thin snow cover while large snow covers inhibit cracking (French, 2007).

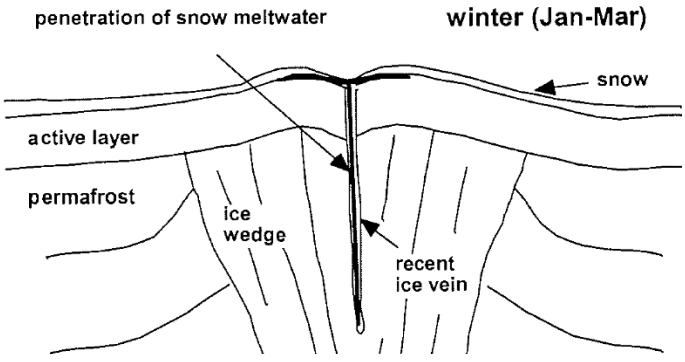

Fig. 2-2 Development of an ice wedge through the penetration of melt water (after Meyer, 2003)

With the air temperature and the snow cover as the main factors, frost cracking is also largely controlled by the ground temperature and the ground-thermal gradient. If an ice wedge is formed after the cracking events is dependent on the amount of moisture available , as the formation mechanism indicate, and if a region lacks of moisture, none or only less developed ice wedges can be observed (French, 2007).

Since it is assumed that the main source of ice wedges is snowmelt water and Michel (1982) and Kleine (2014) showed that the penetrating water freezes rapidly enough to prevent fractionation, the formed ice vein should contain the isotope signal of one discrete winter (Meyer et al., 2002a, 2002a). Meanwhile melting and freezing within the snow cover and the active layer can lead to isotopic fractionation (Nikolayev and Mikhalev, 1995) and therefore can change the isotope signal later preserved in the ice-wedge ice.

3. Methods

3.1. Scientific background

3.1.1. Stable isotope geochemistry: principles of H and O isotopes

Isotope geochemistry is a well approved method to understand processes in nature such as climate or hydrological dynamics and is often used to distinguish these processes or their products. The term isotope consists of the Greek words “iso”, (equal), and “topos”, (place). Consequently, isotopes are variations of atoms, which consist of the same number of protons and electrons and share the same place in the periodic table, but differ in the number of neutrons and therefore in their mass (Markl, 2008). Generally, isotopes are divided in stable and unstable/radioactive isotopes.

The stable isotopes being used most in environmental studies are D/H, ^{18}O /^{16}O and ^{13}C /^{12}C (Clark and Fritz, 1997). In this study, only the stable isotopes of water D / H and ^{18}O /^{16}O are considered. Out of theses, the lighter isotopes ^{1}H and ^{16}O are the more abundant compared to the heavy isotopes (see Tab. 3-1).

Tab. 3-1 Relative environmental abundance of stable hydrogen and oxygen isotopes (after Berglund and Wieser, 2011)

Element	Isotope	Abundance	Isotope	Abundance	Isotope	Abundance
Hydrogen	^{1}H	0.999 885	D	0.000 115		
Oxygen	^{16}O	0.997 57	^{17}O	0.000 38	^{18}O	0.002 05

The electronic structure is responsible for the chemical properties of an element and its nucleus for the physical. Because isotopes have same number and arrangement of electrons, they are similar in their chemical behavior, one the other hand they have certain differences in their physico-chemical behavior due to their differences in mass, leading to different reaction rates (Urey, 1947). Due to their greater mass, heavy isotopes require greater energy to dissociate and have stronger bonds than the light isotopes, which therefore react faster (Clark and Fritz, 1997). The differences in chemical and physical properties arising from variations in atomic mass of isotopes are called *"isotope effects"* (Hoefs, 2009) and lead to isotope fractionation processes (Urey, 1947).

Fractionation processes describe the partitioning of isotopes between two substances or two phases of a substance (i.e. water phases) due to their properties (Hoefs, 2009).

Within these, there are two main phenomena. First the isotope exchange reaction providing an equilibrium isotope distribution and second, are the kinetic processes (Hoefs, 2009).

Isotope exchange processes include all situations, in which the distribution of isotopes changes between different substances, phases or individual molecules, but there is no net reaction (Hoefs, 2009).

The isotope exchange reaction is a special case of a general equilibrium and is expressed as [Eq. 1]:

$$aA_1 + bB_2 = aA_2 + bB_1 \qquad \text{[Eq. 1]}$$

where the subscripts indicate that species A and B contain either the light isotope (1) or the heavy (2) (Hoefs, 2009). For this reaction, it is required that the forward and backward reaction rates are the same, the reaction proceeded often enough to mix the isotopes between the reactant and product reservoirs and that these are well mixed themselves (Clark and Fritz, 1997). Isotope exchange reactions are characterized by the equilibrium constant K which is dependent on the temperature and defined as [Eq. 2]:

$$K = \frac{(\frac{A_2}{A1})^a}{(\frac{B_2}{B_1})^b} \qquad \text{[Eq. 2]}$$

At high temperatures isotope fractionation tend to become zero, but do not decrease monotonically (Hoefs, 2009).

The equilibrium constant is often replaced by the fractionation factor α, which is defined as [Eq. 3]:

$$\alpha_{A-B} = \frac{R_A}{R_B} \quad \text{[Eq. 3]}$$

where R_A is the ratio of a chemical compound A and R_B the one of another compound B.
The fractionation factor alpha, as it is derived from the equilibrium constant, is also temperature dependent (Hoefs, 2009).
The δ-value, expressing the difference between a sample and a standard, is used, because the measurement of the absolute isotopic abundance is difficult and considerably less accurate than measuring relative isotope abundances against a standard and determine relative differences (Clark and Fritz, 1997; Hoefs, 2009).
Therefore, the δ-value for two compounds is defined as [Eq. 4], [Eq. 5]:

$$\delta_A = \left(\frac{R_A}{R_{st}} - 1\right) * 10^3 (‰) \quad \text{[Eq. 4]}$$

and

$$\delta_B = \left(\frac{R_B}{R_{st}} - 1\right) * 10^3 (‰) \quad \text{[Eq. 5]}$$

where R_A and R_B are the respective isotope ratio measurements and R_{st} is the defined ratio of the standard sample (Hoefs, 2009).
The δ-values are related to the fractionation factor by [Eq. 6] (Hoefs, 2009):

$$\delta_A - \delta_B = \delta_{A-B} \approx 10^3 ln\alpha_{A-B} \quad \text{[Eq. 6]}$$

Substances with relatively more heavy isotopes are called enriched with respect to the standard, or, due to their greater weight, isotopically heavier and will show more positive δ-values, while such with relatively less heavy isotopes are called depleted or lighter and will show more negative δ-values than the standard (Clark and Fritz, 1997). For the measurement of the hydrogen and oxygen isotopic composition of water samples, generally the Vienna Standard Mean Ocean Water (V-SMOW) standard is used (Hoefs, 2009). Derived from a first artificial standard established by Craig (1961b) (see also: Clark and Fritz, 1997), V-SMOW is defined as 0‰ as it should represent water of the oceans (Hoefs, 2009). As the second point of the intercalibration for oxygen and hydrogen isotope measurements the Standard Light Antarctic

Precipitation (SLAP) was defined as -55.5‰ for $\delta^{18}O$ (Gonfiantini, 1978), being close to isotopically very light samples from cold regions (Clark and Fritz, 1997).

Among the phase transitions between water in vapor, liquid and ice, evaporation and condensation processes involve the most effective fractionation for water isotopes. The differences in vapor pressure of heavy and light isotopes leads to significant isotope fractionation, enriching the vapor phase in lighter molecules species, while the extent of fractionation is temperature-dependent (Hoefs, 2009).While condensation or distillation processes proceed, a residual vapor reservoir will become progressively depleted with respect to the heavy isotopes and a residual liquid reservoir will become more enriched (Hoefs, 2009).

The secondary effects, the so called kinetic fractionation processes depend on the differences in reaction rates and are associated with incomplete and unidirectional processes like evaporation, dissociation reactions, biologically mediated reaction and diffusion. Furthermore, the knowledge of these processes can provide information about the reaction pathways (Hoefs, 2009).

The process of diffusion also can lead to a significant isotope fractionation, because light isotopes are more mobile than the heavy ones (Hoefs, 2009).

Craig (1961a) found out that, despite the complexity of these processes, water isotopes behave in predictable ways and that hydrogen and oxygen isotopes fractionate similarly. Therefore the δ-values correlate on a global scale within the hydrological cycle. Out of this finding, Craig (1961a) established the relationship of ^{18}O and D in worldwide fresh waters in a $\delta^{18}O$-δD-plot, the so called Global Meteoric Water Line (GMWL) [Eq. 7]:

$$\delta D = 8\delta^{18}O+10 \qquad \text{[Eq. 7]}$$

The constant 10 reflects a surplus of deuterium and is also called the deuterium excess or d-value. Dansgaard (1964) proposed the use of the d-excess for the identification of non-equilibrium fractionations and evaporation rates, as it gives the relative position to the GMWL and would be 0‰ for marine waters e.g. V-SMOW.

After Dansgaard (1964) the d-excess is defined as [Eq. 8]:

$$d = \delta D - 8\delta^{18}O \qquad \text{[Eq. 8]}$$

As the d-excess is dependent on sea surface temperature (SST), wind speed and relative humidity in the moisture source region, it can be used for its identification (Merlivat and Jouzel, 1979).

The slope of 8 in the co-isotope plot is also variable as it represents the ratio of the equilibrium fractionation factors at the time of condensation and is therefore dependent on the condensation temperature, being 8 at 25°C (Clark and Fritz, 1997). Furthermore the slope is only a very close approximation and can also be affected by so called secondary evaporation that takes place after condensation (Clark and Fritz, 1997).

3.1.2. Water isotopes in the hydrological cycle

The ocean is a well-mixed reservoir with a defined isotopic composition of 0‰. When water starts to evaporate from the ocean's surface, the water vapor will be enriched in the lighter isotopes H and ^{16}O because $H_2{}^{16}O$ has a higher vapor pressure than HDO and $H_2{}^{18}O$ and will be depleted in the heavy isotopes (Hoefs, 2009).

When the vapor mass leaves the ocean's surface by rising up it cools and rain will be formed when the dew point is reached (Hoefs, 2009). Atmospheric precipitation through condensation is dominated by equilibrium fractionation between vapor and water because condensation occurs at a humidity of 100% (Clark and Fritz, 1997). When warm air rises, rain is produced as cooling occurs by adiabatic expansion due to lower pressure or radiative heat loss. Along its way to higher latitudes and over continents, the air mass loses its water as precipitation, a process called rainout. It distills the heavy isotopes from the vapor mass and isotopically enriched rain is discarded from the air mass, whereas the residual vapor becomes progressively depleted in ^{18}O and D, a so called Rayleigh distillation. Because of this, later rain will be depleted in respect to earlier rains while enriched with respect to the remaining vapor (Fig. 3-1) (Clark and Fritz, 1997). There may be differences in the isotopic composition of liquid precipitation and solid precipitation as rain drops may undergo evaporation and isotope exchange with vapor in the atmosphere on their way to the surface (Hoefs, 2009). This effect is strongly controlled by the amount of vapor and is described by Dansgaard (1964) as the *"amount effect"*. It is best observed in arid regions, where air is not water-saturated.

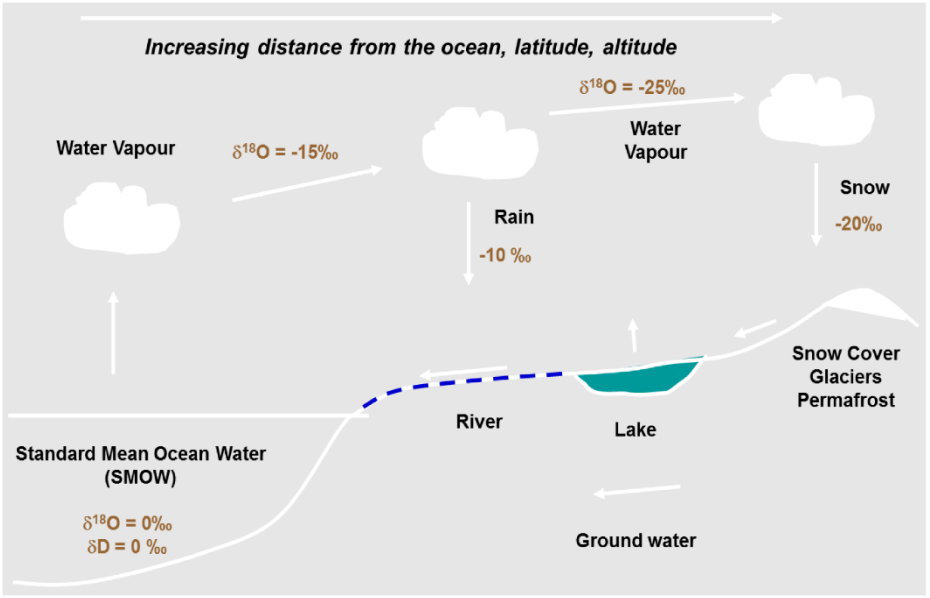

Fig. 3-1 Changes in the isotopic composition of meteoric waters within the hydrological cycle (provided by Hanno Meyer, lecture material)

On the other hand, it is not observed in the Polar Regions, where the temperature effects are predominant (Dansgaard, 1964).

As shown above, decreasing temperature drives the rainout process and so the precipitation will become more and more depleted in ^{18}O and D. However, often trends in the evolving vapor mass are masked because most weather systems acquire new sources of vapor along their path (Clark and Fritz, 1997).

Dansgaard (1964) calculated a relationship for the temperature dependency of meteoric waters on a global scale: $\delta^{18}O = 0.695\ T_{annual}\text{-}13.6$ ‰ SMOW; $\delta D = 5.6\ T_{annual}\text{-}100$ ‰ SMOW.

The strong temperature dependency is accompanied by a partitioning of $\delta^{18}O$ and δD between cold and warm regions (Clark and Fritz, 1997).

Because of the strong temperature dependency of the δ-value and, following global weather trajectories, the polar regions are placed at the end of the Rayleigh distillation. Precipitation at higher latitudes is generally more negative than that at lower latitudes, the so called *„Latitude Effect"*. The δ-value gradients increase polewards but are relatively flat in the tropics and particularly over the oceans (Clark and Fritz, 1997).

As landmasses force rainout from vapor masses, the isotopic composition evolves more rapidly through the vapor masses movement across a continent due to topographic effects and temperature extremes which is called the *"Continental Effect"*. Because continental stations show strong annual variations in temperature they also show strong seasonal differences in the isotope composition of the precipitation but will rather be more isotopically depleted while costal precipitation will rather be less depleted (Clark and Fritz, 1997).

"Seasonality Effects" will be stronger the greater the seasonal extremes in temperature are and stronger seasonal variations in the isotopic composition of the precipitation will be generated. The amplitude of seasonal variations in temperature increases with both the continentality and the latitude of a given site. The latitude also have an effect on the seasonal variations (Clark and Fritz, 1997).

When the orography forces a vapor mass to rise over the landscape and to cool adiabatically, there will be rainout. At higher altitudes, the precipitation will be isotopically depleted, because the average temperature is lower. This effect is called the *„Altitude Effect"*.

For $\delta^{18}O$ a depletion of -0.15 to -0.5 ‰ per 100 m rise in altitude is observed (Bortolami et al., 1979).

3.1.3. Fractionation processes during metamorphism and alteration of the snow cover

The isotopic signal of the snow is primarily dependent upon the temperature at the time of condensation in the atmosphere (Mackay, 1983). Nikolayev and Mikhalev (1995) found out that there is a clear relationship between the mean annual and the mean seasonal air temperature at the Earth's surface and the mean oxygen isotope composition of precipitation in Polar Regions even so these relationship may not be preserved in the permafrost because the freshly deposited snow is strongly deflated and drifted by wind which can, together with the exposure to solar radiation, alter the original isotopic composition. In high latitudes, snow drifting has an especially strong influence on the isotopic composition of snow (Nikolayev and Mikhalev, 1995). Furthermore, the melting and freezing within the active layer and the snow cover during the metamorphosis can lead to isotopic fractionation (Nikolayev and Mikhalev, 1995).

During the alteration and metamorphism of a snow cover several processes lead to a fractionation of its isotopic composition (Epstein and Mayeda, 1953; Moser and Stichler, 1974). The δ-values of the isotopic composition in general rise with increasing metamorphism (Moser and Stichler, 1974).

As mentioned above in section 2.2.1., sublimation processes play an important role during the recrystallization of snow crystals and formation of firn and depth hoar. These sublimation processes happening within the snow cover have to be distinguished from those taking place at the surface of the snow cover.

As shown above in section 3.1.1., every transition between the phases of water will lead to a fractionation due to the differences in vapor pressure. When vapor sublimates from the surface of the snow crystals as described above, it will be enriched in lighter isotopes with respect to

the crystal (Friedman et al., 1991). When the vapor produced within the snow cover re-condensates at the growing crystals, they will be enriched in the heavier isotopes, as they would condensate first due to their lower vapor pressure (Friedman et al., 1991).

During repetitive phase transitions the lighter isotopes will preferably diffuse in the pore space between the firn grains, leading to non-equilibrium fractionations (Sokratov and Golubev, 2009).

The extent of the fractionation during this process is dependent on the temperature gradient, as a higher temperature difference between the bottom and the top increase the diffusion processes accompanying the sublimation processes (Friedman et al., 1991; Sokratov and Golubev, 2009). Arising from the differences in velocity (Hoefs, 2009), the lighter isotopes will preferentially diffuse towards the upper layers, leading to an enrichment of lighter isotopes at the top and an enrichment of heavier isotopes at the bottom. Johnsen et al. (2000) suggest that the diffusion processes will cause a smoothing of the isotopic signal within the snow cover, depending on the mobility of the isotope.

The sublimation processes on the top of the snow cover, causing mass losses during dry periods, are also strongly dependent on the temperature gradient because the processes is mainly driven by the differences in the ambient air temperature and the firn-grain surface temperature in its deeper layers (Stichler et al., 2001).

During daytime sublimation is strongest, because the ambient air has its highest moisture deficit and is accompanied by a high surface temperature of the firn (Stichler et al., 2001).

An experiment on sublimation carried out by Stichler et al. (2001) suggested that this process will cause an enrichment at the surface but that the effect is restricted to a depth of 5 to 7 cm and that the mass loss at the surface has to be considered as it removes the enriched layer instantaneously and therefore limit the actual enrichment and finally ends with the next snowfall. The depth limitation of the sublimation could be caused by condensation and refreezing water vapor during night, forming ice crusts as layer boundaries and blocking the penetration of the heavy isotopes enriched at the surface through diffusion into deeper layers (Stichler et al., 2001).

Direct measurements of the change in isotopic composition do not support this “layer-by-layer” mechanism, suggesting that the concentration at a sublimating surface depend on the intensity of the sublimation and on the self-diffusion of the molecule into the remaining bulk enriching the snow cover with heavy isotopes (Konishchev et al., 2003).

When the snow begins to melt, the melt water will be depleted in heavy isotopes with respect to the remaining bulk, as at any phase transition from solid to liquid the heavy isotopes tend to

remain in the solid phase (Cooper et al., 1993). In this way, the remaining snow cover will become progressively enriched in the heavy water isotopes as melt proceeds (Cooper et al., 1993). Ambach et al. (1972) showed that the isotopic composition of the individual layers within the snow pack remain essentially unchanged during the ablation period despite percolation of melt water or rain.

Near the snow cover surface, exchanges with atmospheric water vapor can take place (Earman et al., 2006) and may be of particularly importance during the early accumulation when the temperatures are low and melting therefore limited (Lee et al., 2010).

Despite the exchange with atmospheric vapor, the re-condensation of vapor sublimated or evaporated from the snow cover surface at its surface will lead to an enrichment in the upper layers (Moser and Stichler, 1974).

3.1.4. Isotope measurements

There are different methods for measuring the isotopic composition of water. Besides laser optical methods, the Alfred Wegener Institute in Potsdam (AWI) uses isotope-ratio-gas-mass-spectrometers (type Finnigan-MAT Delta-S) to measure the hydrogen and oxygen isotope composition of given water samples. It was decided to carry out all measurements at the gas-mass-spectrometers as an approved method at the AWI. Since there was enough sample material, the advantage of the laser-optical method (Picarro) using small amounts of sample was not needed.

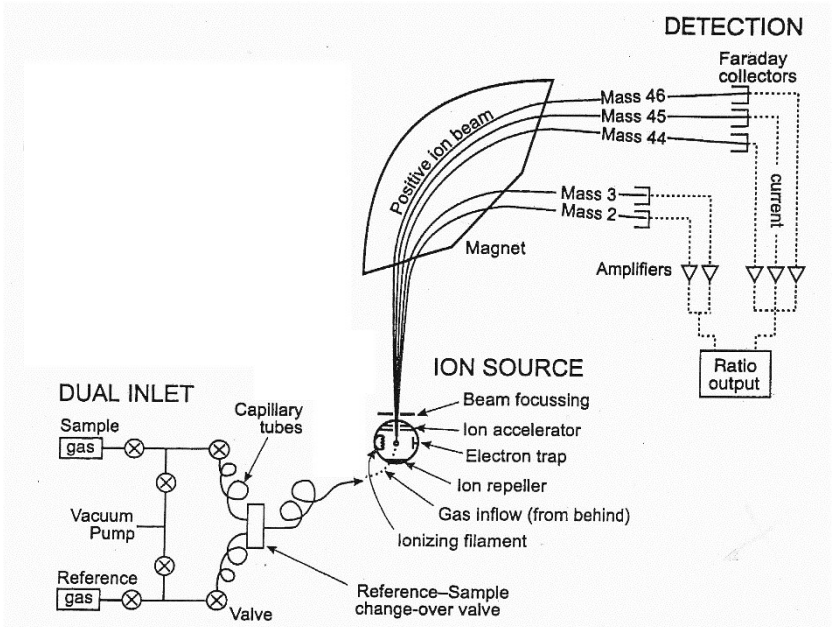

Fig. 3-2 Schematic illustration of a gas-isotope-ratio-mass-spectrometer (IRMS) (modified after Clark and Fritz, 1997)

The principle of mass-spectrometry lies in the differences in deflection depending on the specific mass-to-charge ratio of the isotopes. The gas inserted into the mass-spectrometer gets ionized at an ion source, charged and channeled into a magnetic field in which, because of the resulting Lorenz-force, it is deflected and separated depending on the specific charge of its components which then is registrated in a detector, so called faraday-cups (Markl, 2008).
The main components of a mass-spectrometer (Fig. 3-2) are the ion source, mostly equipped with a tungsten-coated iridium filament forming the ions and accelerating and focusing them, the mass analyzer with an electro-magnet installed over the flight tube to bend the ionized beam, the ion detector, where the intensity of the masses of the ions collected in the faraday cups are converted into an electrical impulse and displayed as an isotope ratio and the inlet system, providing the gas for the measurements (Hoefs, 2009).
There are different peripheral equipment to generate the gas needed for the measurements in a gas-IRMS and different inlet systems exist. The dual-inlet system, as it is used at the AWI, allows the alternate measurement of ratios in a sample and laboratory standard (Clark and Fritz, 1997). Furthermore, two automated equilibration units (MS Analysentechnik, Berlin) to generate the gas are endowed. The equilibration technique allows the automated measurement of both water elements in one run by reducing the amount of sample needed to ~3ml, with no memory effects compared to other methods (Meyer et al., 2000).
Each of the equilibration unit has a capacity of 24 sample bottles. Each of the approx. 25 ml glass bottles are filled with a ca. 3-5 ml aliquot of the water sample. That bottles are attached to a rack, where they are immersed to two thirds of their height into a water shaking bath which is stirred at a frequency of 90 min^{-1} to homogenize the water temperature. The water temperature in the baths is kept at a constant temperature of 18.00 ± 0.01°C within the measuring time to avoid condensation in the upper part of the reaction bottle (Meyer et al., 2000).
The water temperature of the shacking baths, and so the surface temperature of the catalyst sticks, used for H isotope measurements, where the equilibration is happening, should be constant within ±0.05°C because after Friedman, I. and O'Neil, J. R. (1977) the fractionation factor for deuterium has a temperature coefficient of -5.4‰/°C (Meyer et al., 2000). After immersing the reaction bottles into the shaking bath, they are evacuated by a two stage rotary pump.
Because the hydrogen isotope measurement is carried out first, the remaining space in the bottles is first filled with H_2 gas. The hydrogen isotopes are equilibrated between the water sample and the H_2 gas for 120 min, with activated platinum condensed on a hydrophobic stick

working as a catalyst (Meyer et al., 2000). After the complete hydrogen measurement is finished, the sample aliquots are equilibrated with CO_2 for 400 min for the oxygen isotope measurement.

At each unit, the first bottle is filled with the laboratory standard NGT1 and is, after being equilibrated with either H_2 or CO_2 gas, transferred into the standard bellow of the inlet system and used as a reference standard for the whole unit (Meyer et al., 2000).

Into the sample bellow, a variable volume used to regulate the pressure with that the gas is transferred into the gas-IRMS, a gas aliquot of the water sample equilibrated with H_2 or CO_2 is transferred after being separated from water vapor in a cooling at -78°C (Meyer et al., 2000).

The usage of a dual inlet system allows to alternately introduce the sample and reference gases from the bellows into the mass spectrometer trough a viscous leak. Per sample, ten measurements are carried out for statistical reasons.

To calculate the isotopic composition, the ISODAT software is used and the δD and $\delta^{18}O$ values are displayed as permil differences relative to the standard V-SMOW.

If the internal 1σ error is greater than the general ±0.8 ‰ for δD and ±0.1 ‰ for $\delta^{18}O$ the measurement is repeated.

For quality controls and linear corrections, six bottles per unit are filled with four different standards. The selection of the standards depends on the expected isotopic composition of the samples. For water samples from Siberia, the laboratory standards NGT, KARA, SEZ and HDW2 are used and also were chosen for this study.

3.2. Field work

In order to determine the spatial and temporal variability of a snow cover on Samoylov Island and its isotopic modification in the spring season through sublimation, evaporation, redistribution by wind, melting processes, perculation, snowfall etc. over twenty snow profiles were sampled. For each sample site, local site-specific characteristics for predominance of processes influencing the snow cover like exposition, roughness or underlying vegetation were described. The sample sites were selected according to their different geomorphologic characteristics, i.e. is the site a valley fill, is the sample taken on a polygon wall or in a polygon center, and exposition, i.e. is the sample taken at an N- or an S-facing slope, on top of an interpolygonal pond or vegetation cover.

Depth profiles along horizontal transects were sampled in different polygons and in a separate snow field to identify differences in thickness, structure and isotopic composition of the snow cover in the different parts of the polygons and the snowfield and its variations in the depth and

over time. All snow profiles were differentiated into layers of different characteristics (i.e. hardness, grain size and form, sediment content etc.) and sampled. If possible, samples were taken with a density shovel to get a discrete volume of snow to determine snow-to-sediment ratios. Ice crusts observed in different layers were described and sampled with a spatula to get distinct informations of their influence as boundary layers and to determine processes during their formation.

To examine if the different seasons and snow fall events are recognizable and to characterize the seasonal evolution of the snow cover and its isotopic composition and a possible annual cycle, a 1.90 m depth profile (SP13) was sampled on the 23rd of April in a snow field underlain by sandy ground. It was located at 11 m a.s.l. near the research base in the wind shadow of a water pipe, so anthropogenic influences on the profile can not be ruled out. Nevertheless, this sample site was chosen because it provides a thick snow cover, maybe preserving information within its isotopic composition to identify different snow fall events for the complete season and an annual cycle. The whole profile was sampled in parts of 3 cm taken with a density shovel to additionally gain information about the density of the snow and to determine snow-to-sediment ratios.

To observe the spatial variability of the snow cover in sample sites with different characteristics, in two adjacent polygons and in a little distance third snow profiles on the walls and in the centers were sampled as the transects SP7, SP8 and SP21. The polygons were chosen because they were well developed and polygon walls and centers clearly recognizable. Furthermore, they were near the research station, making a frequent sampling easier.

The profile SP7 is situated in a low-center polygon type at 12m a.s.l on the first terrace of Samoylov Island, underlain by vegetation and slightly exposed to the north. The ca. 14 m long

Fig. 3-3 Changes in the snow cover over time

profile was sampled on the 19th of April from the polygon center over the polygon wall to the next center.

Two days later, on the 21st of April, the profile SP8 was sampled in a polygon 20 m to the north of SP7. It was sampled from polygon wall over the center to the next wall. The center was underlain with pond ice and two active frost cracks were observed at the first meter of the profile in the eastern wall of the polygon. These were sampled separately on the 22nd of April. The 11.5m long snow profile SP27 was sampled on the 25th of April in a low center polygon at the northern edge of Samoylov Island. Is was sampled from polygon center over the wall to the next center. Both centers were underlain by pond ice.

To observe changes in the snow cover over time (Fig. 3-3), especially in its isotopic composition and to identify which isotope signal is preserved in the climate archive "ice wedge", the different parts of ice wedge polygon SP8 were resampled one meter to the south as SP47 on the 30th of April. Also the observed frost cracks were resampled. After sampling the profile SP47, a rain event occurred on the 2nd of May. After that event, the snow cover of the observed polygon was fully wet and water was standing in the pond. The thickness of the snow cover was reduced and further frost cracks became visible. To estimate the influence of the rain event, SP8 was sampled again as SP58 on the 3rd of May. As shown above, the meltwater of snow and, to a smaller extent, the developed depth hoar penetrating the frost cracks are considered the main source for the growth of ice wedges. In order to identify the influence of the isotopic composition of snow, ice, depth hoar and water filling the cracks on the isotopic composition of the wedge ice, samples categorized as frost-crack water (FCW), frost-crack ice (FCI), frost-crack depth hoar (FCD), frost-crack snow (FCS) and frost-crack crystals (FCC) were taken out of the now visible troughs above frost cracks.

Additionally bulk snow samples were taken with a liner with a diameter of 59.5 mm within the different sites to further estimate the spatial variability of the isotopic composition of the snow cover and the bulk density in the different landscape units, i.e. the river terraces or on top of the Ice Complex. The aim was to provide data for the comparison with other sites within the Lena Delta, and gain a more comprehensive picture of spatial snow variability in different landscapes.

3.3. Laboratory work

In the laboratory, the still frozen snow samples were melted and filled into 30 ml PE-bottles. If a discrete volume of the samples had been taken with a density shovel, the melted snow was first weighed and then filtered through cellulose acetate filters (CAF) to be able to determine the snow-to-sediment ratio in the layer.

Depending if the sediment were completely settled and a clear liquid was to be found above, the samples were bottled with a pipette before filtering the leftovers in order to safe time. If the samples were murky, they were filtered immediately with a filtration unit. Because the filtration units had to be fully dried out after every sample to avoid contamination, this method was more time-consuming due to drying times of the units.

After drying the CAF with the sediments, they were weighed. To determine the snow-to-sediment ratio, the weight of the plastic bag and the CAF had to be subtracted from the initial weight well as the organic components like leafs or grass, but the results are not part of this study.

The isotopic composition of the samples was measured with a Finnigan MAT Delta-S mass spectrometer as described in section 3.1.4.

4. Results

4.1. Annual snow profile

The profile SP13 is the snow profile with the greatest thickness and is considered separately as it was located in a luvward area behind a water pipe and not in an ice-wedge polygon as the other snow profiles. The $\delta^{18}O$-values at the bottom and at the top are close to each other (bottom: -22.0‰ top: -21.5‰) while in the profile five zones of different isotopic composition can be subdivided (Fig. 4-1).

Zone I (0-50 cm) displays highly variable $\delta^{18}O$ values with a mean of -24.5‰ and a maximum at 30 cm (-15.8‰) and a relatively high bottom $\delta^{18}O$ value (-22.0‰). Minima are observed at 15 cm (-28.7‰) and at 42 cm (-31.1‰).

Zone II (50-85 cm) display relatively constant δ18O values with a mean of -28.7‰, while at 51 cm a smaller maximum (-28.0‰) and at 84 cm a minimum (-29.0‰) can be observed.

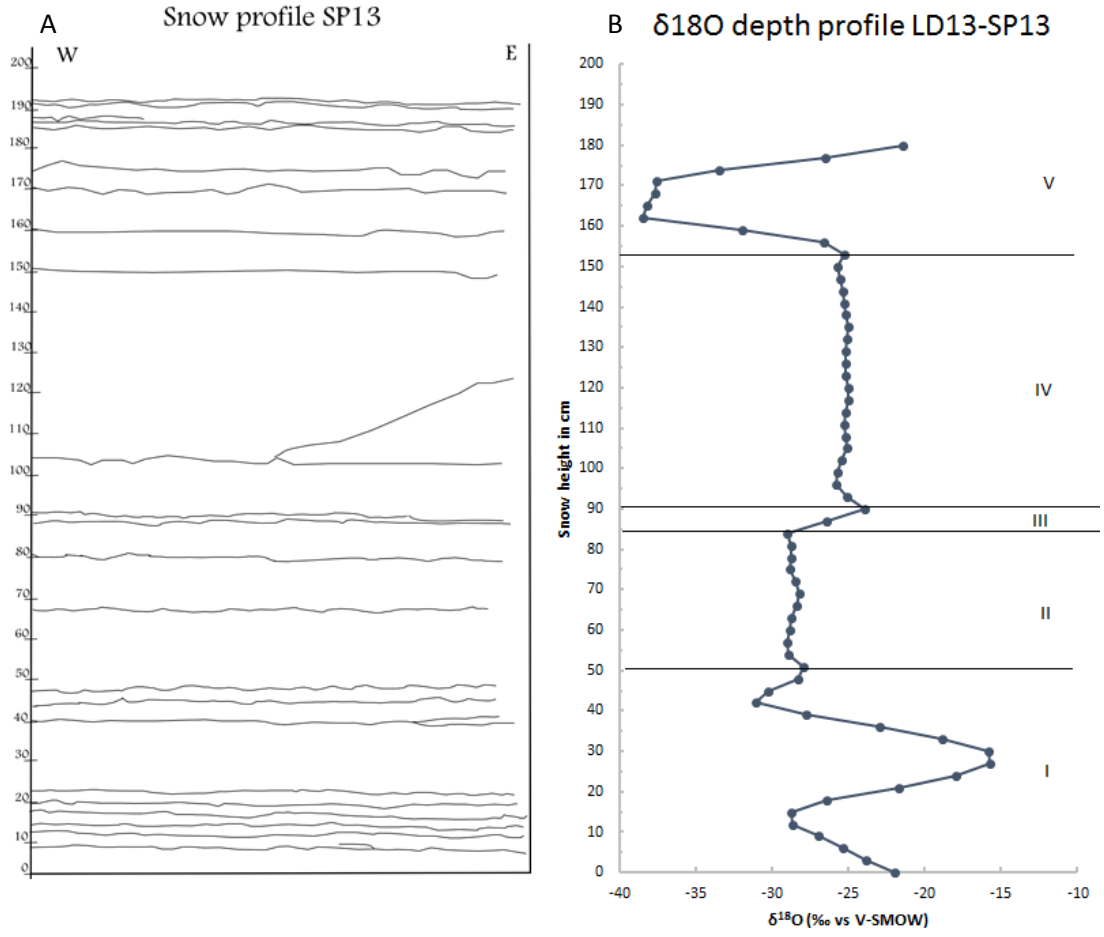

Fig. 4-1 Depth profile of the sampled snow cover SP13 A - scheme of the snow profile with different layers, B - $\delta^{18}O$ depth profile subdivided into isotope zones (I to V)

Zone III (85-90 cm) display a shift between the minimum of zone II and the maximum of zone IV at 90 cm (-24.0‰) with a value being similar to the mean of these two points (-26.5‰).
Zone IV (90-153 cm) again display relatively constant δ18O values with a mean of -25.2‰. A small maximum is observed at 90 cm and a minimum at 96 cm (-25.8‰).
Zone V (153-180 cm) again display highly variable δ18O values with a mean of -31.7 ‰. A minimum at 162 cm (-38.4‰) is observed while the δ18O values increase to the top to a maximum at 180 cm (-21.5‰).

4.2. Spatial comparison of different snow sample sites

In order to understand the spatial variability of the isotopic composition of snow, sample sites with different characteristics were compared. The sites were sampled between the 19th and the 25th of April and hence considered as comparable. Within the time the samples were taken, snow heights in the sampled polygon centers were in general greater than on the polygon walls (Fig. 4-2). While in the polygon centers snow heights ranged between 15 and 40 cm, on the walls only a range between 8 and 15 cm was observed.
SP7, sampled at the 19th of April show a $\delta^{18}O$ range from -34.0‰ to -19.8‰. SP8, sampled on the 21st of April, show a slightly greater range from -36.1‰ to -19.1 ‰. The largest range from -33.3‰ to -16.1 ‰ is found in SP21, sampled on the 25th of April.

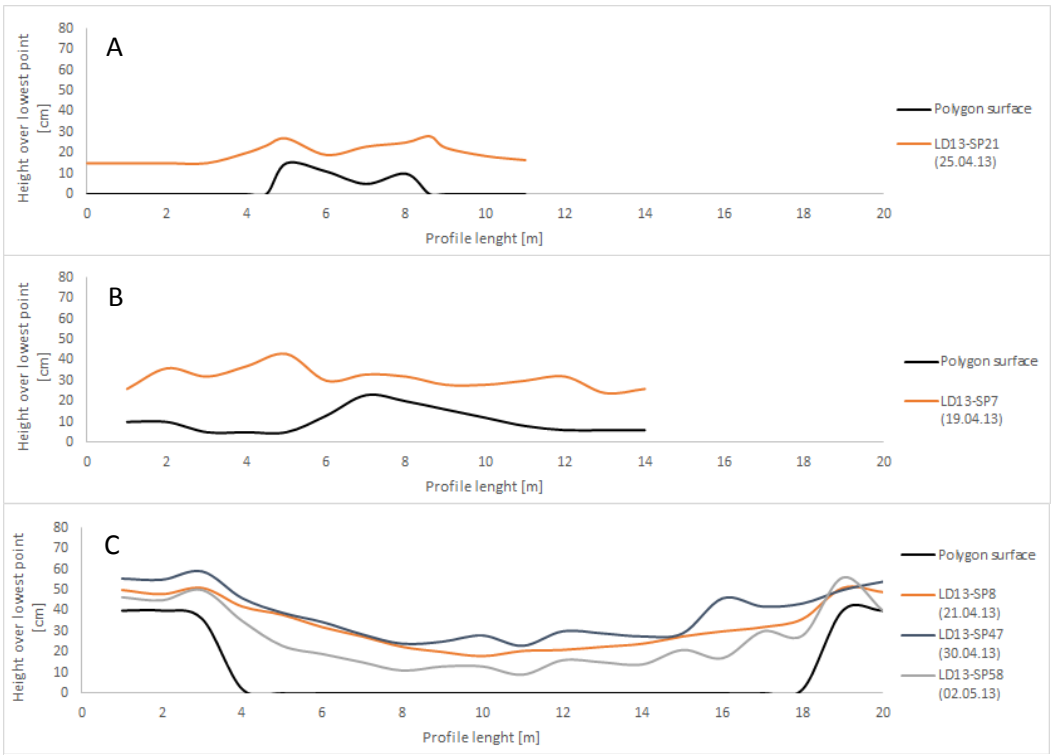

Fig. 4-2 Snow heights of the sampled ice-wedge polygons at the sampling date A - SP7: 19.04.13, B - SP21: 25.04.13, C - SP8: 21.04.13; SP47: 30.04.13;SP58: 02.05.13

The snow profiles SP7 and SP8, taken in adjacent polygons within a short time interval, show similar mean $\delta^{18}O$ values (SP7:-28.7‰, SP8: -28.5‰) while the mean $\delta^{18}O$ value of SP21 is slightly higher (-26.5‰).

The δD-$\delta^{18}O$-diagrams draw a similar picture. All samples plot near the GMWL with SP7 and SP8 having both a slope around 8 and SP21 having a slightly lower slope of 7.4 (Fig. 4-3).

In the co-isotope diagram for SP21 (Fig. 4-3-C), two samples plot lower under the GMWL than the others (red ellipse). These are the samples LD13-SP21-4-7 ($\delta^{18}O$ value: -16.1‰) and LD13-SP21-10-6 ($\delta^{18}O$ value: -16.8‰) both being depth hoar samples taken on the bottom of the snow cover at the centers. With these two samples left out, SP21 would have a slope of 8.44 and an intercept of +26.03 in the δD-$\delta^{18}O$-diagram.

The $\delta^{18}O$ values on the polygon walls range from -27.6‰ at SP21 to -24.0‰ at SP8 (see Tab. 4-1) showing an overall mean $\delta^{18}O$ value of -26.0‰ for all polygon wall snow samples. In the polygon centers, the $\delta^{18}O$ values range from -36.1‰ (SP8) to -16.1‰ (SP21). The mean $\delta^{18}O$ value for all snow samples in the polygon centers is lower than that for the polygon walls with -33.6‰.

The d-excess of the snow at the polygon walls range from 8.1‰ to 26.9‰ with a mean d-excess of 15.7‰ and at the centers from -13.2‰ to 28.9‰ with a mean value of 12.9‰ (compare Tab. 4-1, note that for the spatial comparison SP47 and SP58 are not considered as they were sampled later to show the temporal evolution of SP8).

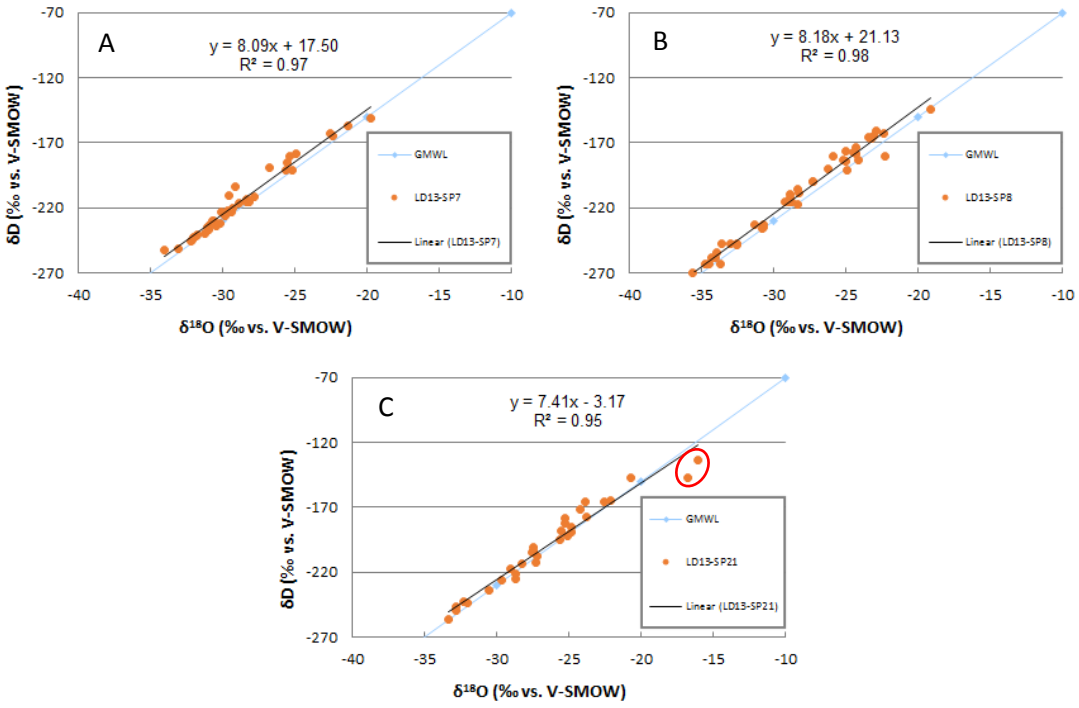

Fig. 4-3 δD-$\delta^{18}O$-diagrams for different sampled polygons A - SP7, B - SP8, C - SP21

Changes in isotopic composition of the snow cover in the centers of the sampled polygons show similar depth profiles for SP7 and SP8 while the curve of SP21 is again slightly different.
In Fig. 4-4, representative depth profiles for the polygon centers are shown. For further plots and more details see App. 1.

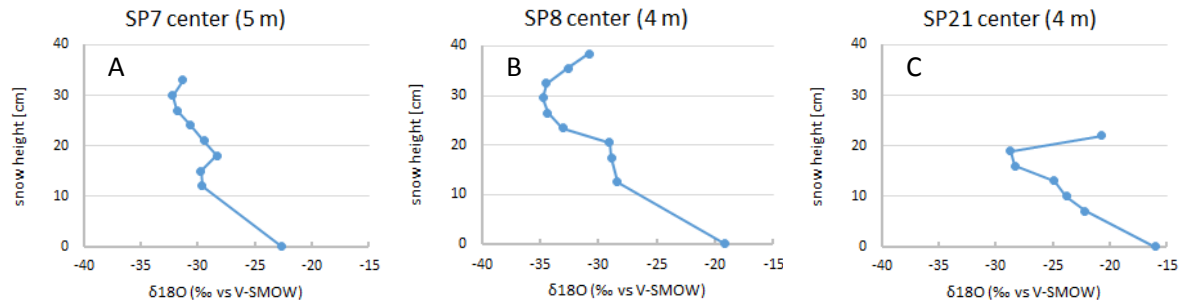

Fig. 4-4 $\delta^{18}O$ depth profiles for representative sites in the polygon centers of the sampled polygons A – SP7 at 5 m, B – SP8 at 4m, C – SP21 at 4 m

The displayed profiles all show a general increase of δ18O values from top to bottom resulting in maximum $\delta^{18}O$ values at the bottom. With increasing height in the profile, a trend towards more negative $\delta^{18}O$ values is observed while in the values in the upper most part trend again towards more positive values after the minimum was reached at 30 cm in SP7-5 and SP8-4 and at 20 cm in SP21-4. The general trend shown in Fig. 4-4 of with maximum $\delta^{18}O$ values at the bottom is found in all depth profiles sampled in the polygon centers, ranging around a mean of -23.1‰ and -21.9‰ for adjacent SP7 and SP8, respectively, whereas SP21 displays slightly heavier $\delta^{18}O$ values around a mean of -19.5‰. In all parts of the polygon centers with thinner snow cover, only parts of the $\delta^{18}O$ curves are preserved while still always showing a secondary maximum in the upper half leading to values between the minimum and maximum at the top like shown for SP21-4 in Fig. 4-4 C.

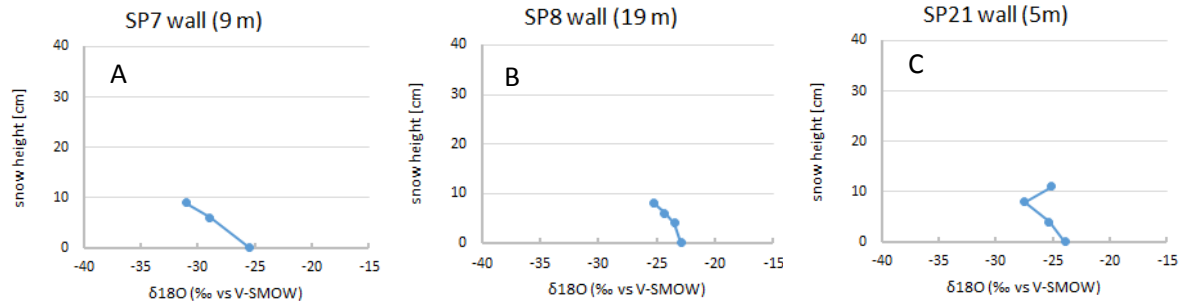

Fig. 4-5 $\delta^{18}O$ depth profiles for representative sites in the polygon walls of the sampled polygons A – SP7 at 9 m, B – SP8 at 19m, C – SP21 at 5 m

On the polygon walls (Fig. 4-5), the mean $\delta^{18}O$ values range from -27.6‰ to -24.0‰ with SP21 showing the lowest mean values and SP8 the highest while SP7 lies with -26.3‰ in between.

Taking a look at the depth profiles it can be seen that the curves show slightly different courses with generally slightly decreasing $\delta^{18}O$ values from bottom to top while some also show a secondary maximum like SP21 at 5 m (Fig. 4-5 C). Nevertheless, as in the polygon centers, the maximum $\delta^{18}O$ values at all polygons walls are found at the bottom, ranging from -27.6‰ in SP21 over -22.4‰ in SP7 to -19.1‰ in SP8.

Tab. 4-1 Minimum, maximum and mean values for $\delta^{18}O$ and d-excess values and slopes and intercepts in δD-$\delta^{18}O$ diagrams for the sampled snow profiles

Snow profile	**N**	**Geomorphological unit**	**$d^{18}O$ (‰) min.**	**$d^{18}O$ (‰) mean**	**$d^{18}O$ (‰) max.**	***d* (‰)min.**	***d* (‰) mean**	***d* (‰) max.**	***slope***	***Intercept (‰)***
SP7	37	all samples	-34.04	-28.71	-19.78	7.3	14.9	28.9	8.1	17.5
	23	Center west	-32.18	-28.55	-19.78	7.3	14.4	28.9		
	6	Wall	-29.07	-26.28	-23.93	10.5	14.7	23.1		
	8	Center east	-33.34	-27.18	-16.77	9.5	16.5	25.5		
SP21	31	all samples	-33.34	-26.53	-16.05	-13.2	12.5	25.1	7.4	-3.2
	14	Center east	-32.81	-26.39	-16.05	-5.1	10.9	18.5		
	10	Wall	-27.58	-27.58	-27.58	9.2	17.7	25.1		
	7	Center west	-33.34	-27.18	-16.77	-13.2	8.2	15.8		
SP8	45	all samples	-36.13	-28.49	-19.14	-1.8	16.0	26.9		
	17	Wall east	-32.55	-26.12	-22.36	8.1	16.7	26.9		
	24	Center	-36.13	-30.92	-19.14	-1.8	14.7	21.4		
	4	Wall west	-25.21	-23.97	-22.89	18.6	20.9	22.4		
SP47	47	all samples	-36.01	-27.09	-13.70	-18.2	15.8	26.8	7.7	8.5
	10	Wall east	-22.62	-20.26	-19.38	11.8	17.7	21.5		
	32	Center	-36.01	-29.28	-13.70	-18.2	14.7	25.3		
	5	Wall west	-31.34	-26.70	-20.40	14.0	19.0	26.8		
SP58	29	all samples	-23.28	-21.03	-20.02	7.6	14.3	25.8	8.0	14.5
	5	Wall east	-33.44	-25.77	-20.02	14.2	15.8	16.5		
	24	Center	-35.35	-29.37	-22.22	7.6	14.0	25.8		
		Wall west	n.d.	n.d.	n.d.	n.d.	n.d.	n.d.		

4.3. Temporal comparisons

To assess the temporal evolution of a snow cover on Samoylov Island, the different parts (center/wall) of one polygon (SP8) were resampled twice: first at the 30th of April (as SP47) and again after a rain event on the 2nd of May (as SP58). Between the 21st and the 30th of April, the whole snow cover (SP47) increased in thickness due to snowfall and snow drift, while on May 2nd, the snow heights were greatly decreased (SP58) in all parts after the rain event, and completely disappeared in some parts (Fig. 4-2 C). The rain event had a $\delta^{18}O$ value of -19.6‰. The mean $\delta^{18}O$ value in SP8 of –28.5‰ increased towards SP47 with -27.1‰ and slightly decreased towards SP58 with -27.9‰. The same pattern is visible in the maximum $\delta^{18}O$ values, whereas for the minimum $\delta^{18}O$ values a constant increase can be observed. While SP8 ranged from $\delta^{18}O$ values of -36.1‰ to -19.1‰, SP47 varied from -36.0‰ to -13.7‰ and SP58 from -35.4‰ to -20.0‰. At the polygon walls, two different trends are observed. While at the eastern polygon wall the mean $\delta^{18}O$ values follow the general trend, first increasing towards SP47 and then slightly decreasing towards SP58, at the western wall an decrease towards SP47 is observed. The same trend is observed in the polygon centers the mean $\delta^{18}O$ values first decrease towards SP47 and then increase again slightly in SP58 (
Tab**. 4-1**).

The snow depth profiles of the different parts of the **polygon center** (at 4, 8 and 18 m), show that the isotope curves in the polygon center only slightly change their pattern with time.

At **4 m** of the profile (Fig. 4-6 C) the isotope record of SP47 is the upper part is similar to that of SP8 but is in the lower 15 cm shifted towards more positive $\delta^{18}O$ values resulting in a less negative $\delta^{18}O$ value of -13.7‰ at the bottom as compared to SP8 (-19.1‰). The isotope profile of SP58 also follows the course of SP8 and SP47, but is at 25 cm height shifted to slightly more positive $\delta^{18}O$ values. SP58 displays a lower $\delta^{18}O$ value than SP8 and SP47 of -22.2‰ at the bottom. At **8m** (Fig. 4-6 D), the $\delta^{18}O$ profile of SP47 is again similar to that of SP8 showing similar $\delta^{18}O$ values of around -22.6‰ at the bottom. SP47 has with $\delta^{18}O$ = -36.1‰ a more negative minimum than SP8 with $\delta^{18}O$ = -34.1‰. As before, the $\delta^{18}O$ values of SP58 display with -26.8‰ the most negative bottom values, while the isotope curve shows a similar pattern than that of SP47 despite the lesser snow depth. At **18m** (Fig. 4-6 E) the $\delta^{18}O$ curve of SP47 is, again, similar to that of SP8, showing both an excursion towards more negative values observed at all polygon center profiles, with a less negative minimum of -34‰ for SP47 than for SP8 (-36‰), whereas the SP47 bottom $\delta^{18}O$ value (-25.7‰) is more negative than that of SP8 (-24.4‰).

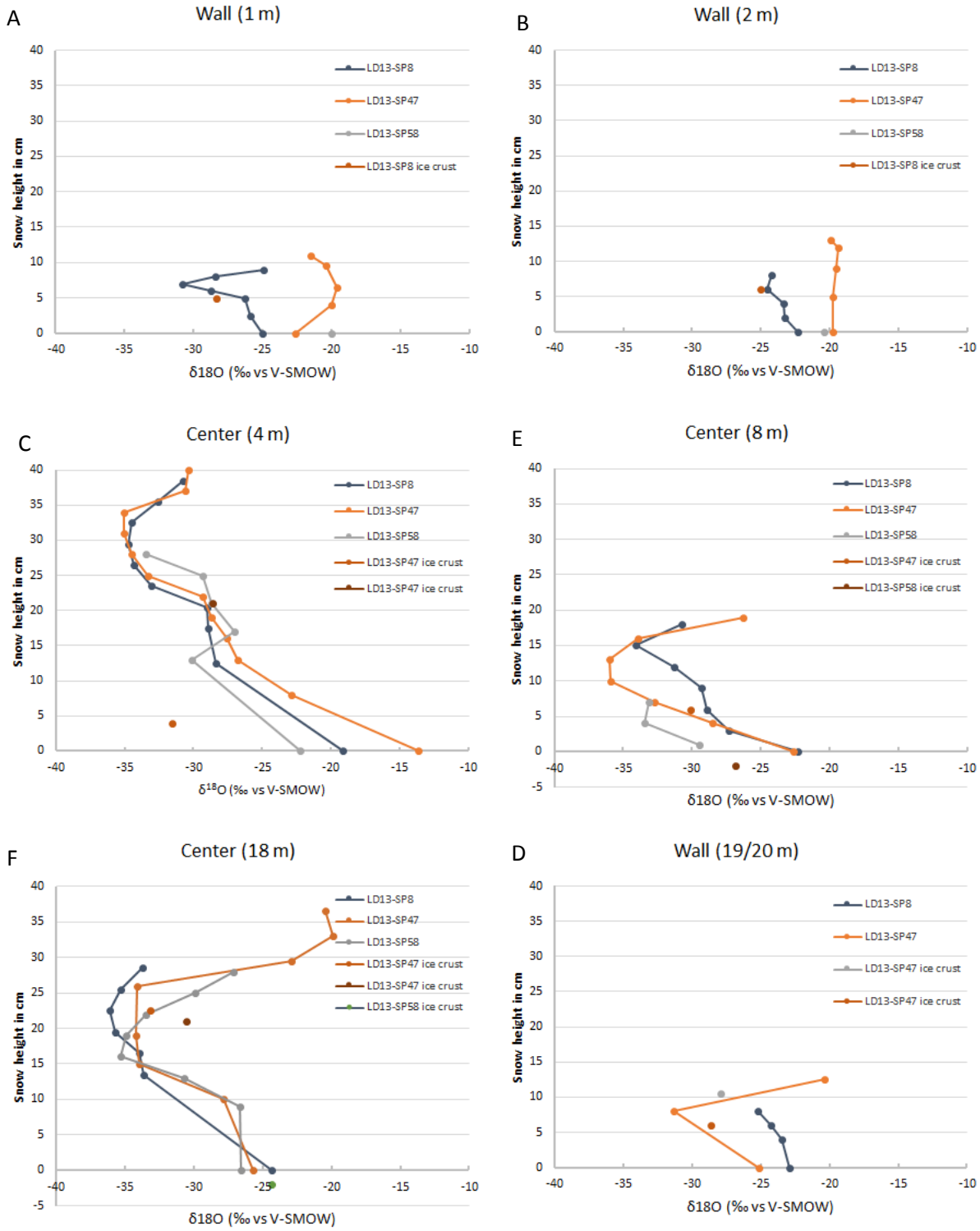

Fig. 4-6 Comparison of $\delta^{18}O$ depth profiles at different parts of the sampled polygon A – Wall (1 m), B – Wall (2 m), C – Center (4 m), D – Center (8 m), E – Center (18 m), F – Wall (19/20 m)

Despite lesser snow depth, the curve of SP58 is similar to that of SP47 with slightly more negative bottom $\delta^{18}O$ value of -26.6‰. In the polygon center, only at 4m the general trend reflected in the mean $\delta^{18}O$ values is observed, while at 8m and 18m the $\delta^{18}O$ values of SP58 are more negative than those of SP47 and SP8. In all snow profiles, ice crusts were additionally identified as they might act as boundaries i.e. for meltwater or diffusion. Ice crusts generally show $\delta^{18}O$ values ranging from -33.2‰ to -24.3‰ with a mean of -28.7‰.

At the **polygon wall**, a completely different picture can be drawn due to the lesser snow depth. For the last sampling (SP58) only one $\delta^{18}O$ value for the eastern and none for the western wall could be measured. In order to get additional information for polygonal walls, the profile 19m of SP8 has been compared to that at 20m of SP47.

At **1m** (Fig. 4-6 A), the isotope curve of SP8 shows a sharp excursion towards more negative $\delta^{18}O$ values at 7 cm with a minimum $\delta^{18}O$ value of -30.9‰, whereas top and bottom $\delta^{18}O$ values are similar yielding around -25‰. In contrast, the $\delta^{18}O$ values of SP47 are more constant and more positive with a maximum of -19.6‰. The $\delta^{18}O$ value at the top is -21.5‰ and at the bottom a minimum of -22.6‰ is observed. The only $\delta^{18}O$ value for SP58 yields -20.0‰.

At **2m** (Fig. 4-6 B), the isotope record is smoother, with SP8 only showing a small minimum and SP47 nearly constant values around -20‰ which are also seen at the bottom and are more positive than the bottom value of SP8 with -22.4‰. The $\delta^{18}O$ value of SP58 is with -20.4‰ slightly more negative than SP47 but also remarkably more positive than the bottom value of SP8.

On the western wall (Fig. 4-6 E), at **19/20m** a different picture is shown: while the depth profile of SP8 displays $\delta^{18}O$ values from -24.3‰ at the top to -22.9‰ at the bottom, it shows in general more positive values than SP47 with a maximum $\delta^{18}O$ value of -20.4‰ at the top while having lower values of -25.2‰ at the bottom and a minimum of -31.3‰.

In a δD-$\delta^{18}O$ diagram, the samples of SP47 and SP58 plot close to the GMWL with slopes of 7.73 and 8.00, and an intercepts of +8.4‰ and +14.5‰, respectively (Fig. 4-7).

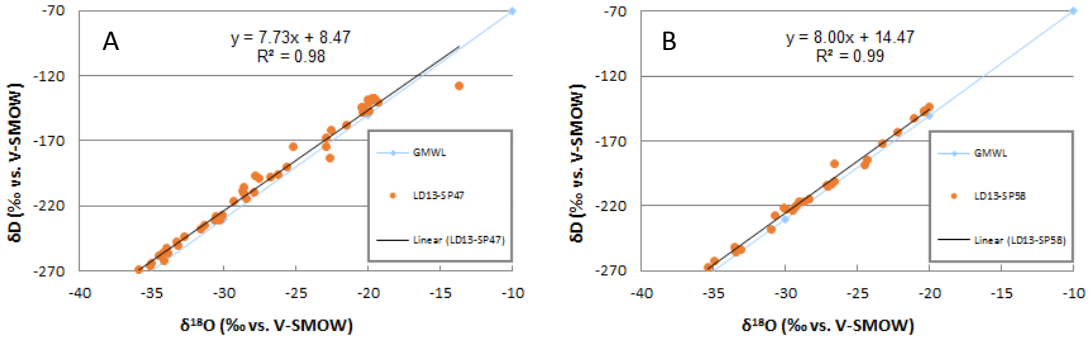

Fig. 4-7 δD-$\delta^{18}O$-diagramms for the resampled profiles A – SP47, B – SP58

The ice samples (FCI) taken out of the frost cracks after the rain event show a range in $\delta^{18}O$ values from –25.4‰ to -20.3‰ with a mean of -23.7‰, being more positive than the ice sample taken out of a frost crack at 1 m in SP8, which has a $\delta^{18}O$ value of -27.3‰. In a δD-$\delta^{18}O$ diagram FCI samples plot with a slope of 8.34 and an intercept of + 22.3‰ (Fig. 4-8). The FCS samples range between values of -29.19‰ and -24.8‰ with a mean of -24.8‰, plotting on the GMWL with a slope of 7.13 (Fig. 4-8) and an intercept of – 9.36‰ (Fig. 4-8) being again more positive than the snow sample taken on 1m in SP8 with -32.6‰.

The FCD samples range from -26.4‰ to -22.9‰ in $\delta^{18}O$ with a mean value of -24.3‰ and they plot on the GMWL with a relatively low slope of 5.97 and an intercept of – 31.7‰ (Fig. 4-8). The depth hoar sample taken at 1m in SP8 lies in the same range with $\delta^{18}O$ = -23.2‰, whereas the ice crystal sample (FCC) shows a $\delta^{18}O$ value of -26.8‰.

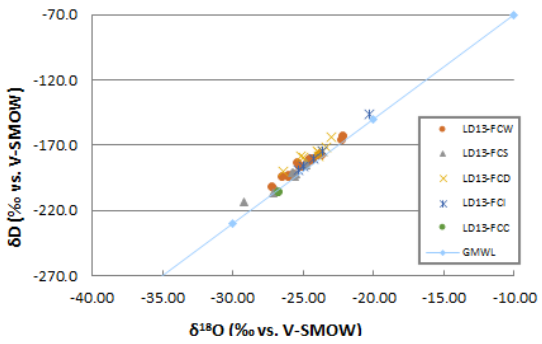

Fig. 4-8 δD-$\delta^{18}O$-diagram for the FC samples (FCW frost crack water, FCS frost crack snow, FCD frost crack depth hoar, FCI frost crack ice, FCC frost crack crystal

5. Discussion

5.1. Isotopic changes in a seasonal snow cover

To characterize seasonal changes and an annual cycle of a snow cover on Samoylov Island, a depth profile (SP13) was sampled on 23rd April 2013. The snow-height sensor showed a first signal on 3rd October 2012 (App. 3), and hence, this is assumed as the start of the snow-fall season. As introduced above, stable oxygen isotopes are indicative for temperature changes: strong peaks towards heavier (+; lighter = -) isotope compositions in the snow pack are therefore assumed to represent warm (cold) pulses, respectively. Phases with stable $\delta^{18}O$ values over several dm are assumed to be indicative for mixing events most likely due to wind drift and cannot be explained by smoothing due to diffusion or percolation (Ambach et al., 1972; Johnsen et al., 2000). It is difficult to clearly define an annual cycle in the isotope profile, because the clear identification and dating of the observed signals is problematic. The first challenge is the identification of snow fall events. Because the precipitation measurements at Samoylov Island exclude snow, snow fall events were estimated from height changes measured by a snow height gauge (Fig. 5-1 C), including both snow fall events and snow height changes due to wind drift. To estimate the ratio of precipitation to wind drift, wind speed measurements have been considered (Fig. 5-1 D), expecting that increases in snow height during high wind speeds are more likely a result of wind drift than of precipitation. The second challenge is the estimation of concrete reasons for decreases in snow heights, i.e. whether they are a result of sublimation/ evaporation or, again, wind drift. To estimate their extent of influence again the measurements of wind speeds and snow-height changes were considered, expecting that during low wind speeds decreases in snow height are more likely a result of sublimation or evaporation. The third challenge is that the snow height gauge only measures at one point and the conditions at the sample sites might have been different as snow height varies with geomorphological position (see Fig. 4-2).

Furthermore, it is obvious that not all temperature pulses (Fig. 5-1 B) are preserved since warmer air masses generally carry a greater amount of precipitation, as mentioned above, while at lower temperatures no snow fall might have taken place and so snow from warmer periods might be overrepresented while colder periods might not be preserved. The use of precipitation data from other weather stations such as i.e. Tiksi, located 120 km to the south east of Samoylov Island, was not possible, because we realized that several precipitation events that took place at Samoylov Island were not registered in Tiksi.

Nevertheless, in the zones I, III and V likely a climate signal can be identified.

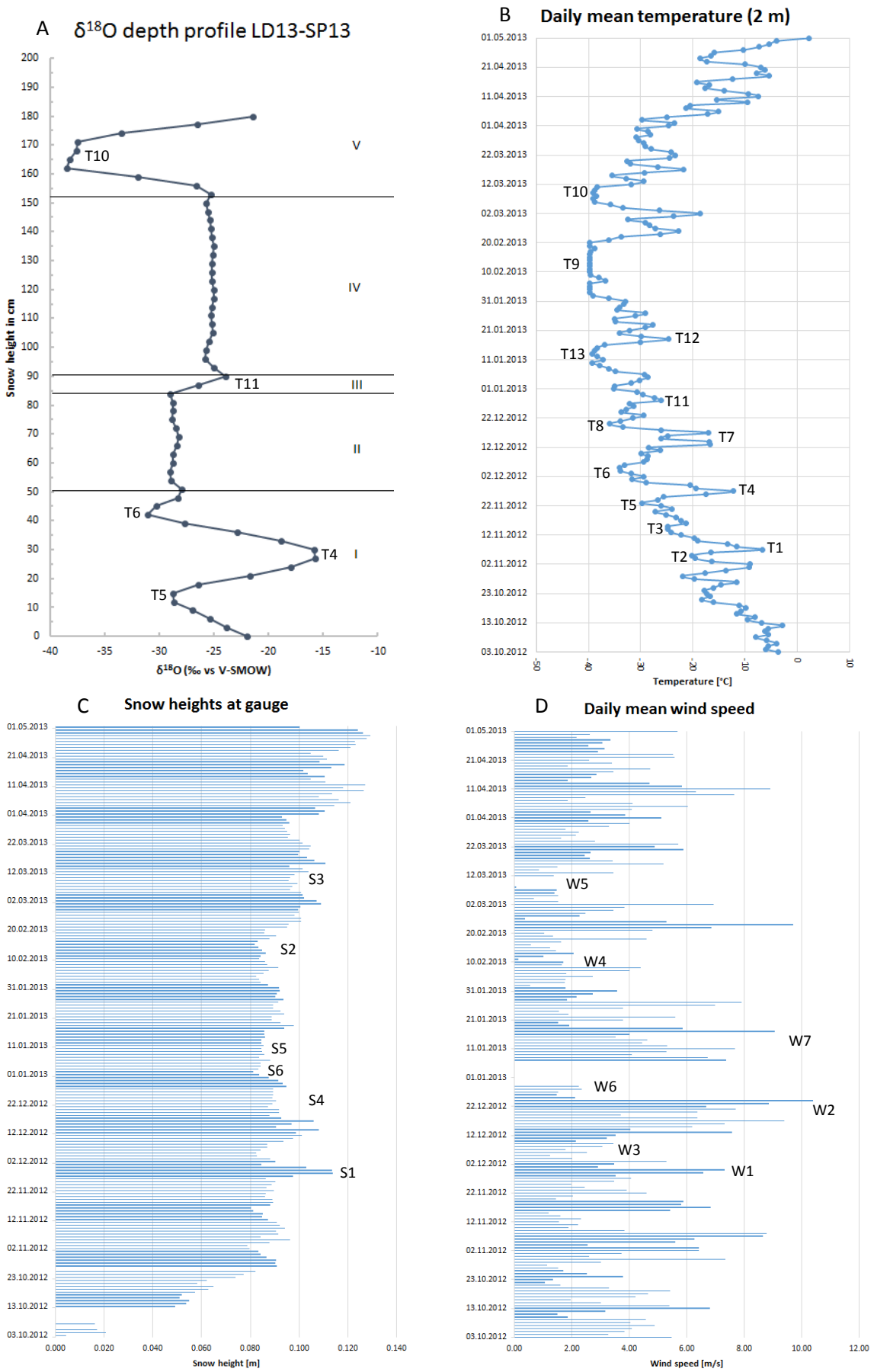

Fig. 5-1 Correlation of weather data from Samoylov Island with the depth profile SP13 and markers for key events A – isotope depth profile with isotope zones, B – daily mean temperature (T), C – daily snow height changes (S), D – daily mean wind speed (W) (source: Samoylov Island weather station)

The observations made for zone I (bottom part) in the $\delta^{18}O$ depth profile suggest, that after the beginning of snow fall in autumn a cold period took place followed by a warm pulse, displaying the highest $\delta^{18}O$ values in the profile, and a second cold pulse in early winter. Possible time points for the warm pulse are (1) around 7 Nov (T1), with a prior cold pulse around 5 Nov (T2) and a subsequent cold pulse around 14 Nov (T3), (2) around 27 Nov (T4), with a prior cold pulse around 23 Nov (T5) and a subsequent cold pulse around 4 Dec (T6), and (3) around 13 and 17 Dec (T7), with a prior cold pulse around 4 Dec (T6) and a subsequent cold pulse around 20 Dec (T8).

Although in this period the warmest temperatures were observed, the first possibility can be excluded because measured increases in snow height at the snow height gauge were always accompanied by strong wind events, leading to the expectation that no snow fall took place during this period and therefore no snow was deposited.

It can be assumed that the zone I represents the second possibility, the time between 23 Nov and 4 Dec, as between the 24 Nov and the 2 Dec (S1) increases in snow heights during lower wind speeds are observed, only interrupted by two strong wind events on 29 and 30 Nov (W1), leading to the assumption that snow fall took place and snow was deposited during this period. During the third possible period, also increases in snow heights were observed but were accompanied by strong wind events between the 13 and 17 Dec and further on till the 24 Dec (W2), leading to the assumption that in the $\delta^{18}O$ profile a due to wind drift homogenized part for this period should be displayed. Furthermore, increasing snow height during lesser wind speeds between 4 and 13 (W3) Dec may resulted in a warming signal following the second cold pulse in the $\delta^{18}O$ profile, further strengthen the assumption that zone I represents the warm phase around the 27 Nov and the cold phases around 23 Nov and 4 Dec.

Zone V at the top of the snow profile shows another cold pulse, displaying the lowest $\delta^{18}O$ values in the profile and therefore representing the lowest temperatures, followed by another warm pulse. Two possible time spans could be reflected in the cold pulse. First, the time between 2 Feb and 20 Feb (T9) and second, the time between 6 Mar and 11 Mar (T10). In the time between 2 Feb and 20 Feb (S2) mostly a decrease in snow heights at the snow height gauge is observed, accompanied by relatively low wind speeds (W4) leading to the assumption that only little or nothing of this period is preserved in the profile. On the other hand, between the 6 and the 11 Mar (S3) increases in snow height accompanied by relatively low wind speeds (W5) are observed, leading to the conclusion that in this period snow fall took place and that it is represented in the cold pulse observed in zone V. Out of this observation, it can be assumed that zone V represents the time between around 2 Mar and the sampling date (23 Apr).

Zones II and IV display nearly constant isotope composition interrupted by zone III. Both zones of constant $\delta^{18}O$ (zone II ca. -30‰, zone IV ca. -26‰) are most likely the result of two strong snow drift events and should ideally correlate with longer periods of higher wind speeds, homogenizing the $\delta^{18}O$ signal preserved in snow. Because zone IV shows less negative $\delta^{18}O$ values than zone II, it can be expected that the temperatures during or prior to the assumed snow drift event(s) were generally higher than the temperatures during or prior to the event displayed in zone II. During autumn and winter, several strong wind events occurred, while the events taken place between 4 Dec and 25 Dec (W2, W3) seem to be the ones responsible for the $\delta^{18}O$ curve in zone II, because up from 25 Dec to 28 Dec (T11) a period with a great increase in temperature as well as increasing snow heights (S4) during relatively low wind speeds (W6) are observed, possible represented in zone III. Another possible period representing zone III and showing a temperature increase could have been the time between 15 and 18 Jan (T12). Because in this period strong winds (W7) are observed, this period is rather represented in the homogenized zone IV.

Because of the observations made, zone IV may be related with strong wind events which took place between the 28 Dec and the 02 Mar. Contrary to the hypothesis that the temperatures in zone IV were higher than in zone II, in this period the lowest temperatures of around -40°C were observed (T10, T13) and can be expected to be the most negative $\delta^{18}O$ values within the profile. Nevertheless, zone IV displays more positive $\delta^{18}O$ values than zone II, which might be a result of a lack of precipitation during the cold periods as mentioned above for the period of 02 to 19 Feb (S2) and is also observed for the period between 7 Jan to 15 Jan (S5) and for the 1 Jan (S6). The reason for this lack of precipitation most likely lies in the estimation that colder air masses may carry lesser moisture available for the formation of snow fall. Furthermore, before and after the cold periods, relatively high temperatures were observed, maybe smoothing out remnants of the cold periods during mixing due to the wind drift.

5.2. Spatial comparisons of the snow cover at different sample sites

A general observation is that the snow height at a sample site depends on its location and on the sample date. Furthermore, it was obvious that the snow cover at the walls of the considered ice-wedge polygons was always thinner than in their centers, which is consistent with observations made by Boike et al. (2013). The depth profiles sampled in the snow cover at the different units of an ice-wedge polygon show similar curves for $\delta^{18}O$ values. At the boundary pond ice-snow or soil-snow, generally a heavier $\delta^{18}O$ is observed, which points to interaction between a phase of heavier (below) to lighter isotope composition (snow), while the resulting

isotope signal is derived from summer precipitation relatively enriched in heavier isotopes, preserved in soil and in pond water (Friedman et al., 1964, 1991).

Isotope measurements of pond ice at Samoylov Island show $\delta^{18}O$ values of -24.8‰ at the top, values between 12‰ and 15.1‰ at its middle and bottom part. The mean $\delta^{18}O$ values of the bottom of the snow cover range from -21.3‰ (SP21), -23.2‰ (SP8), to -23.3‰ (SP7), reinforcing this assumption. This is further supported by Meyer et al. 2002, who saw ion and isotope changes at boundary layers between ground ice and active layer ice.

These exchange processes likely took place before the active layer and pond water were fully frozen, as Cooper et al. (1993) suggested that between the snow and fully frozen water little to no moisture exchange takes place.

The observations suggest that the processes predominant during the alteration of the snow cover are similar despite different underlying surfaces. All $\delta^{18}O$ values curves of the snow cover in the polygon centers show a similar course like that for zone V in SP13. This suggests that mainly snow from early spring is preserved on top of the ice-wedge polygons.

5.3. Temporal evolution of the snow cover

When interpreting the changes in the snow cover and its isotopic composition with time it is necessary to take into account the local weather conditions, i.e. the development of temperature, precipitation events and wind speed and directions. For the meteorological data, see App. 3.

The influence of wind drift events, sublimation/evaporation and precipitation on snow height changes were estimated (as described above in section 5.1 for SP13), dealing with the same challenges.

The snow height measurements show an increase of the snow cover between the 21st of April and the 30th of April at the snow height gauge, which may be a result of snow fall events as until the 1st of May only little wind speeds were observed.

The increase in snow height is also reflected between SP8 and SP47 at the eastern polygon wall and the western part of the profile. At 4m and 8m the snow thickness is rather similar between the 21st and 30th of April (Fig. 4-2 C). Possible reasons for this observation are losses in thickness due to a local higher sublimation rate or snow drifting through wind. The reduction due to wind drift seems to be more likely, and is supported by the fact that the mean wind direction between the sampling dates was east, which is in line with the observed distribution. Contrary to this hypothesis, the snow heights at the eastern wall increased between the sampling dates which may be due to i.e. vegetation acting as natural barrier.

Furthermore, as mentioned above, in this interval only small mean wind speeds were observed, making a redistribution due to wind drift unlikely. On the other hand, sublimation would cause an enrichment in heavy isotopes resulting in more positive $\delta^{18}O$ values in the upper layers. However, at 4m in the profile no such changes were observed in the upper part and at the 8m even more negative $\delta^{18}O$ values for SP47 than for SP8 were found. One more positive $\delta^{18}O$ value for SP47 at the surface of the snow cover at 8m is most likely a result of fresh snow as the towards the 30th of April increasing temperatures should be reflected in more positive $\delta^{18}O$ values in precipitation. The same is observed at 18m where the snow height increased between the sampling of SP8 and SP47, displaying a strong increase in $\delta^{18}O$ values in the upper 10cm of the profile as it was also observed for SP13 in section 5.1.

At the polygon centers, the lower 20cm of the profiles are shifted towards more positive $\delta^{18}O$ values, displaying an enrichment of heavier isotopes due to sublimation processes at the snow grain surfaces during the metamorphism of the snow cover and the depth hoar formation in the deeper layers as described in section 3.1.3.

At 8m (Fig. 4-6 D) the middle part from 5cm to 15cm shows more negative $\delta^{18}O$ values for SP47 than for SP8. These differences in 8m are likely the result of shifted sample site.

At the eastern polygon wall the $\delta^{18}O$ values of the snow cover at SP47 evolved towards more positive values compared to SP8 and at the western wall towards more negative values while the initial curves of SP8 are similar in course, value range and snow height at 2m and 19m (Fig. 4-6 B,F). The $\delta^{18}O$ curve of SP8 at 1m (Fig. 4-6 A) shows a similar course like the one sampled nine days later (SP47) at the eastern wall at 20m (Fig. 4-6 F). This observation might be a result of the distance of one meter between the sampling points, suggesting that different sites were sampled (at 19 and 20m) and a temporal comparison is difficult.

The shift towards more positive $\delta^{18}O$ values at the top of the snow cover in the polygon centers may display a mixture of (1) enrichment of heavier isotopes due to sublimation and (2) increasing $\delta^{18}O$ values in freshly-deposited snow due to increasing temperatures.

It was expected that the rain event, which took place on 2nd of April would have a great impact on the isotope composition as it fully saturated the snow cover with water and reduced the snow heights. At the eastern wall, the remaining snow cover showed $\delta^{18}O$ values of around -20‰, being similar than that of the rain with -19‰. Accordingly, the $\delta^{18}O$ values did not change significantly towards the sampling after the rain event (SP58).

In the polygon centers, the similarity of the $\delta^{18}O$ curves with time (from SP8 to SP47 and SP58) is striking. However, there are some smaller differences: while the upper part of snow cover, when preserved after the reduction of the snow height like at 4 m and 18 m (Fig. 4-6 C, E),

shows more positive values than in SP47 and the lower halfs are equal or more negative. At all sample sites, the bottom values of SP58 are more negative than that of SP47. The snow height at 4m and 18m (Fig. 4-2) is less reduced after the rain event what might be connected to their position at the foot of the polygon walls and not in the polygon center where the water running off the polygon walls is collected.

Because of the observation that the values of SP58 are not shifted extremely towards more positive $\delta^{18}O$ values of about -19‰ measured in the rain water it is assumed, that the percolation of the rain water has no significant influence on the isotope signal. This has also been suggested by Ambach et al. (1972) and Moser and Stichler (1974). The lighter $\delta^{18}O$ values observed at the bottom of the polygon centers are most likely connected to the collection of initial runoff snow-melt water from the polygon walls in the depression, which is enriched in the lighter isotopes compared to the remaining snow (Cooper et al., 1993). The accumulation of lighter isotopes at the bottom of the snow cover in the polygon centers seems plausible as the runoff takes place at the underground surface and under the snow cover.

The ice sample taken out of a frost crack (at 1m during the sampling of SP8; 21st April) show a more negative $\delta^{18}O$ value (-27.3‰) than the mean value of the frost-crack-ice (FCI) samples (-23.7‰) taken on 3rd of May. The same was observed for the snow sample (-32.6‰) taken at 1m on the 21st of April and the frost-crack-snow (FCS) samples (-26.2‰) taken on 3rd of May. The depth hoar sample taken at 1m in SP8 (-23.2‰) in contrary is in the range of the frost-crack-depth-hoar (FCD) sample $\delta^{18}O$ values taken on 3rd of May (-26.4‰ to -23.0‰). The increase in $\delta^{18}O$ values in the FCI and FCS samples might be a result of isotopically heavier precipitation due to the observed rising temperatures but are rather the product of fractionation processes during the snow metamorphism. The depth hoar may have the same range of $\delta^{18}O$ values because the FCD samples are remnants of depth hoar formed under the snow cover during an earlier period.

5.4. Correlation with recent ice wedges at Samoylov Island

As described above, formation of ice wedges is dependent on meltwater penetrating open frost cracks and producing new annual veins. Therefore, it is expected that the isotope signal stored in the ice wedges is derived from snow melt water filling the cracks. Because of this, $\delta^{18}O$ values observed in the ice wedges need to be compared to the ones observed in the fillings of the cracks and at the bottom of the snow cover at the polygon walls. The $\delta^{18}O$ values at the bottom are expected to provide the preserved isotope signal as the percolation of melt water from the upper snow layers and precipitation should have no significant influence on the signal

as shown above and suggested by Ambach et al. (1972) and also observed in this study as described above. According Kleine (2014), the isotope signals preserved in ice wedges range between average $\delta^{18}O$ values of -22.9‰ and -22.3 ‰ for the time period between 2002/3 and 2009/10, while showing great ranges within the years, varying between -25‰ and -20‰ in $\delta^{18}O$.The bottoms samples of SP58 display $\delta^{18}O$ values between -26‰ and -20‰ thus, a variation, which is comparable to that observed by Kleine (2014). The depth-hoar samples (FCD) with a range between $\delta^{18}O$ values of -26.4‰ and -22.9‰ and a mean of -24.3‰ also fit well into this range. The same is observed for the ice samples FCI with a range between -25.4‰ and -20.3‰ and a mean of -23.7‰. The snow samples show a more negative range with values between -29.2‰ and -24.8‰ with a mean value of -26.2‰ being at the lower end of the observed range for ice wedges. The same is observed for the sampled ice crystal FCC with a $\delta^{18}O$ value of -26.8‰ being situated at the lower end of the range observed by Kleine (2014). As mentioned above in section 2.2.2, Michel (1982) and Kleine (2014) showed that the freezing of the penetrating water is fast enough to prevent it from fractionation processes during the freezing and therefore its isotope composition should be preserved in the formed ice. The water samples FCW taken out of the frost crack after the rain event show with $\delta^{18}O$ values between -27.3‰ and -22.2‰ a slightly more negative range than that observed in the ice wedges.

Kleine (2014) also showed that there are two penetration periods for the frost cracks being responsible for the great ranges over the year. The first period is in December, when frost cracks open (Kleine, 2014) and snow might fall into the cracks and depth hoar may develop (French, 2007). A second period in April/May, when the snow melt starts (Boike et al., 2013) and the frost cracks are filled with snow melt. As the sampling took place in April/May, only the second, but expected to be the more relevant, filling of the cracks was sampled, and the influence of the primary filling can not be estimated. The data suggest, that the isotope signal preserved in the annual veins of the ice wedge is mainly derived from snow of the bottom of the snow cover and depth hoar and ice developing in the troughs of the frost cracks. The snow (FCS) and water (FCW) samples may undergo further alteration due to evaporation, leading to an enrichment in heavier isotopes, before refreezing in the open frost cracks. As shown in section 5.2., snow samples at the bottom of the snow cover are influenced by moisture exchange with the underlying soil before the underground were fully frozen, while at the polygon walls this influence seems to be overwritten by the alteration processes due to lesser snow heights.

6. Conclusions

The data show, that the snow cover thickness at Samoylov Island during the snow period is highly variable. It was observed, that the thickness of the snow cover in the centers of the ice-wedge polygons was greater than on their walls, which is consistent with observations by Boike et al. (2013). The spatial variability of the snow cover is mainly dependent on the location of the sample site, i.e. exposition to wind or location on different geomorphologic, while being smaller as the temporal snow height variability.

It was difficult to characterize an annual cycle within the snow cover because strong winter winds caused a homogenization of the $\delta^{18}O$ profile in over 50% of the snow cover. Furthermore the differentiation of the processes leading to changes in snow cover height and altering the isotopic composition of the snow is challenging. Nevertheless, it was possible to identify a climate signal for late-autumn, mid-winter and early spring in the isotope composition. The signal for early spring at the top of the annual snow profile, showing a cold and a warm phase, was also noticeable in snow profile at the ice-wedge polygons.

The snow at the bottom of the snow cover shows an influence of moisture exchange with underground, as suggested by Friedman et al. (1991).

It has been shown that the snow cover and its isotopic composition undergo changes over time due to sublimation, evaporation and wind drift processes, while percolating rain water highly reduced the thickness of the snow cover but had no significant influence on its isotopic composition as suggested by Ambach et al. (1972). Nevertheless, it was observed that initial-runoff-snow-melt water has an influence on the isotopic composition of the snow at the bottom of depressions. Furthermore it was observed, that thinner snow packs are stronger influenced by alteration processes than thicker snow packs.

The observations suggest, that the isotope signal preserved in the annual veins of ice wedges best corresponds to that of snow of the bottom of the snow cover, depth hoar and ice from snow melt developing in the troughs above frost cracks. Therefore, the ice veins forming ice wedges should rather reflect the isotope signal of early spring temperatures where snow undergoes strong metamorphic changes and is influenced by moisture of precipitation of the previous summer stored in the active layer and in ponds in the ice-wedge polygon centers.

7. Outlook

To better understand the made observations and better distinguish the processes predominant during the alteration of the snow cover, precipitation measurements including snow fall would be necessary, as the estimation of snow fall events out of the correlation of wind speeds and a local measuring snow height gauge are problematic.

Furthermore, more samples should be taken at the polygon walls in order to better understand the temporal evolution and to estimate if there are differences to other sample sites.

References

ACIA, 2004. Impacts of a warming Arctic: Arctic Climate Impact Assessment - ACIA Overview report-. Cambridge University Press, Cambridge, U.K., 140 pp.

Akhmadeeva, I., Becker, H., Friedrich K., Wagener, D., Pfeiffer, E. M. D., Quass, W., Zhurbenko, M., Zollner E., Boike, J., 1999. Modern Processes in Permafrost Affected soil, in: Rachold, V., Grigoriev, M.N. (Eds.), Russian-German Cooperation System Laptev Sea 2000: Expeditions in Siberia 1998, vol. 315. Berichte zur Polarforschung 315. Alfred-Wegner-Institut für Polar-und Meeresforschung, Bremerhaven, pp. 19–80.

Ambach, W., Eisner, H., Pessl, K., 1972. Isotopic oxygen composition of firn, old snow and precipitation in Alpine regions. Zeitschrift für Gletscherkunde und Glazialgeologie (8), 125–135.

Berglund, M. and Wieser, M.E., 2011. Isotopic compositions of the elements 2009 (IUPAC Technical Report). Pure and Applied Chemistry 83 (2), 397–410.

Boike, J., Wille, C., Abnizova, A., 2008. Climatology and summer energy and water balance of polygonal tundra in the Lena River Delta, Siberia. J. Geophys. Res. 113 (G3).

Boike, J., Grüber, M., Langer, M., Piel, K., Scheritz, M., 2012. Orthomosaic Samoylov Island, Lena Delta, Siberia. PANGAEA, Bremerhaven.

Boike, J., Kattenstroth, B., Abramova, K., Bornemann, N., Chetverova, A., Fedorova, I., Fröb, K., Grigoriev, M., Grüber, M., Kutzbach, L., Langer, M., Minke, M., Muster, S., Piel, K., Pfeiffer, E.-M., Stoof, G., Westermann, S., Wischnewski, K., Wille, C., Hubberten, H.-W., 2013. Baseline characteristics of climate, permafrost and land cover from a new permafrost observatory in the Lena River Delta, Siberia (1998–2011). Biogeosciences 10 (3), 2105–2128.

Bortolami, G.C., B. Ricci, G. F. Susella, G. M. Zuppi, 1979. Isotope hydrology of the Val Corsaglia, Maritime Alps, Piedmont Italy, in: Isotope hydrology, 1978. Proceedings of an International Symposium on Isotope Hydrology. International Atomic Energy Agency; [Sold by UNIPUB], Vienna, [New York], pp. 327–350.

Clark, I.D., Fritz, P., 1997. Environmental isotopes in hydrogeology. Lewis Publ., Boca Raton [u.a.], 328 S.

Cooper, L.W., Solis, C., Kane, D.L., Hinzman, L.D., 1993. Application of Oxygen-18 Tracer Techniques to Arctic Hydrological Processes. Arctic and Alpine Research 25 (3), 247.

Costard, F., Gautier, E., Brunstein, D., Hammadi, J., Fedorov, A., Yang, D., Dupeyrat, L., 2007. Impact of the global warming on the fluvial thermal erosion over the Lena River in Central Siberia. Geophys. Res. Lett. 34 (14).

Craig, H., 1961a. Isotopic Variations in Meteoric Waters. Science (133), 1702–1703.

Craig, H., 1961b. Standard for Reporting Concentrations of Deuterium and Oxygen-18 in Natural Waters. Science 133 (3467), 1833–1834, (in eng).

Dansgaard, W., 1964. Stable isotopes in precipitation. Tellus (16), 436–468.

Earman, S., Campbell, A.R., Phillips, F.M., Newman, B.D., 2006. Isotopic exchange between snow and atmospheric water vapor: Estimation of the snowmelt component of groundwater recharge in the southwestern United States. J. Geophys. Res. 111 (D9).

Epstein, S. and Mayeda, T., 1953. Variations of 18O content of waters from natural sources. Geochimica et Cosmochimica Acta (4), 213–244.

French, H.M., 2007. The periglacial environment, 3rd ed. Wiley & Sons, Chichester [u.a.].

Friedman, I. and O'Neil, J. R., 1977. Compilation of stable isotope fractionation factors of geochemical interest. USGPO (440-KK).

Friedman, I., Redfield, A.C., Schoen, B., Harris, J., 1964. The variation of the deuterium content of natural waters in the hydrologic cycle. Rev. Geophys. 2 (1), 177–224.

Friedman, I., Benson, C., Gleason, J., 1991. Isotopic changes during snow metamorphism, in: Taylor, H.P., O'Neil, J.R., Kaplan, I.R. (Eds.), Stable isotope geochemistry. A tribute to Samuel Epstein. Spcial publication no. 3. Geochemical Society, San Antonio, Tex., U.S.A., pp. 211–221.

Gonfiantini, R., 1978. Standards for stable isotope measurements in natural compounds. Nature 271 (5645), 534–536.

Gordeev, V. and Shevchenko, V.P., 1995. Chemical composition of suspended sediments in the Lena River and its mixing zone, in: Kassens, H. (Ed.), Russian-German cooperation: Laptev-Sea system, vol. 176. Berichte zur Polarforschung 176. Alfred-Wegner-Institut für Polar-und Meeresforschung, Bremerhaven, pp. 154–169.

Grigoriev, M.N., 1993. Criomorphogenesis in the Lena Delta. Permafrost Institute Press, Yakutsk, 176pp, (in Russian).

Hoefs, J., 2009. Stable Isotope Geochemistry, 6th Edition ed. Springer, Berlin, Heidelberg, 293 pp.

Hubberten, H.-W., Dirk Wagner, Eva-Maria Pfeiffer, Julia Boike, Alexander Yu. Gukov, 2006. The Russian-German Research Station Samoylov, Lena Delta - A Key Site for Polar Research in the Siberian Arctic. Polarforschung (73), 111–116.

Johnsen, S.J., Clausen, H.B., Cuffey, K.M., Hoffmann, G., Schwander, J., Creyts, T., 2000. Diffusion of stable isotopes in polar firn and ice: the isotope effect in firn diffusion. Physics of ice core records (159), 121–140.

Kleine, C., 2014. Recent cryogenic processes at Samoylov Island North Siberia for calibrating a stable-isotope thermometer for ice wedges. Bachelor Thesis, Potsdam, 82 pp.

Konishchev, V.N., Golubev, V.N., Sokratov, S.A., 2003. Sublimation from a seasonal snow cover and an isotopic content of ice wedges in the light of a palaeoclimate reconstruction, in: Permafrost: Proceedings of the Eighth International Conference on Permafrost. Internatinal Conference on Permafrost, Zürich, Switzerland. 21-25 July. Swets & Zeitlinger, Lisse, pp. 585–590.

Lee, J., Feng, X., Faiia, A.M., Posmentier, E.S., Kirchner, J.W., Osterhuber, R., Taylor, S., 2010. Isotopic evolution of a seasonal snowcover and its melt by isotopic exchange between liquid water and ice. Chemical Geology 270 (1-4), 126–134.

Mackay, J.R., 1974. Ice-wedges cracks, Garry Island, Northwest Territories. Canadian Journal of Earth Sciences (11), 1366–1383.

Mackay, J.R., 1983. Oxygen isotope variations in permafrost, Tuktoyaktuk Peninsula area, Northwest Territories. Current Research, Part B, Geological Survey of Canada (83-1B), 67–74.

Mackay, J.R., 1993. Air temperature, snow cover, creep of frozen ground, and the time of ice-wedge cracking, western. Canadian Journal of Earth Sciences (30), 1720–1729.

Markl, G., 2008. Minerale und Gesteine: Mineralogie - Petrologie - Geochemie, 2., verb. u. erw. Aufl ed. Spektrum, Akad. Verl., Heidelberg, XIV, 610 S.

Merlivat, L. and Jouzel, J., 1979. Global climatic interpretation of the deuterium-oxygen 18 relationship for precipitation. J. Geophys. Res. 84 (C8), 5029–5033.

Meyer, H., Schönicke, L., Wand, U., Hubberten, H.W., Friedrichsen, H., 2000. Isotope Studies of Hydrogen and Oxygen in Ground Ice - Experiences with the Equilibration Technique. Isotopes in Environmental and Health Studies 36 (2), 133–149.

Meyer, H., Dereviagin, A., Siegert, C., Schirrmeister, L., Hubberten, H.-W., 2002a. Palaeoclimate Reconstruction on Big Lyakhovsky Island, North Siberia-Hydrogen and Oxygen Isotopes in Ice Wedges. Permafrost Periglac. Process. 13 (2), 91–105.

Meyer, H., Dereviagin, A., Siegert, C., Hubberten, H.-W., 2002b. Paleoelimate Studies on Bykovsky Peninsula, North Siberia, Hydrogen and Oxygen Isotopes in Ground Ice. Polarforschung 2000 (70), 37–51.

Meyer, H., 2003. 3.3 Studies on recent crygenesis. The Expedition LENA 2002, in: Grigoriev, M.N., Rachold, V., Bolshiyanov, D. (Eds.), Russian-German cooperation SYSTEM LAPTEV SEA : the expedition LENA 2002, vol. 466. Berichte zur Polarforschung 466. Alfred-Wegner-Institut für Polar-und Meeresforschung, Bremerhaven, pp. 29–48.

Meyer, H., Schirrmeister, L., Yoshikawa, K., Opel, T., Wetterich, S., Hubberten, H.-W., Brown, J., 2010. Permafrost evidence for severe winter cooling during the Younger Dryas in northern Alaska. Geophys. Res. Lett. 37 (3).

Michel, F.A., 1982. Isotope investigations of permafrost waters in northern Canada. PhD thesis, Waterloo, Canada.

Moser, H. and Stichler, W., 1974. Deuterium and oxygen-18 contents as an index of the properties of snow covers. International Association of Hydrological Sciences Publication (114), 122–135.

Nikolayev, V.I. and Mikhalev, D.V., 1995. An Oxygen-Isotope Paleothermometer from Ice in Siberian Permafrost. Quaternary Research (43), 14–21.

Opel, T., Dereviagin, A.Y., Meyer, H., Schirrmeister, L., Wetterich, S., 2010. Palaeoclimatic information from stable water isotopes of Holocene ice wedges on the Dmitrii Laptev Strait, northeast Siberia, Russia. Permafrost Periglac. Process. 22 (1), 84–100.

Péwé, T.L., 1966. Ice-wedge in Alaska: Classification, distribution and climatic significance, in: 01st International Conference on Permafrost - Proceedings. International Conference on Permafrost (ICOP), Lafayette Indianna. 11-15 November 1963. National Academy of Sciences-National Research Council, Washington, D.C., pp. 76–81.

Romanovskii, N.N. and Hubberten, H.-W., 2001. Results of permafrost modelling of the lowlands and shelf of the Laptev Sea Region, Russia. Permafrost Periglac. Process. 12 (2), 191–202.

Sachs, T., Wille, C., Boike, J., Kutzbach, L., 2008. Environmental controls on ecosystem-scale CH 4 emission from polygonal tundra in the Lena River Delta, Siberia. J. Geophys. Res. 113.

Schwamborn, G., Rachold, V., Grigoriev, M.N., 2002. Late Quaternary sedimentation history of the Lena Delta. Quaternary International 89 (1), 119–134.

Singh, V.P., Singh, P., Haritashya, U.K. (Eds.), 2011. Encyclopedia of snow, ice and glaciers. The encyclopedia of earth sciences series. Springer, Dordrecht, London, 1 online resource.

Sokratov, S.A. and Golubev, V.N., 2009. Snow isotopic content change by sublimation. Journal of Glaciology 55 (193), 823–828.

Stichler, W., Schotterer, U., Fröhlich, K., Ginot, P., Kull, C., Gäggeler, H., Pouyaud, B., 2001. Influence of sublimation on stable isotope records recovered from high-altitude glaciers in the tropical Andes. J. Geophys. Res. 106 (D19), 22613.

Urey, H.C., 1947. The thermodynamic properties of isotopic substances. J. Chem. Soc., 562–581.

Vaikmäe, R., 1989. Oxygen isotopes in permafrost and ground ice: A new tool for paleoclimatic investigations, in: Fifth Working Meeting Isotopes in Nature. Proceedings, Leipzig. 25-29.09.1989. Central Institute of Isotope and Radiation Research, Leipzig, pp. 543–553.

van Everdingen, R. (Ed.), ed. 1998 revised 2005. Multi-language glossary of permafrost and related ground-ice terms. CO: National Snow and Ice Data Center/World Data Center for Glaciology, Boulder, 90 pp.

Vasil'chuk, Y., 1991. Reconstruction of the palaeoclimate of the late Pleistocene and Holocene on the basis of isotope studies of subsurface ice and waters of the permafrost zone. Water Resurces (17), 640–674.

Wilhelm, F., 1975. Schnee- und Gletscherkunde. Lehrbuch der allgemeinen Geographie Bd. 3, T. 3. De Gruyter, Berlin, New York, vii, 434.

Zhang, T., Barry, R.G., Knowles, K., Heginbottom, J.A., Brown, J., 1999. Statistics and characteristics of permafrost and ground-ice distribution in the Northern Hemisphere 1. Polar Geography 23 (2), 132–154.

Appendix

Index of Appendices

App. 1 Considered samples with isotope data

Nr.	Sample	date	type	depth min (cm)	depth max (cm)	$d^{18}O$ (‰) vs. SMOW	1 s	δD (‰) vs. SMOW	1 s	d excess
31	LD13-SP-7-1-1	19.04.2013	SP	0	3	-28.17	0.05	-215.72	0.22	9.65
32	LD13-SP-7-1-2	19.04.2013	SP	3	6	-25.64	0.05	-191.18	0.23	13.95
33	LD13-SP-7-1-3	19.04.2013	SP	6	9	-25.52	0.08	-184.91	0.17	19.28
34	LD13-SP-7-1-4	19.04.2013	SP	9	16	-21.34	0.06	-157.19	0.37	13.53
35	LD13-SP-7-2	19.04.2013	SP	0	26	-27.86	0.06	-211.22	0.21	11.62
36	LD13-SP-7-3-1	19.04.2013	SP	0	3	-30.52	0.04	-234.15	0.18	9.98
37	LD13-SP-7-3-2	19.04.2013	SP	3	6	-32.04	0.04	-243.28	0.23	13.01
38	LD13-SP-7-3-3	19.04.2013	SP	6	9	-31.08	0.05	-234.73	0.32	13.88
39	LD13-SP-7-3-4	19.04.2013	SP	9	12	-30.89	0.04	-232.82	0.34	14.31
40	LD13-SP-7-3-5	19.04.2013	SP	12	15	-30.75	0.05	-229.78	0.14	16.19
41	LD13-SP-7-3-6	19.04.2013	SP	15	18	-29.13	0.03	-204.19	0.24	28.85
42	LD13-SP-7-3-7	19.04.2013	SP	18	27	-19.78	0.06	-150.95	0.34	7.31
43	LD13-SP-7-4	19.04.2013	SP	0	32	-28.36	0.03	-215.70	0.20	11.14
44	LD13-SP-7-5-1	19.04.2013	SP	0	3	-31.30	0.04	-240.01	0.22	10.42
45	LD13-SP-7-5-2	19.04.2013	SP	3	6	-32.18	0.06	-244.90	0.26	12.52
46	LD13-SP-7-5-3	19.04.2013	SP	6	9	-31.81	0.04	-240.98	0.27	13.50
47	LD13-SP-7-5-4	19.04.2013	SP	9	12	-30.62	0.04	-230.11	0.30	14.87
48	LD13-SP-7-5-5	19.04.2013	SP	12	15	-29.44	0.01	-223.45	0.29	12.08
49	LD13-SP-7-5-6	19.04.2013	SP	15	18	-28.33	0.04	-213.75	0.22	12.90
50	LD13-SP-7-5-7	19.04.2013	SP	18	21	-29.71	0.04	-222.67	0.24	14.98
51	LD13-SP-7-5-8	19.04.2013	SP	21	24	-29.59	0.07	-210.62	0.37	26.08
52	LD13-SP-7-5-9	19.04.2013	SP	24	36	-22.62	0.02	-163.32	0.25	17.64
53	LD13-SP-7-6	19.04.2013	SP	0	19.5	-29.89	0.03	-226.53	0.15	12.57
54	LD13-SP-7-7-1	19.04.2013	SP	0	3	-25.25	0.06	-191.45	0.28	10.54
55	LD13-SP-7-7-2	19.04.2013	SP	3	10	-22.42	0.02	-164.91	0.28	14.43
56	LD13-SP-7-9-1	19.04.2013	SP	0	3	-31.00	0.04	-237.37	0.24	10.62
57	LD13-SP-7-9-2	19.04.2013	SP	3	6	-28.94	0.02	-216.24	0.26	15.25
58	LD13-SP-7-9-3	19.04.2013	SP	6	12	-25.42	0.03	-180.28	0.27	23.05
59	LD13-SP-7-10	19.04.2013	SP	0	11 or 17	-29.33	0.04	-220.5	0.3	14.1
60	LD13-SP-7-11-1	19.04.2013	SP	0	3	-30.19	0.04	-232.08	0.26	9.47
61	LD13-SP-7-11-2	19.04.2013	SP	3	6	-33.09	0.02	-251.93	0.19	12.82
62	LD13-SP-7-11-3	19.04.2013	SP	6	9	-34.04	0.05	-252.35	0.23	20.00
63	LD13-SP-7-11-4	19.04.2013	SP	9	18	-26.80	0.04	-188.86	0.17	25.54
64	LD13-SP-7-12	19.04.2013	SP	0	22	-32.19	0.05	-245.7	0.3	11.8
65	LD13-SP-7-13-1	19.04.2013	SP	0	3	-31.85	0.06	-242.00	0.21	12.78
66	LD13-SP-7-13-2	19.04.2013	SP	3	6	-30.13	0.03	-223.06	0.29	17.95
67	LD13-SP-7-13-3	19.04.2013	SP	6	18	-24.98	0.04	-178.45	0.33	21.38
118	LD13-SP-8-1-1	21.04.2013	SP	0	1	-24.93	0.02	-191.3	0.3	8.1
119	LD13-SP-8-1-2	21.04.2013	SP	1	2	-28.40	0.04	-217.1	0.2	10.1
120	LD13-SP-8-1-3	21.04.2013	SP	2	3	-30.83	0.03	-235.7	0.3	10.9
121	LD13-SP-8-1-4	21.04.2013	SP	3	4	-28.78	0.04	-215.2	0.2	15.0

Nr.	Sample	date	type	depth min (cm)	depth max (cm)	$d^{18}O$ (‰) vs. SMOW	1 s	δD (‰) vs. SMOW	1 s	d excess
122	LD13-SP-8-1-5	21.04.2013	SP	4	5	-26.25	0.03	-190.4	0.3	19.6
123	LD13-SP-8-1-6	21.04.2013	SP	5	7.5	-25.88	0.02	-180.1	0.4	26.9
124	LD13-SP-8-1-7	21.04.2013	SP	7.5	10	-25.01	0.05	-176.2	0.3	23.9
125	LD13-SP-8-1-8	21.04.2013	SP	4.5	5	-28.31	0.03	-208.6	0.4	17.8
126	LD13-SP-8-2-1	21.04.2013	SP	0	1	-24.19	0.03	-183.5	0.2	9.8
127	LD13-SP-8-2-2	21.04.2013	SP	1	3	-24.55	0.03	-177.4	0.3	19.0
128	LD13-SP-8-2-3	21.04.2013	SP	3	5	-23.32	0.03	-166.8	0.3	19.8
129	LD13-SP-8-2-4	21.04.2013	SP	5	7	-23.25	0.03	-166.7	0.2	19.1
130	LD13-SP-8-2-5	21.04.2013	SP	7	9	-22.36	0.03	-162.6	0.3	16.2
131	LD13-SP-8-2-6	21.04.2013	SP	2.5	3	-25.04	0.04	-184.7	0.3	15.6
132	LD13-SP-8-4-1	21.04.2013	SP	0	3	-30.78	0.03	-234.8	0.3	11.4
133	LD13-SP-8-4-2	21.04.2013	SP	3	6	-32.57	0.05	-249.0	0.2	11.0
134	LD13-SP-8-4-3	21.04.2013	SP	6	9	-34.47	0.03	-263.3	0.2	12.6
135	LD13-SP-8-4-4	21.04.2013	SP	9	12	-34.74	0.03	-263.4	0.2	14.9
136	LD13-SP-8-4-5	21.04.2013	SP	12	15	-34.33	0.04	-258.6	0.2	16.6
137	LD13-SP-8-4-6	21.04.2013	SP	15	18	-33.03	0.04	-247.5	0.2	16.5
138	LD13-SP-8-4-7	21.04.2013	SP	18	21	-29.02	0.03	-215.3	0.2	17.1
139	LD13-SP-8-4-8	21.04.2013	SP	21	24	-28.90	0.05	-212.3	0.4	19.2
140	LD13-SP-8-4-9	21.04.2013	SP	24	29	-28.40	0.03	-206.1	0.2	21.2
141	LD13-SP-8-4-10	21.04.2013	SP	29	41.5	-19.14	0.03	-144.0	0.1	9.2
142	LD13-SP-8-8-1	21.04.2013	SP	0	3	-30.74	0.02	-232.8	0.3	12.9
143	LD13-SP-8-8-2	21.04.2013	SP	3	6	-34.07	0.06	-258.3	0.2	14.2
144	LD13-SP-8-8-3	21.04.2013	SP	6	9	-31.31	0.05	-233.5	0.3	17.0
145	LD13-SP-8-8-4	21.04.2013	SP	9	12	-29.28	0.04	-216.1	0.2	18.2
146	LD13-SP-8-8-5	21.04.2013	SP	12	15	-28.93	0.04	-210.0	0.3	21.4
147	LD13-SP-8-8-6	21.04.2013	SP	15	18	-27.29	0.05	-199.9	0.2	18.4
148	LD13-SP-8-8-7	21.04.2013	SP	18	21	-22.30	0.02	-180.2	0.4	-1.8
155	LD13-SP-8-19-1	22.04.2013	SP	0	1	-25.21	0.05	-183.1	0.2	18.6
156	LD13-SP-8-19-2	22.04.2013	SP	1	3	-24.30	0.04	-173.5	0.4	20.9
157	LD13-SP-8-19-3	22.04.2013	SP	3	5	-23.49	0.03	-166.2	0.2	21.8
158	LD13-SP-8-19-4	22.04.2013	SP	5	9	-22.89	0.03	-161.1	0.2	22.4
159	LD13-SP-8-18-1	22.04.2013	SP	0	3	-33.74	0.06	-263.4	0.2	6.5
160	LD13-SP-8-18-2	22.04.2013	SP	3	6	-35.29	0.04	-270.5	0.2	11.8
161	LD13-SP-8-18-3	22.04.2013	SP	6	9	-36.13	0.03	-275.5	0.3	13.5
162	LD13-SP-8-18-4	22.04.2013	SP	9	12	-35.68	0.02	-269.9	0.2	15.5
163	LD13-SP-8-18-5	22.04.2013	SP	12	15	-33.96	0.04	-254.1	0.2	17.6
164	LD13-SP-8-18-6	22.04.2013	SP	15	18	-33.61	0.03	-247.9	0.3	21.0
165	LD13-SP-8-18-7	22.04.2013	SP	18	31.5	-24.35	0.03	-178.9	0.3	15.9
166	LD13-SP-8-1-9	22.04.2013	SP	0	6	-32.55	0.04	-248.0	0.2	12.4
167	LD13-SP-8-1-10	22.04.2013	SP	6	9.5	-27.31	0.03	-199.5	0.3	19.0
168	LD13-SP-8-1-11	22.04.2013	SP	9.5	24	-23.15	0.03	-164.8	0.2	20.5
180	LD13-SP-13-1	23.04.2013	SP	0	1	-21.45	0.03	-155.9	0.2	15.7
181	LD13-SP-13-2	23.04.2013	SP	1	4	-26.51	0.01	-200.8	0.3	11.2
182	LD13-SP-13-3	23.04.2013	SP	4	7	-33.45	0.03	-260.4	0.3	7.2

Nr.	Sample	date	type	depth min (cm)	depth max (cm)	$d^{18}O$ (‰) vs. SMOW	1 s	δD (‰) vs. SMOW	1 s	d excess
183	LD13-SP-13-4	23.04.2013	SP	7	10	-37.52	0.04	-288.1	0.2	12.0
184	LD13-SP-13-5	23.04.2013	SP	10	13	-37.61	0.03	-288.5	0.2	12.4
185	LD13-SP-13-6	23.04.2013	SP	13	16	-38.19	0.03	-293.0	0.3	12.5
186	LD13-SP-13-7	23.04.2013	SP	16	19	-38.43	0.03	-294.4	0.3	13.1
187	LD13-SP-13-8	23.04.2013	SP	19	22	-31.96	0.03	-233.6	0.3	22.1
188	LD13-SP-13-9	23.04.2013	SP	22	25	-26.58	0.02	-196.6	0.3	16.0
189	LD13-SP-13-10	23.04.2013	SP	25	28	-25.29	0.01	-191.1	0.2	11.2
190	LD13-SP-13-11	23.04.2013	SP	28	31	-25.70	0.02	-193.9	0.3	11.7
191	LD13-SP-13-12	23.04.2013	SP	31	34	-25.52	0.03	-193.4	0.2	10.7
192	LD13-SP-13-13	23.04.2013	SP	34	37	-25.37	0.03	-192.1	0.4	10.9
193	LD13-SP-13-14	23.04.2013	SP	37	40	-25.24	0.02	-190.6	0.3	11.4
194	LD13-SP-13-15	23.04.2013	SP	40	43	-25.16	0.03	-190.8	0.2	10.5
195	LD13-SP-13-16	23.04.2013	SP	43	46	-25.00	0.03	-190.0	0.3	9.9
196	LD13-SP-13-17	23.04.2013	SP	46	49	-25.06	0.02	-190.4	0.3	10.2
197	LD13-SP-13-18	23.04.2013	SP	49	52	-25.20	0.02	-190.7	0.3	10.9
198	LD13-SP-13-19	23.04.2013	SP	52	55	-25.21	0.03	-190.7	0.4	11.0
199	LD13-SP-13-20	23.04.2013	SP	55	58	-25.15	0.02	-190.2	0.3	10.9
200	LD13-SP-13-21	23.04.2013	SP	58	61	-25.01	0.03	-188.9	0.5	11.1
201	LD13-SP-13-22	23.04.2013	SP	61	64	-25.00	0.07	-189.9	3.2	10.1
202	LD13-SP-13-23	23.04.2013	SP	64	67	-25.16	0.03	-189.2	0.3	12.0
203	LD13-SP-13-24	23.04.2013	SP	67	70	-25.30	0.04	-189.3	0.2	13.0
204	LD13-SP-13-25	23.04.2013	SP	70	73	-25.18	0.03	-191.0	0.3	10.4
205	LD13-SP-13-26	23.04.2013	SP	73	76	-25.10	0.04	-191.2	0.3	9.6
206	LD13-SP-13-27	23.04.2013	SP	76	79	-25.44	0.02	-192.2	0.4	11.2
207	LD13-SP-13-28	23.04.2013	SP	79	82	-25.70	0.01	-193.1	0.3	12.5
208	LD13-SP-13-29	23.04.2013	SP	82	85	-25.77	0.02	-194.8	0.2	11.4
209	LD13-SP-13-30	23.04.2013	SP	85	88	-25.05	0.07	-186.9	0.2	13.5
210	LD13-SP-13-31	23.04.2013	SP	88	91	-23.95	0.02	-177.8	0.3	13.8
211	LD13-SP-13-32	23.04.2013	SP	91	94	-26.45	0.02	-192.1	0.2	19.5
212	LD13-SP-13-33	23.04.2013	SP	94	97	-29.03	0.02	-215.8	0.3	16.4
213	LD13-SP-13-34	23.04.2013	SP	97	100	-28.73	0.05	-211.1	0.4	18.7
214	LD13-SP-13-35	23.04.2013	SP	100	103	-28.78	0.03	-215.2	0.3	15.1
215	LD13-SP-13-36	23.04.2013	SP	103	106	-28.80	0.02	-215.1	0.3	15.3
216	LD13-SP-13-37	23.04.2013	SP	106	109	-28.47	0.04	-212.3	0.3	15.4
217	LD13-SP-13-38	23.04.2013	SP	109	112	-28.22	0.04	-211.1	0.3	14.7
218	LD13-SP-13-39	23.04.2013	SP	112	115	-28.42	0.02	-210.6	0.3	16.7
219	LD13-SP-13-40	23.04.2013	SP	115	118	-28.71	0.05	-214.1	0.3	15.6
220	LD13-SP-13-41	23.04.2013	SP	118	121	-28.79	0.03	-214.7	0.2	15.6
221	LD13-SP-13-42	23.04.2013	SP	121	124	-28.98	0.03	-216.9	0.2	14.9
222	LD13-SP-13-43	23.04.2013	SP	124	127	-28.93	0.04	-214.7	0.2	16.8
223	LD13-SP-13-44	23.04.2013	SP	127	130	-27.95	0.02	-207.7	0.3	15.8
224	LD13-SP-13-45	23.04.2013	SP	130	133	-28.29	0.05	-207.7	0.4	18.6
225	LD13-SP-13-46	23.04.2013	SP	133	136	-30.25	0.03	-225.9	0.3	16.1
226	LD13-SP-13-47	23.04.2013	SP	136	139	-31.08	0.03	-231.7	0.1	16.9

Nr.	Sample	date	type	depth min (cm)	depth max (cm)	$d^{18}O$ (‰) vs. SMOW	1 s	δD (‰) vs. SMOW	1 s	d excess
227	LD13-SP-13-48	23.04.2013	SP	139	142	-27.72	0.02	-204.6	0.3	17.2
228	LD13-SP-13-49	23.04.2013	SP	142	145	-22.91	0.03	-165.3	0.4	18.0
229	LD13-SP-13-50	23.04.2013	SP	145	148	-18.84	0.04	-136.3	0.4	14.4
230	LD13-SP-13-51	23.04.2013	SP	148	151	-15.81	0.02	-112.1	0.3	14.4
231	LD13-SP-13-52	23.04.2013	SP	151	154	-15.72	0.02	-113.6	0.4	12.2
232	LD13-SP-13-53	23.04.2013	SP	154	157	-17.93	0.03	-133.7	0.2	9.9
233	LD13-SP-13-54	23.04.2013	SP	157	160	-21.72	0.03	-164.3	0.1	9.5
234	LD13-SP-13-55	23.04.2013	SP	160	163	-26.41	0.04	-202.0	0.3	9.1
235	LD13-SP-13-56	23.04.2013	SP	163	166	-28.73	0.04	-219.3	0.2	10.5
236	LD13-SP-13-57	23.04.2013	SP	166	169	-28.63	0.05	-213.4	0.3	15.6
237	LD13-SP-13-58	23.04.2013	SP	169	172	-26.95	0.05	-197.9	0.2	17.6
238	LD13-SP-13-59	23.04.2013	SP	172	175	-25.34	0.01	-187.7	0.3	14.5
239	LD13-SP-13-60	23.04.2013	SP	175	178	-23.87	0.02	-180.6	0.4	9.8
240	LD13-SP-13-61	23.04.2013	SP	178	181	-22.00	0.04	-165.3	0.2	18.5
250	LD13-SP-21-2-1	25.04.2013	SP	0	3	-27.33	0.02	-212.42	0.21	6.21
251	LD13-SP-21-2-2	25.04.2013	SP	3	6	-32.32	0.03	-242.78	0.45	15.75
252	LD13-SP-21-2-3	25.04.2013	SP	6	8	-32.81	0.03	-249.61	0.30	12.89
253	LD13-SP-21-2-4	25.04.2013	SP	8	11	-32.07	0.04	-244.17	0.25	12.38
254	LD13-SP-21-2-5	25.04.2013	SP	11	15	-25.62	0.04	-195.04	0.14	9.92
255	LD13-SP-21-2-6	25.04.2013	SP	0	15	-29.70	0.04	-226.1	0.2	11.5
256	LD13-SP-21-4-1	25.04.2013	SP	0	1	-20.72	0.04	-147.33	0.37	18.47
257	LD13-SP-21-4-2	25.04.2013	SP	1	4	-28.71	0.02	-221.23	0.11	8.49
258	LD13-SP-21-4-3	25.04.2013	SP	4	7	-28.30	0.03	-213.31	0.19	13.07
259	LD13-SP-21-4-4	25.04.2013	SP	7	10	-24.88	0.05	-184.96	0.13	14.12
260	LD13-SP-21-4-5	25.04.2013	SP	10	13	-23.80	0.02	-177.21	0.25	13.22
261	LD13-SP-21-4-6	25.04.2013	SP	13	16	-22.17	0.03	-165.30	0.32	12.06
262	LD13-SP-21-4-7	25.04.2013	SP	16	23	-16.05	0.05	-133.53	0.14	-5.10
263	LD13-SP-21-4-8	25.04.2013	SP	0	23	-24.90	0.05	-189.4	0.4	9.8
264	LD13-SP-21-5-1	25.04.2013	SP	0	2	-25.12	0.03	-191.71	0.13	9.24
265	LD13-SP-21-5-2	25.04.2013	SP	2	5	-27.47	0.05	-204.13	0.32	15.66
266	LD13-SP-21-5-3	25.04.2013	SP	5	9	-25.33	0.04	-178.17	0.54	24.50
267	LD13-SP-21-5-4	25.04.2013	SP	9	13	-23.93	0.07	-166.35	0.33	25.10
268	LD13-SP-21-5-5	25.04.2013	SP	0	13	-25.33	0.03	-182.6	0.5	20.0
269	LD13-SP-21-7-1	25.04.2013	SP	0	3	-27.27	0.03	-208.00	0.38	10.14
270	LD13-SP-21-7-2	25.04.2013	SP	3	6	-29.07	0.06	-217.31	0.28	15.23
271	LD13-SP-21-7-3	25.04.2013	SP	6	11	-27.45	0.04	-200.80	0.18	18.82
272	LD13-SP-21-7-4	25.04.2013	SP	11	18	-24.23	0.03	-171.48	0.38	22.37
273	LD13-SP-21-7-5	25.04.2013	SP	0	18	-27.58	0.03	-205.1	0.3	15.6
274	LD13-SP-21-10-1	25.04.2013	SP	0	1	-22.55	0.04	-166.22	0.24	14.16
275	LD13-SP-21-10-2	25.04.2013	SP	1	4	-30.52	0.06	-234.38	0.22	9.81
276	LD13-SP-21-10-3	25.04.2013	SP	4	7	-33.34	0.04	-256.33	0.27	10.37
277	LD13-SP-21-10-4	25.04.2013	SP	7	10	-32.81	0.03	-246.67	0.23	15.83
278	LD13-SP-21-10-5	25.04.2013	SP	10	14	-25.52	0.05	-188.71	0.23	15.48
279	LD13-SP-21-10-6	25.04.2013	SP	14	18	-16.77	0.05	-147.29	0.35	-13.16

Nr.	Sample	date	type	depth min (cm)	depth max (cm)	$d^{18}O$ (‰) vs. SMOW	1 s	δD (‰) vs. SMOW	1 s	d excess
280	LD13-SP-21-10-7	25.04.2013	SP	0	18	-28.74	0.05	-225.3	0.2	4.7
416	LD13-BH-6-1	29.04.2013	LI	0	6	-24.82	0.03	-191.63	0.21	6.97
417	LD13-BH-6-2	29.04.2013	LI	6	13	-12.23	0.04	-104.14	0.20	-6.31
418	LD13-BH-6-3	29.04.2013	LI	13	19	-12.00	0.05	-102.07	0.31	-6.06
419	LD13-BH-6-4	29.04.2013	LI	19	25	-12.20	0.04	-103.62	0.22	-6.03
420	LD13-BH-6-5	29.04.2013	LI	25	31	-12.19	0.05	-103.60	0.31	-6.09
421	LD13-BH-6-6	29.04.2013	LI	31	38	-12.47	0.04	-105.49	0.31	-5.72
422	LD13-BH-6-7	29.04.2013	LI	38	46	-12.85	0.03	-107.86	0.29	-5.06
423	LD13-BH-6-8	29.04.2013	LI	46	52	-13.28	0.03	-110.72	0.30	-4.44
424	LD13-BH-6-9	29.04.2013	LI	52	58	-14.06	0.05	-115.65	0.26	-3.19
425	LD13-BH-6-10	29.04.2013	LI	58	64	-14.72	0.05	-120.25	0.30	-2.46
426	LD13-BH-6-11	29.04.2013	LI	64	70	-15.13	0.03	-123.04	0.28	-1.98
427	LD13-SP-47-1-1	30.04.2013	SP	0	1	-21.52	0.04	-157.88	0.24	14.30
428	LD13-SP-47-1-2	30.04.2013	SP	1	2.5	-20.37	0.03	-144.85	0.35	18.14
429	LD13-SP-47-1-3	30.04.2013	SP	2.5	5.5	-19.58	0.05	-138.01	0.31	18.61
430	LD13-SP-47-1-4	30.04.2013	SP	5.5	8	-20.04	0.04	-138.84	0.18	21.48
431	LD13-SP-47-1-5	30.04.2013	SP	8	12	-22.62	0.05	-162.47	0.20	18.52
432	LD13-SP-47-2-1	30.04.2013	SP	0	1	-19.93	0.04	-147.57	0.34	11.85
433	LD13-SP-47-2-2	30.04.2013	SP	1	2	-19.38	0.06	-140.12	0.32	14.89
434	LD13-SP-47-2-3	30.04.2013	SP	2	5	-19.57	0.05	-137.80	0.26	18.79
435	LD13-SP-47-2-4	30.04.2013	SP	5	9	-19.82	0.04	-137.37	0.41	21.15
436	LD13-SP-47-2-5	30.04.2013	SP	9	14	-19.75	0.03	-138.36	0.24	19.66
437	LD13-SP-47-4-1	30.04.2013	SP	0	3	-30.33	0.02	-231.40	0.25	11.22
438	LD13-SP-47-4-2	30.04.2013	SP	3	6	-30.62	0.05	-231.23	0.13	13.73
439	LD13-SP-47-4-3	30.04.2013	SP	6	9	-35.08	0.07	-265.94	0.23	14.69
440	LD13-SP-47-4-4	30.04.2013	SP	9	12	-35.04	0.03	-264.19	0.27	16.14
441	LD13-SP-47-4-5	30.04.2013	SP	12	15	-34.51	0.04	-258.06	0.22	18.01
442	LD13-SP-47-4-6	30.04.2013	SP	15	18	-33.28	0.03	-247.62	0.23	18.63
443	LD13-SP-47-4-7	30.04.2013	SP	18	21	-29.33	0.03	-216.95	0.20	17.68
444	LD13-SP-47-4-8	30.04.2013	SP	21	24	-28.72	0.01	-209.23	0.35	20.54
445	LD13-SP-47-4-9	30.04.2013	SP	24	27	-27.57	0.04	-198.99	0.13	21.59
446	LD13-SP-47-4-10	30.04.2013	SP	27	30	-26.76	0.04	-198.02	0.49	16.06
447	LD13-SP-47-4-11	30.04.2013	SP	30	35	-22.90	0.04	-174.54	0.15	8.64
448	LD13-SP-47-4-12	30.04.2013	SP	35	43	-13.70	0.03	-127.71	0.27	-18.15
449	LD13-SP-47-4-13	30.04.2013	SP	38	39	-31.58	0.02	-237.71	0.22	14.91
450	LD13-SP-47-4-14	30.04.2013	SP	20	22	-28.61	0.03	-210.69	0.21	18.17
451	LD13-SP-47-8-1	30.04.2013	SP	0	4.5	-26.30	0.03	-196.21	0.40	14.23
452	LD13-SP-47-8-2	30.04.2013	SP	4.5	7.5	-33.90	0.05	-256.18	0.20	15.02
453	LD13-SP-47-8-3	30.04.2013	SP	7.5	10.5	-36.01	0.01	-270.93	0.18	17.15
454	LD13-SP-47-8-4	30.04.2013	SP	10.5	13.5	-35.92	0.03	-269.24	0.28	18.16
455	LD13-SP-47-8-5	30.04.2013	SP	13.5	16.5	-32.76	0.03	-244.06	0.24	18.01
456	LD13-SP-47-8-6	30.04.2013	SP	16.5	19.5	-28.49	0.02	-214.41	0.15	13.53
457	LD13-SP-47-8-7	30.04.2013	SP	19.5	23.5	-22.64	0.03	-183.83	0.31	-2.46
458	LD13-SP-47-8-8	30.04.2013	SP	16.5	17.5	-30.10	0.05	-226.84	0.17	13.94

Nr.	Sample	date	type	depth min (cm)	depth max (cm)	$d^{18}O$ (‰) vs. SMOW	1 s	δD (‰) vs. SMOW	1 s	d excess
459	LD13-SP-47-18-1	30.04.2013	SP	0	3.5	-20.47	0.02	-144.90	0.14	18.85
460	LD13-SP-47-18-2	30.04.2013	SP	3.5	7	-19.92	0.04	-140.30	0.23	19.08
461	LD13-SP-47-18-3	30.04.2013	SP	7	10.5	-22.90	0.03	-167.81	0.22	15.37
462	LD13-SP-47-18-4	30.04.2013	SP	10.5	14	-34.16	0.02	-262.81	0.15	10.45
463	LD13-SP-47-18-5	30.04.2013	SP	14	17.5	-33.18	0.04	-251.03	0.26	14.39
464	LD13-SP-47-18-6	30.04.2013	SP	17.5	21	-34.22	0.03	-256.53	0.19	17.24
465	LD13-SP-47-18-7	30.04.2013	SP	21	25	-34.00	0.03	-252.57	0.14	19.41
466	LD13-SP-47-18-8	30.04.2013	SP	25	30	-27.87	0.03	-197.55	0.27	25.30
467	LD13-SP-47-18-9	30.04.2013	SP	30	40	-25.66	0.05	-189.80	0.13	14.99
468	LD13-SP-47-18-10	30.04.2013	SP	17	19	-30.52	0.02	-228.58	0.26	15.59
469	LD13-SP-47-20-1	30.04.2013	SP	0	3	-20.40	0.03	-148.09	0.26	15.13
470	LD13-SP-47-20-2	30.04.2013	SP	3	5	-27.93	0.03	-209.47	0.13	14.00
471	LD13-SP-47-20-3	30.04.2013	SP	5	7.5	-31.34	0.01	-234.60	0.40	16.14
472	LD13-SP-47-20-4	30.04.2013	SP	7.5	9.5	-28.65	0.05	-206.04	0.25	23.02
473	LD13-SP-47-20-5	30.04.2013	SP	9.5	15.5	-25.18	0.03	-174.34	0.31	26.75
517	LD13-SP-58-1-1	03.05.2013	SP	0	6.5	-20.02	0.05	-143.62	0.32	16.52
518	LD13-SP-58-1-2	03.05.2013	SP			-21.07	0.06	-152.07	0.25	16.48
519	LD13-SP-58-2-1	03.05.2013	SP	0	5	-20.40	0.05	-147.85	0.25	15.34
520	LD13-SP-58-2-2	03.05.2013	SP			-20.38	0.06	-146.78	0.20	16.30
521	LD13-SP-58-3	02.05.2013	SP	0	15	-23.28	0.03	-172.1	0.4	14.2
522	LD13-SP-58-4-1	03.05.2013	SP	28	31	-33.44	0.03	-252.82	0.22	14.68
523	LD13-SP-58-4-2	03.05.2013	SP	25	28	-29.30	0.05	-221.05	0.33	13.33
524	LD13-SP-58-4-3	03.05.2013	SP	21	25	-28.72	0.03	-217.00	0.31	12.80
525	LD13-SP-58-4-4	03.05.2013	SP	17	21	-27.03	0.03	-204.98	0.24	11.24
526	LD13-SP-58-4-5	03.05.2013	SP	13	17	-30.11	0.02	-221.70	0.18	19.18
527	LD13-SP-58-4-6	03.05.2013	SP	0	13	-22.22	0.07	-163.29	0.24	14.50
528	LD13-SP-58-4-7	03.05.2013	SP	bottom		-24.54	0.04	-188.75	0.37	7.58
529	LD13-SP-58-4-8	03.05.2013	SP	31	32	-31.03	0.05	-237.73	0.27	10.48
530	LD13-SP-58-4-9	02.05.2013	SP	0	35	-29.22	0.03	-219.7	0.3	14.1
531	LD13-SP-58-8-1	03.05.2013	SP	7	10	-33.13	0.04	-253.30	0.28	11.74
532	LD13-SP-58-8-2	03.05.2013	SP	4	7	-33.46	0.06	-255.77	0.34	11.91
533	LD13-SP-58-8-3	03.05.2013	SP	1	4	-29.48	0.04	-223.53	0.32	12.29
534	LD13-SP-58-8-4	03.05.2013	SP	-2	1	-26.83	0.03	-202.78	0.20	11.83
535	LD13-SP-58-8-5	03.05.2013	SP			-29.07	0.04	-216.72	0.17	15.86
536	LD13-SP-58-10	02.05.2013	SP	0	18	-28.36	0.02	-215.0	0.3	11.8
537	LD13-SP-58-18-1	03.05.2013	SP	28	29	-27.11	0.03	-203.8	0.2	13.1
538	LD13-SP-58-18-2	03.05.2013	SP	25	28	-29.93	0.02	-222.80	0.21	16.62
539	LD13-SP-58-18-3	03.05.2013	SP	22	25	-33.50	0.02	-251.70	0.47	16.32
540	LD13-SP-58-18-4	03.05.2013	SP	19	22	-34.91	0.03	-262.94	0.17	16.36
541	LD13-SP-58-18-5	03.05.2013	SP	16	19	-35.35	0.02	-267.15	0.16	15.63
542	LD13-SP-58-18-6	03.05.2013	SP	13	16	-30.70	0.03	-227.57	0.42	18.01
543	LD13-SP-58-18-7	03.05.2013	SP	9	13	-26.65	0.02	-187.40	0.24	25.80
544	LD13-SP-58-18-8	03.05.2013	SP	0	9	-26.60	0.03	-201.14	0.15	11.63
545	LD13-SP-58-18-9	03.05.2013	SP	-2	0	-24.32	0.13	-184.61	0.36	9.95

Nr.	Sample	date	type	depth min (cm)	depth max (cm)	$d^{18}O$ (‰) vs. SMOW	1 s	δD (‰) vs. SMOW	1 s	d excess
546	LD13-FCW-1	03.05.2013	FCW			-25.69	0.02	-191.8	0.4	13.8
547	LD13-FCW-2	04.05.2013	FCW			-26.49	0.03	-193.7	0.5	18.2
548	LD13-FCW-3	04.05.2013	FCW			-26.07	0.02	-194.3	0.3	14.3
549	LD13-FCW-4	04.05.2013	FCW			-24.49	0.03	-180.3	0.2	15.6
550	LD13-FCW-5	04.05.2013	FCW			-24.64	0.02	-181.0	0.3	16.1
551	LD13-FCW-6	04.05.2013	FCW			-24.42	0.03	-181.0	0.3	14.4
552	LD13-FCW-7	04.05.2013	FCW			-23.92	0.00	-177.4	0.4	14.0
553	LD13-FCW-8	04.05.2013	FCW			-24.35	0.02	-180.5	0.3	14.3
554	LD13-FCW-9	04.05.2013	FCW			-24.66	0.03	-183.6	0.3	13.7
555	LD13-FCW-10	04.05.2013	FCW			-22.21	0.03	-162.6	0.4	15.0
556	LD13-FCW-11	04.05.2013	FCW			-22.29	0.02	-165.4	0.4	12.9
557	LD13-FCW-12	04.05.2013	FCW			-26.04	0.03	-192.7	0.4	15.6
558	LD13-FCW-13	04.05.2013	FCW			-27.27	0.01	-201.8	0.2	16.4
559	LD13-FCW-14	04.05.2013	FCW			-25.44	0.03	-183.7	0.4	19.8
560	LD13-FCS-1	04.05.2013	FCS			-25.52	0.01	-192.6	0.5	11.6
561	LD13-FCS-2	04.05.2013	FCS			-25.63	0.04	-193.9	0.4	11.2
562	LD13-FCS-3	04.05.2013	FCS			-26.83	0.01	-204.9	0.2	9.7
563	LD13-FCS-4	04.05.2013	FCS			-27.13	0.02	-206.7	0.4	10.3
564	LD13-FCS-5	04.05.2013	FCS			-25.76	0.02	-191.2	0.4	14.8
565	LD13-FCS-6	04.05.2013	FCS			-25.69	0.01	-191.6	0.4	14.0
566	LD13-FCS-7	04.05.2013	FCS			-29.19	0.02	-213.7	0.2	19.8
567	LD13-FCD-1	04.05.2013	FCD			-24.02	0.05	-174.20	0.40	18.00
568	LD13-FCD-2	04.05.2013	FCD			-25.15	0.04	-178.90	0.20	22.30
569	LD13-FCD-3	04.05.2013	FCD			-23.38	0.05	-172.10	0.20	15.00
570	LD13-FCD-4	04.05.2013	FCD			-24.97	0.04	-179.80	0.20	20.00
571	LD13-FCD-5	04.05.2013	FCD			-22.97	0.05	-164.40	0.30	19.40
572	LD13-FCD-6	04.05.2013	FCD			-23.90	0.01	-178.80	0.20	12.50
573	LD13-FCD-7	04.05.2013	FCD			-26.43	0.03	-190.00	0.40	21.40
574	LD13-FCD-8	04.05.2013	FCD			-23.59	0.02	-174.20	0.20	14.50
575	LD13-FCC-1	04.05.2013	FCC			-26.76	0.03	-205.8	0.4	8.3
576	LD13-FCI-1	04.05.2013	FCI			-25.38	0.03	-189.2	0.4	13.8
577	LD13-FCI-2	04.05.2013	FCI			-24.21	0.04	-180.3	0.3	13.4
578	LD13-FCI-3	04.05.2013	FCI			-23.62	0.05	-174.9	0.1	14.1
580	LD13-FCI-5	05.05.2013	FCI			-20.27	0.04	-146.7	0.3	15.4
582	LD13-FCI-7	05.05.2013	FCI			-25.01	0.06	-186.3	0.2	13.8
583	LD13-FCS-8	05.05.2013	FCS			-24.81	0.02	-185.3	0.4	13.1
604	LD13-FCW-15	06.05.2013	FCW			-25.17	0.03	-186.7	0.3	14.6
605	LD13-FCW-16	06.05.2013	FCW			-24.31	0.02	-180.4	0.1	14.1
606	LD13-FCW-17	06.05.2013	FCW			-23.72	0.03	-177.3	0.3	12.5
607	LD13-FCW-18	06.05.2013	FCW			-23.81	0.00	-176.9	0.3	13.6
608	LD13-FCW-19	06.05.2013	FCW			-25.23	0.02	-186.0	0.4	15.8
609	LD13-FCS-9	06.05.2013	FCS			-24.79	0.02	-183.1	0.2	15.2
610	LD13-FCD-9	06.05.2013	FCD			-23.92	0.04	-175.50	0.30	15.90

App. 2 $\delta^{18}O$ depth profiles for different sample sites at different ice-wedge polygons

Snow profile LD13-SP7

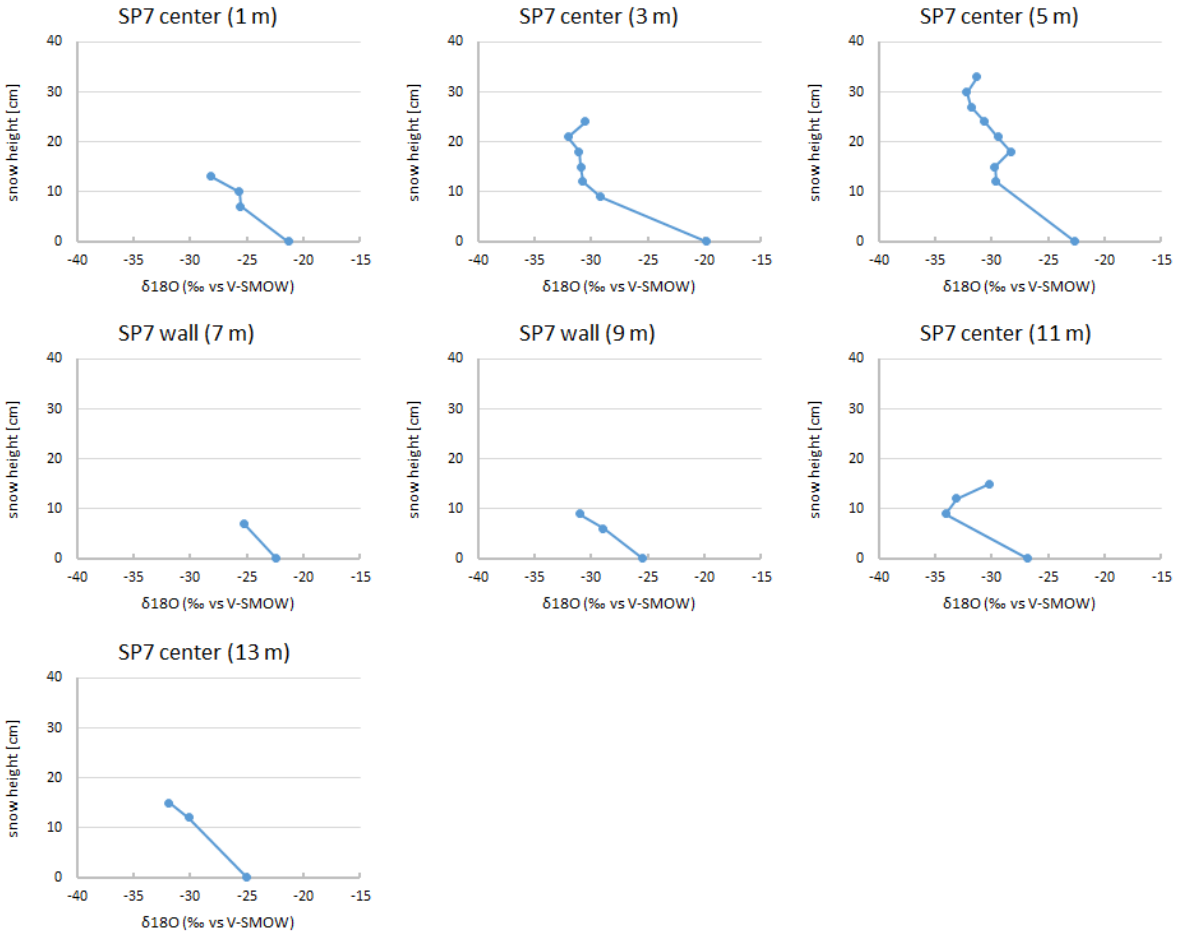

Snow profile LD13-SP8

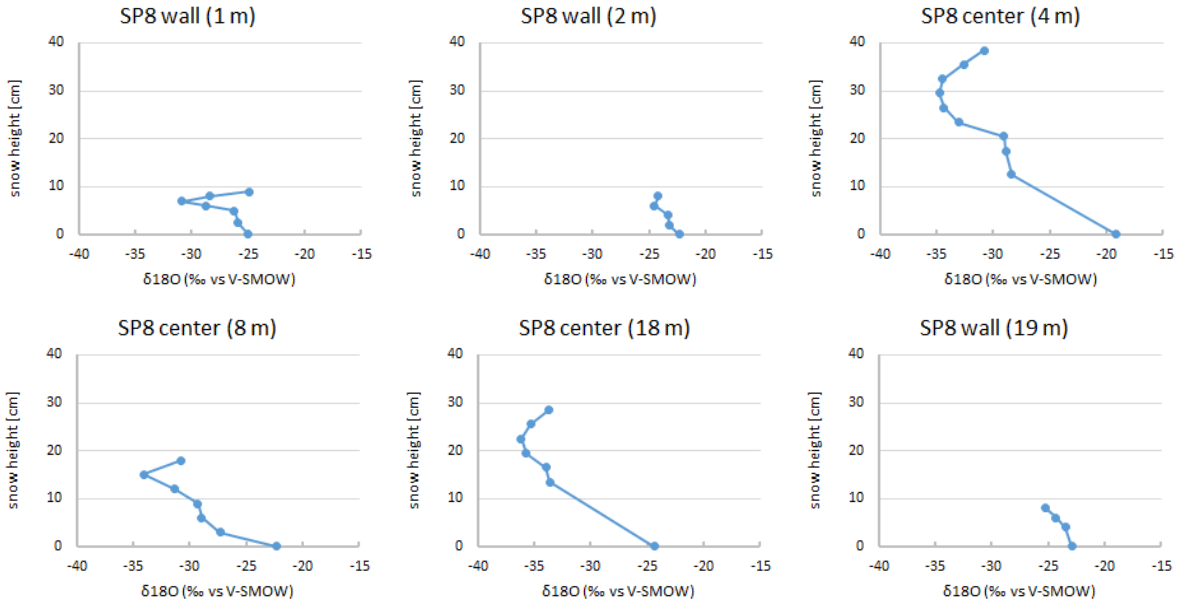

Snow profile LD13-SP21

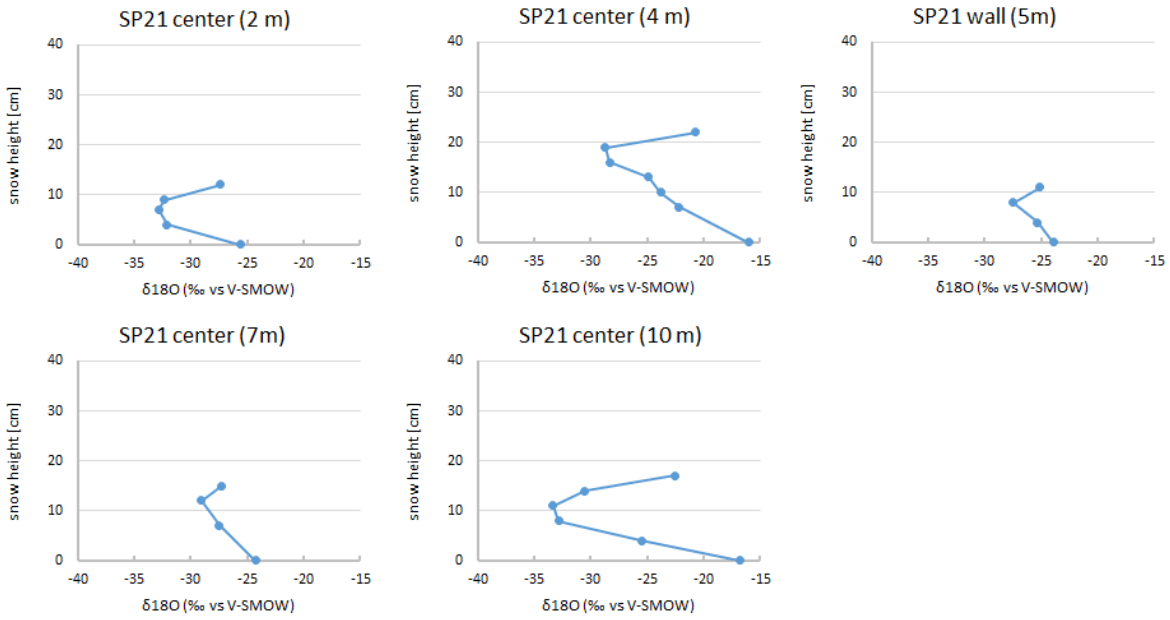

App. 3 Weather data from Samoylov Island for 2012 and 2013 (Source: Samoylov Island weather Station)

Date	Temp_Avg (2 m)	Temp_Min (2 m)	Temp_Max (2 m)	Wind speed (mean)	Wind dir (mean)	Rain_Tot	Snow height
	Deg C	Deg C	Deg C	m/s	m/s	Counts	m
01.01.2012	-20.55	-23.17	-18.35	4.25	197	0.00	0.071
02.01.2012	-24.78	-28.18	-21.36	3.42	215	0.00	0.082
03.01.2012	-27.30	-32.13	-23.95	3.92	188	0.00	0.084
04.01.2012	-30.13	-32.21	-27.30	4.83	153	0.00	0.076
05.01.2012	-33.27	-36.33	-27.18	1.90	331	0.00	0.066
06.01.2012	-37.12	-38.65	-35.54	1.07	265	0.00	0.065
07.01.2012	-35.56	-36.64	-34.57	1.51	174	0.00	0.060
08.01.2012	-35.70	-36.44	-34.88	2.07	173	0.00	0.056
09.01.2012	-32.57	-34.77	-31.56	6.67	169	0.00	0.061
10.01.2012	-30.61	-32.14	-28.46	8.50	175	0.00	0.090
11.01.2012	-31.65	-33.52	-30.56	4.80	211	0.00	0.097
12.01.2012	-34.90	-35.75	-33.34	2.59	212	0.00	0.094
13.01.2012	-37.38	-39.59	-35.58	1.93	148	0.00	0.091
14.01.2012	-37.96	-39.71	-35.69	2.16	354	0.00	0.092
15.01.2012	-36.88	-37.58	-35.38	1.14	307	0.00	0.090
16.01.2012	-32.20	-37.58	-27.68	1.80	108	0.00	0.094
17.01.2012	-33.54	-36.62	-30.72	2.45	309	0.00	0.093
18.01.2012	-22.74	-30.29	-18.56	4.72	351	0.00	0.102
19.01.2012	-29.05	-30.55	-24.59	10.06	193	0.00	0.097
20.01.2012	-27.76	-29.55	-26.36	7.69	193	0.00	0.098
21.01.2012	-30.92	-31.61	-29.71	6.59	165	0.00	0.097
22.01.2012	-28.68	-31.46	-27.18	4.59	177	0.00	0.099
23.01.2012	-29.70	-31.25	-27.38	6.26	191	0.00	0.098
24.01.2012	-33.07	-35.62	-29.86	3.13	163	0.00	0.095

Date	Temp_Avg (2 m)	Temp_Min (2 m)	Temp_Max (2 m)	Wind speed (mean)	Wind dir (mean)	Rain_Tot	Snow height
	Deg C	Deg C	Deg C	m/s	m/s	Counts	m
25.01.2012	-34.92	-36.17	-33.99	1.45	189	0.00	0.096
26.01.2012	-35.72	-36.63	-34.13	1.75	158	0.00	0.094
27.01.2012	-35.71	-36.86	-34.65	1.71	156	0.00	0.092
28.01.2012	-32.04	-36.97	-26.79	1.77	178	0.00	0.096
29.01.2012	-27.22	-32.23	-21.83	3.42	230	0.00	0.101
30.01.2012	-17.85	-22.22	-15.46	9.19	262	0.00	0.104
31.01.2012	-14.82	-17.66	-13.58	7.04	232	0.00	0.117
01.02.2012	-13.69	-14.83	-12.34	6.84	263	0.00	0.126
02.02.2012	-18.22	-26.07	-14.60	5.29	252	0.00	0.102
03.02.2012	-26.19	-31.53	-21.60	3.00	77	0.00	0.096
04.02.2012	-25.86	-30.92	-23.01	3.50	283	0.00	0.098
05.02.2012	-21.32	-27.20	-16.47	4.97	186	0.00	0.119
06.02.2012	-22.61	-27.62	-18.58	5.82	185	0.00	0.115
07.02.2012	-33.99	-39.68	-28.36	3.09	35	0.00	0.092
08.02.2012	-33.50	-39.72	-28.16	4.55	300	0.00	0.093
09.02.2012	-22.97	-27.45	-20.75	7.24	284	0.00	0.103
10.02.2012	-23.88	-25.21	-22.48	7.05	230	0.00	0.101
11.02.2012	-24.73	-26.35	-22.97	8.38	186	0.00	0.100
12.02.2012	-24.56	-26.86	-23.36	7.16	178	0.00	0.100
13.02.2012	-25.17	-27.01	-23.35	5.16	180	0.00	0.101
14.02.2012	-25.99	-27.59	-24.49	6.16	175	0.00	0.100
15.02.2012	-16.71	-25.63	-13.83	7.76	243	0.00	0.109
16.02.2012	-18.93	-25.21	-14.76	5.19	279	0.00	0.103
17.02.2012	-24.25	-25.97	-21.74	3.66	273	0.00	0.099
18.02.2012	-28.16	-33.14	-25.20	2.88	265	0.00	0.096
19.02.2012	-32.40	-33.73	-30.41	3.26	160	0.00	0.095
20.02.2012	-33.94	-35.01	-32.53	4.42	147	0.00	0.094
21.02.2012	-35.27	-37.06	-33.14	2.03	106	0.00	0.093
22.02.2012	-34.30	-36.11	-31.25	1.61	86	0.00	0.094
23.02.2012	-33.36	-35.36	-31.60	1.50	90	0.00	0.096
24.02.2012	-33.62	-36.09	-30.40	3.19	92	0.00	0.095
25.02.2012	-38.05	-39.73	-34.99	2.28	125	0.00	0.091
26.02.2012	-38.38	-39.66	-37.11	3.01	138	0.00	0.092
27.02.2012	-38.98	-39.73	-37.03	0.69	86	0.00	0.089
28.02.2012	-39.22	-39.73	-38.13	0.42	76	0.00	0.089
29.02.2012	-39.05	-39.73	-38.29	0.22	69	0.00	0.089
01.03.2012	-36.77	-39.36	-35.06	0.19	79	0.00	0.092
02.03.2012	-35.27	-37.93	-31.39	0.31	74	0.00	0.091
03.03.2012	-35.85	-37.57	-33.80	2.66	146	0.00	0.091
04.03.2012	-37.14	-38.89	-34.70	1.00	93	0.00	0.088
05.03.2012	-36.63	-38.73	-34.25	3.35	179	0.00	0.089
06.03.2012	-27.76	-33.96	-25.20	6.35	178	0.00	0.102
07.03.2012	-21.73	-25.93	-18.57	8.89	225	0.00	0.104

Date	Temp_Avg (2 m)	Temp_Min (2 m)	Temp_Max (2 m)	Wind speed (mean)	Wind dir (mean)	Rain_Tot	Snow height
	Deg C	Deg C	Deg C	m/s	m/s	Counts	m
08.03.2012	-19.33	-22.63	-17.24	7.16	292	0.00	0.103
09.03.2012	-29.24	-33.46	-23.47	7.07	332	0.00	0.095
10.03.2012	-33.53	-37.40	-28.85	3.36	6	0.00	0.094
11.03.2012	-33.33	-39.23	-28.16	2.75	332	0.00	0.095
12.03.2012	-37.70	-39.39	-34.32	0.76	35	0.00	0.090
13.03.2012	-38.37	-39.73	-34.52	0.74	322	0.00	0.089
14.03.2012	-38.66	-39.73	-34.24	0.38	198	0.00	0.087
15.03.2012	-38.39	-39.73	-33.70	NaN	NaN	0.00	0.087
16.03.2012	-33.16	-38.99	-30.13	7.41	165	0.00	0.098
17.03.2012	-30.66	-33.67	-27.24	4.11	158	0.00	0.097
18.03.2012	-28.77	-33.05	-25.85	4.89	165	0.00	0.099
19.03.2012	-23.10	-25.56	-21.43	6.77	160	0.00	0.103
20.03.2012	-22.10	-29.37	-16.64	3.28	102	0.00	0.101
21.03.2012	-29.40	-33.75	-22.94	2.04	35	0.00	0.093
22.03.2012	-29.42	-32.92	-25.04	3.43	335	0.00	0.097
23.03.2012	-29.51	-35.82	-24.17	1.94	11	0.00	0.100
24.03.2012	-29.17	-33.86	-26.53	3.68	166	0.00	0.102
25.03.2012	-27.16	-31.86	-23.24	3.21	93	0.00	0.122
26.03.2012	-28.98	-31.48	-27.29	3.60	78	0.00	0.124
27.03.2012	-27.60	-29.59	-25.09	4.52	70	0.00	0.122
28.03.2012	-29.30	-35.43	-24.69	3.51	30	0.00	0.114
29.03.2012	-30.53	-33.86	-25.63	1.72	232	0.00	0.112
30.03.2012	-26.50	-31.95	-24.01	2.73	139	0.00	0.116
31.03.2012	-23.98	-28.57	-19.77	3.17	144	0.00	0.116
01.04.2012	-19.79	-25.84	-15.59	1.72	96	0.00	0.119
02.04.2012	-21.10	-28.08	-14.91	3.79	66	0.00	0.112
03.04.2012	-23.94	-27.13	-21.14	2.88	59	0.00	0.110
04.04.2012	-19.89	-24.37	-14.23	4.45	124	0.00	0.105
05.04.2012	-17.96	-23.57	-12.50	4.42	147	0.00	0.104
06.04.2012	-19.48	-24.33	-14.16	2.66	140	0.00	0.100
07.04.2012	-18.43	-21.26	-14.16	3.33	92	0.00	0.102
08.04.2012	-21.01	-25.43	-17.63	3.99	55	0.00	0.101
09.04.2012	-21.26	-26.05	-15.93	2.16	310	0.00	0.103
10.04.2012	-25.50	-30.19	-19.48	1.32	318	0.00	0.097
11.04.2012	-25.86	-29.34	-22.83	1.28	262	0.00	0.089
12.04.2012	-20.78	-24.79	-12.96	1.93	47	0.00	0.097
13.04.2012	-20.06	-23.41	-16.85	3.67	321	0.00	0.121
14.04.2012	-18.80	-24.63	-14.17	2.41	209	0.00	0.164
15.04.2012	-18.04	-23.95	-10.67	2.38	62	0.00	0.163
16.04.2012	-18.25	-21.37	-15.52	2.75	339	0.00	0.159
17.04.2012	-15.20	-20.56	-9.79	5.73	323	0.00	0.157
18.04.2012	-18.55	-21.38	-16.11	4.91	269	0.00	0.104
19.04.2012	-20.60	-27.14	-15.80	2.87	224	0.00	0.098

Date	Temp_Avg (2 m)	Temp_Min (2 m)	Temp_Max (2 m)	Wind speed (mean)	Wind dir (mean)	Rain_Tot	Snow height
	Deg C	Deg C	Deg C	m/s	m/s	Counts	m
20.04.2012	-19.36	-24.27	-14.64	1.86	104	0.00	0.100
21.04.2012	-15.40	-18.35	-13.19	5.58	82	0.00	0.108
22.04.2012	-12.90	-15.42	-11.10	5.46	99	0.00	0.131
23.04.2012	-16.13	-21.13	-11.04	3.69	103	0.00	0.165
24.04.2012	-14.20	-15.72	-12.72	5.37	96	0.00	0.165
25.04.2012	-16.13	-19.37	-14.01	5.55	74	0.00	0.155
26.04.2012	-15.24	-17.13	-14.58	4.57	67	0.00	0.157
27.04.2012	-14.54	-17.67	-12.21	3.16	33	0.00	0.152
28.04.2012	-17.88	-23.09	-14.31	3.31	22	0.00	0.162
29.04.2012	-21.49	-28.76	-15.42	2.58	7	0.00	0.159
30.04.2012	-21.80	-27.78	-17.68	2.63	23	0.00	0.152
01.05.2012	-20.86	-24.51	-18.82	3.69	62	0.00	0.152
02.05.2012	-20.42	-25.41	-16.92	3.52	70	0.00	0.152
03.05.2012	-18.13	-22.74	-14.40	3.47	111	0.00	0.153
04.05.2012	-4.62	-13.58	-0.75	6.04	163	0.00	0.170
05.05.2012	1.85	-1.08	3.09	7.85	181	0.00	0.161
06.05.2012	3.98	2.36	5.71	5.83	201	0.00	0.114
07.05.2012	2.34	-2.48	4.87	4.14	218	0.00	0.044
08.05.2012	-4.92	-7.38	-2.93	4.14	317	0.00	0.035
09.05.2012	-7.28	-8.23	-5.62	5.02	26	0.00	0.038
10.05.2012	-6.48	-7.29	-5.99	5.65	81	0.00	0.055
11.05.2012	-7.33	-10.41	-5.41	5.21	54	0.00	0.053
12.05.2012	-7.46	-10.69	-5.03	2.69	95	0.00	0.050
13.05.2012	-3.26	-4.92	-1.20	6.70	123	0.00	0.056
14.05.2012	-4.12	-8.03	-0.50	8.50	111	0.00	0.051
15.05.2012	-5.21	-6.69	-3.92	11.13	86	0.00	0.058
16.05.2012	-5.67	-6.82	-4.72	6.16	5	0.00	0.066
17.05.2012	-6.12	-7.41	-5.07	4.46	272	0.00	0.066
18.05.2012	-4.92	-5.62	-4.23	2.21	92	0.00	0.065
19.05.2012	-5.47	-8.26	-1.69	2.90	185	0.00	0.072
20.05.2012	-4.17	-8.76	0.94	1.44	271	0.00	0.076
21.05.2012	-4.73	-6.47	-3.18	3.69	168	0.00	0.077
22.05.2012	-0.78	-3.99	0.63	4.30	152	0.00	0.086
23.05.2012	1.73	0.02	3.32	2.22	133	0.00	0.060
24.05.2012	3.69	1.51	5.60	2.92	124	0.00	0.064
25.05.2012	5.87	3.13	9.33	5.21	154	0.00	0.058
26.05.2012	6.03	1.95	11.08	5.64	194	0.00	0.042
27.05.2012	3.41	1.33	5.78	3.38	186	0.00	0.025
28.05.2012	3.94	-0.30	7.88	3.75	207	0.00	0.014
29.05.2012	4.71	0.91	6.56	5.57	241	0.00	0.006
30.05.2012	7.87	3.10	11.54	3.17	195	0.00	-0.004
31.05.2012	8.26	1.17	15.81	4.34	279	0.00	-0.013
01.06.2012	3.33	0.17	4.85	6.54	288	0.00	-0.012

Date	Temp_Avg (2 m)	Temp_Min (2 m)	Temp_Max (2 m)	Wind speed (mean)	Wind dir (mean)	Rain_Tot	Snow height
	Deg C	Deg C	Deg C	m/s	m/s	Counts	m
02.06.2012	0.50	-0.44	1.55	8.70	311	0.00	-0.009
03.06.2012	1.14	-0.08	2.02	5.00	327	0.00	-0.009
04.06.2012	2.61	1.13	4.31	3.58	58	0.00	-0.012
05.06.2012	1.40	-0.72	3.46	6.13	65	0.00	-0.011
06.06.2012	1.25	0.47	2.56	4.23	327	0.00	-0.010
07.06.2012	5.30	2.82	7.07	4.91	171	0.00	-0.012
08.06.2012	5.34	2.68	7.32	5.07	227	0.00	-0.009
09.06.2012	8.13	5.00	9.92	3.88	85	0.00	-0.009
10.06.2012	12.10	9.69	15.84	3.12	129	0.00	-0.007
11.06.2012	12.93	9.27	17.68	3.26	55	0.00	-0.009
12.06.2012	11.24	8.87	14.22	4.83	71	0.00	-0.009
13.06.2012	15.98	12.11	19.98	2.74	110	0.00	-0.012
14.06.2012	18.46	14.07	21.81	2.00	86	0.00	-0.014
15.06.2012	9.62	2.45	24.42	4.91	39	0.00	-0.011
16.06.2012	5.69	3.38	8.67	3.99	106	0.00	-0.010
17.06.2012	8.52	5.12	10.94	1.71	104	0.00	-0.007
18.06.2012	6.83	2.40	13.40	5.10	341	0.00	-0.006
19.06.2012	3.34	1.80	4.88	5.18	3	0.00	-0.004
20.06.2012	4.05	1.63	6.50	4.88	332	0.00	-0.005
21.06.2012	3.91	1.95	6.04	3.97	331	0.00	-0.006
22.06.2012	7.35	3.71	11.56	2.00	319	0.00	-0.012
23.06.2012	15.60	12.30	18.42	3.56	241	0.00	-0.009
24.06.2012	14.41	7.70	20.12	5.87	253	0.00	-0.003
25.06.2012	8.24	6.51	10.48	4.67	279	0.00	-0.004
26.06.2012	11.56	8.36	14.81	3.53	139	0.00	0.001
27.06.2012	7.59	2.88	15.88	5.15	358	0.00	-0.005
28.06.2012	4.49	2.78	7.20	4.24	16	0.00	-0.002
29.06.2012	9.38	3.71	14.52	4.90	275	0.00	-0.004
30.06.2012	3.01	1.65	4.45	6.72	314	0.00	-0.005
01.07.2012	13.39	3.43	17.83	2.82	220	0.00	0.000
02.07.2012	7.32	4.32	14.31	6.26	300	0.00	-0.002
03.07.2012	5.02	2.94	7.30	3.79	359	0.00	-0.002
04.07.2012	6.31	4.47	7.85	3.64	46	0.00	-0.002
05.07.2012	4.67	2.69	6.39	4.89	340	0.00	-0.003
06.07.2012	4.13	2.92	5.32	3.65	300	0.00	-0.005
07.07.2012	9.41	4.79	16.03	2.74	164	0.00	-0.006
08.07.2012	15.24	12.30	17.12	6.34	165	0.00	0.005
09.07.2012	14.90	11.72	18.93	4.28	223	0.00	0.000
10.07.2012	16.33	13.11	19.96	2.74	4	0.00	-0.004
11.07.2012	17.91	15.72	22.27	5.10	158	0.00	-0.002
12.07.2012	12.46	10.26	15.16	4.01	259	0.00	0.000
13.07.2012	16.54	13.28	19.98	4.48	199	0.00	-0.002
14.07.2012	11.25	4.58	16.38	5.73	241	0.00	-0.002

Date	Temp_Avg (2 m)	Temp_Min (2 m)	Temp_Max (2 m)	Wind speed (mean)	Wind dir (mean)	Rain_Tot	Snow height
	Deg C	Deg C	Deg C	m/s	m/s	Counts	m
15.07.2012	7.56	5.41	10.14	5.52	274	0.00	-0.001
16.07.2012	10.63	-31.36	13.83	3.39	268	0.00	-0.001
17.07.2012	17.55	13.66	21.08	3.83	220	0.00	-0.002
18.07.2012	13.58	5.02	23.68	5.13	243	0.00	-0.005
19.07.2012	9.17	5.82	10.96	3.22	NaN	0.00	-0.007
20.07.2012	10.39	8.28	13.42	4.09	NaN	0.00	-0.005
21.07.2012	7.96	3.25	14.38	4.57	NaN	0.00	-0.006
22.07.2012	8.60	3.92	13.14	3.02	NaN	0.00	-0.005
23.07.2012	15.72	10.98	21.22	4.44	NaN	0.00	-0.001
24.07.2012	13.86	11.38	16.31	2.77	NaN	0.00	-0.008
25.07.2012	15.87	13.13	19.10	3.58	NaN	0.00	-0.006
26.07.2012	11.75	6.12	24.87	6.03	NaN	0.00	-0.011
27.07.2012	7.90	6.86	9.19	3.20	NaN	0.00	-0.006
28.07.2012	14.65	8.16	17.77	5.42	NaN	0.00	-0.003
29.07.2012	14.94	10.59	20.84	4.00	NaN	0.00	-0.005
30.07.2012	12.63	9.44	16.26	4.50	NaN	0.00	-0.008
31.07.2012	8.83	7.89	9.87	4.94	NaN	0.00	-0.012
01.08.2012	13.35	10.37	16.18	3.92	NaN	0.00	-0.009
02.08.2012	9.97	7.84	12.04	3.77	NaN	0.00	-0.009
03.08.2012	10.77	4.97	16.42	3.84	NaN	0.00	-0.007
04.08.2012	4.70	4.30	5.39	5.10	NaN	0.00	-0.010
05.08.2012	7.39	5.66	8.93	4.60	NaN	0.00	-0.006
06.08.2012	10.46	8.56	11.89	2.50	NaN	0.00	-0.009
07.08.2012	12.94	8.65	15.99	2.15	NaN	0.00	-0.010
08.08.2012	16.57	11.53	21.75	3.14	NaN	0.00	-0.007
09.08.2012	16.54	11.06	22.26	2.58	NaN	0.00	-0.004
10.08.2012	17.89	14.64	21.94	3.66	NaN	0.00	-0.006
11.08.2012	15.05	9.48	23.02	4.00	NaN	0.00	-0.006
12.08.2012	9.01	8.07	10.40	4.16	NaN	0.00	-0.009
13.08.2012	9.61	5.03	12.42	2.46	NaN	0.00	-0.012
14.08.2012	10.57	7.57	13.53	3.17	NaN	0.00	-0.011
15.08.2012	9.30	8.07	10.60	5.67	NaN	0.00	-0.007
16.08.2012	9.70	8.61	11.05	5.73	NaN	0.00	-0.009
17.08.2012	9.56	8.98	10.46	6.24	NaN	0.00	-0.013
18.08.2012	9.62	8.94	10.95	5.34	NaN	0.00	-0.015
19.08.2012	9.86	8.57	11.42	4.32	NaN	0.00	-0.018
20.08.2012	9.04	7.78	11.02	3.21	NaN	0.00	-0.007
21.08.2012	6.59	5.76	8.06	5.75	NaN	0.00	-0.009
22.08.2012	5.42	4.71	6.71	6.32	NaN	0.00	-0.015
23.08.2012	5.31	3.04	6.66	2.85	NaN	0.00	-0.011
24.08.2012	7.31	5.52	8.44	1.07	NaN	0.00	-0.011
25.08.2012	8.46	6.64	10.04	1.72	NaN	0.00	-0.012
26.08.2012	7.69	5.13	9.79	2.67	NaN	0.00	-0.011

Date	Temp_Avg (2 m)	Temp_Min (2 m)	Temp_Max (2 m)	Wind speed (mean)	Wind dir (mean)	Rain_Tot	Snow height
	Deg C	Deg C	Deg C	m/s	m/s	Counts	m
27.08.2012	6.93	5.49	8.61	2.99	NaN	0.00	-0.007
28.08.2012	6.56	5.68	7.51	3.55	NaN	0.00	-0.010
29.08.2012	4.96	3.61	6.77	4.86	NaN	0.00	-0.014
30.08.2012	4.94	4.02	5.91	4.42	NaN	0.00	-0.011
31.08.2012	4.34	2.23	6.84	4.00	25	0.00	-0.013
01.09.2012	3.80	1.93	6.31	2.58	316	0.00	-0.009
02.09.2012	4.87	2.89	6.71	2.38	248	0.00	-0.008
03.09.2012	6.20	2.29	9.72	1.96	159	0.00	-0.011
04.09.2012	6.66	4.96	9.20	4.73	303	0.00	-0.010
05.09.2012	5.17	2.89	8.53	3.50	358	0.00	-0.010
06.09.2012	5.06	2.94	7.07	1.63	178	0.00	-0.009
07.09.2012	5.35	3.26	8.60	2.42	102	0.00	-0.013
08.09.2012	4.19	3.31	4.91	3.38	101	0.00	-0.007
09.09.2012	4.47	3.19	5.57	5.43	113	0.00	-0.009
10.09.2012	4.23	3.13	5.27	7.37	123	0.00	-0.007
11.09.2012	4.52	2.47	6.78	7.58	120	0.00	-0.006
12.09.2012	3.02	1.24	5.22	8.39	99	0.00	-0.006
13.09.2012	1.54	0.55	2.50	7.63	98	0.00	-0.005
14.09.2012	2.07	0.69	3.49	6.72	94	0.00	-0.007
15.09.2012	2.05	-0.32	4.75	4.25	66	0.00	-0.006
16.09.2012	1.78	-0.71	4.15	3.13	92	0.00	-0.009
17.09.2012	1.92	-0.19	4.49	2.79	48	0.00	-0.010
18.09.2012	1.49	0.05	3.21	4.16	96	0.00	-0.010
19.09.2012	0.84	-1.47	3.46	4.06	99	0.00	-0.013
20.09.2012	0.60	-3.16	4.22	3.08	139	0.00	-0.013
21.09.2012	3.82	-0.60	5.16	3.77	259	0.00	-0.007
22.09.2012	5.36	3.70	6.85	5.34	269	0.00	-0.013
23.09.2012	5.78	2.89	7.21	3.57	239	0.00	-0.014
24.09.2012	5.65	2.62	7.75	3.22	214	0.00	-0.006
25.09.2012	3.37	0.61	6.79	2.19	129	0.00	-0.010
26.09.2012	4.35	2.28	5.36	2.14	128	0.00	-0.012
27.09.2012	4.83	2.90	6.52	1.46	29	0.00	-0.021
28.09.2012	2.69	0.67	4.44	2.95	217	0.00	-0.023
29.09.2012	-0.24	-1.84	1.41	3.79	281	0.00	-0.016
30.09.2012	0.54	-1.27	1.65	5.61	182	0.00	-0.013
01.10.2012	-0.10	-0.79	0.62	2.64	320	0.00	-0.016
02.10.2012	-0.04	-1.37	1.40	4.70	325	0.00	-0.011
03.10.2012	-3.69	-5.59	-0.94	5.48	280	0.00	0.005
04.10.2012	-6.02	-8.12	-4.66	3.27	257	0.00	0.021
05.10.2012	-5.58	-7.37	-4.37	3.84	230	0.00	0.017
06.10.2012	-3.98	-5.80	-2.44	4.10	234	0.00	NaN
07.10.2012	-5.97	-7.96	-3.72	4.88	190	0.00	0.016
08.10.2012	-7.88	-9.78	-4.52	4.03	177	0.00	0.000

Date	Temp_Avg (2 m)	Temp_Min (2 m)	Temp_Max (2 m)	Wind speed (mean)	Wind dir (mean)	Rain_Tot	Snow height
	Deg C	Deg C	Deg C	m/s	m/s	Counts	m
09.10.2012	-5.56	-7.61	-4.62	4.57	198	0.00	NaN
10.10.2012	-6.26	-10.91	-4.01	1.87	187	0.00	NaN
11.10.2012	-5.61	-8.51	-2.75	1.49	169	0.00	NaN
12.10.2012	-2.82	-4.42	-1.57	3.16	8	0.00	NaN
13.10.2012	-6.88	-7.96	-4.16	6.82	256	0.00	0.049
14.10.2012	-9.55	-11.61	-7.52	5.41	229	0.00	0.054
15.10.2012	-8.18	-9.79	-7.44	3.01	247	0.00	0.055
16.10.2012	-11.55	-13.30	-9.57	1.97	251	0.00	0.051
17.10.2012	-10.84	-12.27	-9.89	4.22	270	0.00	0.052
18.10.2012	-9.89	-11.70	-8.66	4.65	268	0.00	0.057
19.10.2012	-11.06	-15.81	-7.65	5.43	256	0.00	0.063
20.10.2012	-16.11	-17.31	-14.96	3.31	237	0.00	0.065
21.10.2012	-18.34	-20.97	-14.59	1.61	226	0.00	0.058
22.10.2012	-16.78	-20.56	-14.12	1.06	294	0.00	0.062
23.10.2012	-17.34	-21.52	-12.57	1.34	17	0.00	0.074
24.10.2012	-17.86	-21.65	-13.34	3.79	81	0.00	0.077
25.10.2012	-16.01	-19.66	-13.49	2.52	74	0.00	0.082
26.10.2012	-14.63	-16.23	-12.09	1.70	18	0.00	NaN
27.10.2012	-11.64	-13.01	-9.81	1.52	331	0.00	0.091
28.10.2012	-19.79	-24.99	-12.59	1.15	79	0.00	0.090
29.10.2012	-22.03	-25.63	-18.31	3.01	154	0.00	0.091
30.10.2012	-17.74	-18.86	-16.97	7.36	175	0.00	0.087
31.10.2012	-13.61	-17.71	-10.99	2.60	127	0.00	0.084
01.11.2012	-9.20	-12.95	-1.72	3.73	167	0.00	0.083
02.11.2012	-9.06	-12.71	-7.26	6.43	188	0.00	0.080
03.11.2012	-16.39	-18.73	-12.91	6.43	198	0.00	0.079
04.11.2012	-19.61	-20.90	-18.37	2.55	231	0.00	0.088
05.11.2012	-20.27	-21.19	-18.66	5.59	235	0.00	0.096
06.11.2012	-16.60	-19.56	-11.49	6.26	203	0.00	0.084
07.11.2012	-6.63	-11.19	-2.82	8.66	259	0.00	0.091
08.11.2012	-11.58	-12.67	-10.39	8.78	256	0.00	0.091
09.11.2012	-13.43	-16.99	-10.01	3.85	255	0.00	0.094
10.11.2012	-19.07	-20.16	-16.83	1.89	160	0.00	0.092
11.11.2012	-19.76	-21.07	-18.32	2.23	161	0.00	0.091
12.11.2012	-22.26	-23.96	-20.61	1.56	159	0.00	0.087
13.11.2012	-24.15	-24.66	-23.44	2.32	177	0.00	0.085
14.11.2012	-24.83	-25.86	-24.07	1.60	187	0.00	0.085
15.11.2012	-24.78	-25.82	-23.79	1.20	234	0.00	0.081
16.11.2012	-21.37	-23.81	-18.35	5.42	253	0.00	0.080
17.11.2012	-22.32	-23.55	-21.08	6.83	217	0.00	0.088
18.11.2012	-23.21	-25.41	-22.25	5.82	184	0.00	0.089
19.11.2012	-25.10	-26.14	-23.61	5.88	168	0.00	0.089
20.11.2012	-27.19	-29.86	-25.59	1.45	173	0.00	0.086

Date	Temp_Avg (2 m)	Temp_Min (2 m)	Temp_Max (2 m)	Wind speed (mean)	Wind dir (mean)	Rain_Tot	Snow height
	Deg C	Deg C	Deg C	m/s	m/s	Counts	m
21.11.2012	-24.07	-29.15	-21.66	2.05	282	0.00	0.086
22.11.2012	-26.09	-28.85	-21.68	4.60	194	0.00	0.090
23.11.2012	-29.83	-31.19	-28.77	3.92	161	0.00	0.087
24.11.2012	-26.80	-31.15	-24.22	2.45	235	0.00	0.089
25.11.2012	-25.62	-28.22	-24.55	2.00	195	0.00	0.090
26.11.2012	-17.48	-24.34	-11.29	3.46	354	0.00	0.086
27.11.2012	-12.24	-13.29	-11.28	4.05	25	0.00	0.097
28.11.2012	-19.48	-24.02	-12.42	3.53	89	0.00	0.114
29.11.2012	-20.47	-26.95	-9.81	6.58	207	0.00	0.114
30.11.2012	-28.92	-30.64	-26.62	7.32	186	0.00	0.103
01.12.2012	-31.61	-33.75	-29.20	2.91	184	0.00	0.085
02.12.2012	-29.37	-32.41	-28.13	3.48	240	0.00	0.090
03.12.2012	-31.85	-33.35	-30.72	5.30	168	0.00	0.088
04.12.2012	-33.90	-36.87	-30.16	2.01	158	0.00	0.083
05.12.2012	-34.06	-35.99	-32.46	1.25	263	0.00	0.083
06.12.2012	-33.05	-35.16	-30.66	2.53	319	0.00	0.084
07.12.2012	-29.40	-30.53	-28.02	1.78	290	0.00	0.087
08.12.2012	-28.79	-30.68	-27.08	3.07	191	0.00	0.087
09.12.2012	-28.58	-31.13	-26.86	3.46	251	0.00	0.094
10.12.2012	-29.98	-32.16	-27.83	2.14	236	0.00	0.097
11.12.2012	-26.22	-30.05	-24.53	3.23	223	0.00	0.101
12.12.2012	-28.48	-31.65	-25.02	3.53	167	0.00	0.099
13.12.2012	-16.68	-30.63	-6.47	7.58	256	0.00	0.108
14.12.2012	-16.83	-21.25	-9.06	4.05	211	0.00	0.091
15.12.2012	-26.05	-32.56	-15.25	6.18	29	0.00	0.097
16.12.2012	-24.86	-30.97	-19.15	7.31	243	0.00	0.106
17.12.2012	-17.02	-19.99	-13.44	9.41	211	0.00	0.093
18.12.2012	-26.09	-31.88	-19.29	6.38	297	0.00	0.088
19.12.2012	-33.43	-35.67	-30.23	3.72	261	0.00	0.092
20.12.2012	-36.03	-37.24	-35.02	6.38	175	0.00	0.092
21.12.2012	-33.86	-35.51	-32.30	7.72	154	0.00	0.087
22.12.2012	-31.42	-36.27	-26.34	6.67	322	0.00	0.089
23.12.2012	-29.36	-31.80	-25.94	8.86	263	0.00	0.091
24.12.2012	-33.70	-35.10	-29.64	10.41	166	0.00	0.089
25.12.2012	-32.79	-35.10	-28.30	2.11	129	0.00	0.089
26.12.2012	-31.38	-32.91	-30.51	1.46	170	0.00	0.089
27.12.2012	-32.06	-32.99	-30.80	1.52	10	0.00	0.089
28.12.2012	-26.09	-31.46	-22.14	2.34	121	0.00	0.095
29.12.2012	-27.43	-29.29	-23.81	2.24	147	0.00	0.093
30.12.2012	-29.54	-30.62	-26.61	NaN	NaN	0.00	0.092
31.12.2012	-30.72	-34.62	-27.42	NaN	NaN	0.00	0.088
01.01.2013	-35.16	-36.68	-33.04	0.00	NaN	0.00	0.084
02.01.2013	-35.03	-37.58	-32.85	0.00	NaN	0.00	0.081

Date	Temp_Avg (2 m)	Temp_Min (2 m)	Temp_Max (2 m)	Wind speed (mean)	Wind dir (mean)	Rain_Tot	Snow height
	Deg C	Deg C	Deg C	m/s	m/s	Counts	m
03.01.2013	-31.84	-34.11	-28.68	0.00	NaN	0.00	0.083
04.01.2013	-30.29	-33.16	-26.96	0.00	NaN	0.00	0.084
05.01.2013	-28.57	-30.83	-27.13	0.00	NaN	0.00	0.084
06.01.2013	-29.30	-31.54	-26.39	0.00	NaN	0.00	0.088
07.01.2013	-34.88	-36.23	-31.02	7.38	163	0.00	0.084
08.01.2013	-36.03	-36.60	-35.32	6.73	164	0.00	0.086
09.01.2013	-37.84	-38.96	-36.23	4.09	166	0.00	0.085
10.01.2013	-39.27	-39.62	-38.74	5.30	170	0.00	0.085
11.01.2013	-37.15	-38.80	-35.51	7.68	164	0.00	0.085
12.01.2013	-38.36	-39.36	-36.21	5.33	156	0.00	0.084
13.01.2013	-39.24	-39.59	-38.75	4.44	156	0.00	0.084
14.01.2013	-38.82	-39.56	-37.89	4.62	153	0.00	0.086
15.01.2013	-38.40	-39.30	-37.70	3.54	166	0.00	0.086
16.01.2013	-36.83	-39.25	-34.20	4.01	174	0.00	0.086
17.01.2013	-30.10	-36.57	-22.55	9.07	159	0.00	0.094
18.01.2013	-24.70	-28.16	-22.39	5.86	164	0.00	0.098
19.01.2013	-29.86	-33.26	-23.38	1.92	158	0.00	0.092
20.01.2013	-34.11	-35.64	-31.86	1.54	334	0.00	0.089
21.01.2013	-32.07	-35.77	-30.10	3.79	47	0.00	0.089
22.01.2013	-29.12	-32.64	-26.35	5.59	80	0.00	0.094
23.01.2013	-27.65	-33.62	-22.73	1.89	44	0.00	0.092
24.01.2013	-34.81	-37.15	-33.15	1.56	18	0.00	0.089
25.01.2013	-35.07	-37.55	-33.48	3.77	179	0.00	0.089
26.01.2013	-31.01	-33.84	-28.56	7.00	175	0.00	0.091
27.01.2013	-29.09	-30.69	-27.49	7.90	166	0.00	0.094
28.01.2013	-34.48	-37.15	-31.24	1.84	120	0.00	0.090
29.01.2013	-34.01	-36.19	-32.06	2.18	146	1.00	0.091
30.01.2013	-33.23	-37.46	-27.11	2.75	179	0.00	0.092
31.01.2013	-32.94	-36.58	-30.07	3.58	152	0.00	0.092
01.02.2013	-36.10	-38.57	-33.34	1.79	8	0.00	0.087
02.02.2013	-39.16	-39.73	-38.11	0.55	160	0.00	0.084
03.02.2013	-39.70	-39.73	-39.22	1.77	171	0.00	0.084
04.02.2013	-39.73	-39.73	-39.73	1.79	161	0.00	0.082
05.02.2013	-39.69	-39.73	-39.46	2.74	162	0.00	0.086
06.02.2013	-39.71	-39.73	-39.44	1.81	157	0.00	0.087
07.02.2013	-36.80	-39.15	-35.87	4.02	165	0.00	0.092
08.02.2013	-38.08	-39.63	-36.42	4.39	165	0.00	0.087
09.02.2013	-39.67	-39.73	-39.30	1.65	158	0.00	0.086
10.02.2013	-39.73	-39.73	-39.73	1.71	171	0.00	0.084
11.02.2013	-39.73	-39.73	-39.73	0.14	175	0.00	0.084
12.02.2013	-39.73	-39.73	-39.73	1.03	141	0.00	0.086
13.02.2013	-39.73	-39.73	-39.73	2.08	143	0.00	0.085
14.02.2013	-39.73	-39.73	-39.73	1.45	140	0.00	0.083

Date	Temp_Avg (2 m)	Temp_Min (2 m)	Temp_Max (2 m)	Wind speed (mean)	Wind dir (mean)	Rain_Tot	Snow height
	Deg C	Deg C	Deg C	m/s	m/s	Counts	m
15.02.2013	-39.73	-39.73	-39.73	1.24	326	0.00	0.082
16.02.2013	-39.73	-39.73	-39.73	0.57	139	0.00	0.083
17.02.2013	-39.62	-39.73	-38.80	1.64	157	0.00	0.088
18.02.2013	-38.84	-39.73	-37.66	4.60	172	0.00	0.090
19.02.2013	-39.70	-39.73	-39.28	1.34	65	0.00	0.086
20.02.2013	-39.73	-39.73	-39.73	1.04	243	0.00	0.086
21.02.2013	-36.09	-39.73	-32.91	4.80	171	0.00	0.095
22.02.2013	-33.68	-34.58	-32.25	6.85	163	0.00	0.096
23.02.2013	-26.18	-32.92	-23.23	9.71	182	0.00	0.101
24.02.2013	-22.79	-24.59	-20.97	5.30	189	0.00	0.101
25.02.2013	-27.26	-30.84	-24.10	0.37	21	0.00	0.098
26.02.2013	-28.31	-30.36	-26.51	2.26	100	0.00	0.100
27.02.2013	-29.05	-36.10	-23.95	2.48	192	0.00	0.100
28.02.2013	-32.45	-36.38	-29.32	3.46	175	0.00	0.101
01.03.2013	-23.69	-28.81	-22.08	3.84	203	0.00	0.109
02.03.2013	-18.66	-22.22	-16.85	6.93	183	0.00	0.107
03.03.2013	-26.45	-33.95	-19.37	1.53	304	0.00	0.102
04.03.2013	-33.33	-37.27	-28.29	0.68	22	0.00	0.102
05.03.2013	-35.78	-39.33	-32.54	1.54	93	0.00	0.101
06.03.2013	-38.84	-39.73	-36.71	1.41	298	0.00	0.096
07.03.2013	-39.15	-39.73	-37.29	1.47	157	0.00	0.097
08.03.2013	-38.44	-39.73	-36.18	0.06	164	0.00	0.099
09.03.2013	-39.15	-39.73	-37.85	0.00	NaN	0.00	0.096
10.03.2013	-38.75	-39.73	-35.27	0.00	NaN	0.00	0.096
11.03.2013	-38.40	-39.73	-34.34	0.00	NaN	0.00	0.098
12.03.2013	-31.86	-38.97	-28.79	1.38	297	0.00	0.104
13.03.2013	-29.40	-32.68	-27.37	3.45	268	0.00	0.101
14.03.2013	-32.72	-35.84	-28.23	0.86	204	0.00	0.096
15.03.2013	-35.48	-39.51	-31.16	1.50	99	0.00	0.111
16.03.2013	-29.23	-36.48	-21.28	5.20	354	0.00	0.106
17.03.2013	-21.75	-26.51	-19.51	3.41	37	0.00	0.103
18.03.2013	-26.76	-31.62	-24.14	2.64	52	0.00	0.100
19.03.2013	-32.00	-36.83	-27.57	2.44	79	0.00	0.100
20.03.2013	-32.61	-36.60	-29.27	2.65	65	0.00	0.104
21.03.2013	-24.48	-28.63	-21.46	5.89	82	0.00	0.105
22.03.2013	-23.45	-26.47	-21.30	4.89	75	0.00	0.101
23.03.2013	-24.15	-27.59	-21.60	5.70	89	0.00	0.100
24.03.2013	-28.06	-33.41	-24.22	2.81	103	0.00	0.095
25.03.2013	-29.12	-31.49	-26.09	1.63	152	0.00	0.096
26.03.2013	-29.45	-32.42	-24.78	2.13	321	0.00	0.095
27.03.2013	-30.37	-33.16	-26.18	2.25	305	0.00	0.094
28.03.2013	-30.83	-33.77	-27.08	1.78	302	0.00	0.093
29.03.2013	-28.11	-31.54	-24.56	3.31	320	0.00	0.096

Date	Temp_Avg (2 m)	Temp_Min (2 m)	Temp_Max (2 m)	Wind speed (mean)	Wind dir (mean)	Rain_Tot	Snow height
	Deg C	Deg C	Deg C	m/s	m/s	Counts	m
30.03.2013	-28.56	-31.73	-25.71	4.01	334	0.00	0.095
31.03.2013	-30.72	-35.16	-26.26	2.59	344	0.00	0.093
01.04.2013	-24.64	-30.57	-21.79	5.12	15	0.00	0.108
02.04.2013	-23.60	-30.94	-19.57	3.85	50	0.00	0.111
03.04.2013	-29.78	-34.86	-24.30	2.66	106	0.00	0.107
04.04.2013	-25.04	-28.45	-20.57	4.08	160	0.00	0.115
05.04.2013	-17.11	-20.94	-13.55	6.04	166	0.00	0.121
06.04.2013	-15.19	-21.51	-9.81	4.13	151	0.00	0.116
07.04.2013	-21.28	-27.87	-13.68	1.86	29	0.00	0.108
08.04.2013	-20.50	-25.36	-14.50	2.48	139	0.00	0.114
09.04.2013	-9.51	-15.26	-4.31	7.66	219	0.00	0.127
10.04.2013	-15.43	-17.84	-13.85	6.31	226	0.00	0.118
11.04.2013	-7.46	-14.80	-4.25	8.91	167	0.00	0.127
12.04.2013	-9.32	-15.36	-0.86	5.84	302	0.00	0.111
13.04.2013	-13.98	-17.27	-9.85	4.69	278	0.00	0.105
14.04.2013	-17.66	-23.48	-13.68	1.86	308	0.00	0.111
15.04.2013	-16.86	-21.55	-12.57	2.69	356	0.00	0.104
16.04.2013	-19.29	-22.95	-15.08	2.87	167	0.00	0.102
17.04.2013	-12.37	-18.59	-9.40	3.46	158	0.00	0.113
18.04.2013	-5.47	-9.16	-1.60	4.74	194	0.00	0.119
19.04.2013	-7.85	-15.26	-2.32	1.85	242	0.00	0.108
20.04.2013	-6.27	-13.01	-0.36	3.39	155	0.00	0.111
21.04.2013	-6.99	-11.99	-0.76	2.61	37	1.00	0.110
22.04.2013	-10.05	-15.64	-6.12	5.59	348	0.00	0.105
23.04.2013	-17.39	-23.16	-13.66	5.53	337	0.00	0.116
24.04.2013	-18.61	-20.97	-16.18	2.91	341	0.00	0.121
25.04.2013	-16.49	-20.02	-13.16	3.15	44	0.00	0.123
26.04.2013	-15.99	-21.24	-11.45	2.58	114	0.00	0.123
27.04.2013	-10.35	-15.99	-7.55	3.06	87	0.00	0.128
28.04.2013	-7.34	-10.87	-4.25	3.34	108	0.00	0.129
29.04.2013	-5.37	-11.82	1.10	2.17	73	0.00	0.126
30.04.2013	-3.91	-8.09	-0.88	2.64	104	0.00	0.124
01.05.2013	2.19	-0.33	3.55	5.68	150	0.00	0.100
02.05.2013	1.81	-1.52	4.23	6.63	207	20.00	0.018
03.05.2013	-3.93	-5.55	-1.27	4.69	263	0.00	0.018
04.05.2013	-1.72	-5.91	1.54	2.06	210	4.00	-0.011
05.05.2013	-1.62	-5.14	1.02	2.29	277	0.00	-0.019
06.05.2013	-2.42	-5.83	0.24	2.22	67	0.00	-0.023
07.05.2013	-4.17	-5.74	-1.94	4.91	82	0.00	-0.025
08.05.2013	-3.70	-5.25	-1.87	5.35	94	0.00	-0.021
09.05.2013	-4.56	-6.53	-3.20	6.27	86	0.00	-0.021
10.05.2013	-5.80	-6.57	-4.86	5.86	64	0.00	-0.016
11.05.2013	-4.01	-5.86	-2.21	4.90	125	0.00	-0.014

Date	Temp_Avg (2 m)	Temp_Min (2 m)	Temp_Max (2 m)	Wind speed (mean)	Wind dir (mean)	Rain_Tot	Snow height
	Deg C	Deg C	Deg C	m/s	m/s	Counts	m
12.05.2013	1.09	-2.90	3.02	5.57	150	0.00	-0.016
13.05.2013	4.65	1.72	7.17	3.06	135	0.00	-0.017
14.05.2013	3.04	-2.30	10.73	4.02	319	0.00	-0.024
15.05.2013	-4.20	-8.56	-1.39	7.59	85	0.00	-0.031
16.05.2013	-8.91	-11.61	-6.05	9.18	100	0.00	-0.028
17.05.2013	-6.54	-9.28	-4.16	5.62	77	0.00	-0.026
18.05.2013	-7.31	-9.67	-3.80	4.92	58	0.00	-0.026
19.05.2013	-8.36	-9.50	-7.47	4.07	47	0.00	-0.030
20.05.2013	-6.41	-7.54	-5.31	3.05	2	0.00	-0.025
21.05.2013	-4.52	-6.50	-2.69	2.95	181	0.00	-0.025
22.05.2013	-0.80	-2.48	1.15	2.92	35	0.00	-0.022
23.05.2013	2.30	-1.45	8.41	3.26	303	0.00	-0.020
24.05.2013	-2.55	-5.82	0.67	3.63	1	0.00	-0.027
25.05.2013	-4.02	-5.24	-2.28	4.49	297	0.00	-0.024
26.05.2013	1.87	-3.94	7.18	4.08	223	0.00	-0.017
27.05.2013	5.90	1.09	10.34	2.45	304	0.00	-0.020
28.05.2013	4.30	1.43	6.89	2.25	103	0.00	-0.023
29.05.2013	7.00	1.68	12.78	3.28	138	4.00	-0.021
30.05.2013	3.18	-0.72	10.46	3.52	34	0.00	-0.026
31.05.2013	0.19	-1.05	1.73	4.41	56	0.00	-0.030
01.06.2013	-0.94	-1.95	0.02	4.60	56	1.00	-0.029
02.06.2013	-1.63	-3.54	0.37	5.71	84	0.00	-0.023
03.06.2013	-2.64	-3.58	-1.70	6.13	83	0.00	-0.021
04.06.2013	-2.51	-3.76	-0.94	5.92	70	0.00	-0.020
05.06.2013	-3.26	-4.12	-2.56	6.05	87	0.00	-0.022
06.06.2013	-1.49	-2.59	-0.68	4.50	79	0.00	-0.027
07.06.2013	2.13	-0.78	5.06	2.51	228	9.00	-0.021
08.06.2013	3.08	2.12	3.79	4.99	272	1.00	-0.018
09.06.2013	1.43	-1.80	5.89	5.83	276	4.00	-0.018
10.06.2013	1.38	-1.07	2.82	4.16	263	0.00	-0.017
11.06.2013	5.78	2.78	8.76	3.72	127	0.00	-0.020
12.06.2013	5.23	-0.84	14.29	3.98	266	0.00	-0.021
13.06.2013	7.92	1.51	15.16	3.41	165	55.00	-0.017
14.06.2013	17.80	12.05	23.66	3.71	200	1.00	-0.014
15.06.2013	12.58	9.65	15.78	3.72	69	1.00	-0.019
16.06.2013	9.07	1.43	23.03	5.63	346	10.00	-0.022
17.06.2013	3.52	1.55	6.04	3.10	88	1.00	-0.019
18.06.2013	8.20	0.54	17.36	5.42	300	0.00	-0.018
19.06.2013	5.81	2.86	8.61	2.93	272	0.00	-0.017
20.06.2013	9.39	5.91	11.52	5.37	155	41.00	-0.015
21.06.2013	5.90	2.07	9.06	5.02	1	0.00	-0.017
22.06.2013	5.61	1.47	9.98	6.24	84	0.00	-0.019
23.06.2013	1.68	1.28	2.06	8.39	82	1.00	-0.019

XXX

Date	Temp_Avg (2 m)	Temp_Min (2 m)	Temp_Max (2 m)	Wind speed (mean)	Wind dir (mean)	Rain_Tot	Snow height
	Deg C	Deg C	Deg C	m/s	m/s	Counts	m
24.06.2013	1.97	1.19	2.79	7.39	64	4.00	-0.019
25.06.2013	3.95	2.25	8.37	5.16	113	7.00	-0.018
26.06.2013	8.73	5.25	11.42	3.78	239	6.00	-0.013
27.06.2013	7.53	5.55	9.80	4.10	251	2.00	-0.012
28.06.2013	4.94	2.66	8.54	4.95	328	0.00	-0.017
29.06.2013	6.23	4.83	8.10	6.05	86	0.00	-0.016
30.06.2013	7.54	5.55	10.51	4.72	73	0.00	-0.019
01.07.2013	6.02	3.28	7.89	5.11	11	2.00	NaN
02.07.2013	3.65	0.68	6.91	5.29	328	29.00	-0.022
03.07.2013	6.00	0.81	9.81	4.27	267	7.00	-0.008
04.07.2013	8.16	3.61	13.26	4.47	273	9.00	-0.014
05.07.2013	4.56	2.74	6.15	4.03	312	6.00	-0.019
06.07.2013	4.52	1.54	7.12	4.66	323	0.00	-0.016
07.07.2013	4.09	3.15	5.14	5.43	352	19.00	-0.018
08.07.2013	4.42	3.59	7.16	4.97	323	208.00	-0.015
09.07.2013	10.47	6.70	13.18	3.63	190	0.00	-0.014
10.07.2013	12.38	8.12	16.84	3.44	100	0.00	-0.015
11.07.2013	8.96	7.96	11.03	4.83	341	110.00	-0.018
12.07.2013	12.29	10.05	14.77	3.22	26	0.00	-0.016
13.07.2013	13.15	8.70	17.88	3.81	121	0.00	-0.016
14.07.2013	12.05	7.23	16.37	3.64	122	0.00	-0.016
15.07.2013	9.53	6.85	12.88	3.88	98	0.00	-0.018
16.07.2013	12.31	8.10	15.95	3.72	91	0.00	-0.020
17.07.2013	11.82	8.41	15.04	4.29	86	0.00	-0.016
18.07.2013	12.68	9.94	15.53	3.64	68	0.00	-0.017
19.07.2013	9.92	5.63	16.26	3.19	344	0.00	-0.019
20.07.2013	6.98	3.82	11.78	3.91	356	0.00	-0.019
21.07.2013	4.41	3.20	5.74	6.26	313	3.00	-0.016
22.07.2013	4.97	2.49	8.04	3.87	313	3.00	-0.014
23.07.2013	11.02	4.20	14.33	1.86	198	0.00	-0.018
24.07.2013	16.51	12.08	20.60	2.54	188	0.00	-0.016
25.07.2013	14.98	7.67	22.52	4.27	59	19.00	-0.015
26.07.2013	6.11	4.46	7.81	4.44	68	4.00	-0.018
27.07.2013	8.17	6.45	9.81	4.13	112	0.00	-0.023
28.07.2013	11.90	8.86	14.92	2.12	84	0.00	-0.022
29.07.2013	8.57	5.95	11.87	4.55	69	0.00	-0.024
30.07.2013	6.41	4.47	9.57	5.40	82	24.00	-0.017
31.07.2013	6.76	5.63	8.50	3.41	40	0.00	-0.015
01.08.2013	5.99	2.15	9.53	3.48	95	0.00	-0.020
02.08.2013	7.26	3.69	10.76	3.05	101	0.00	-0.023
03.08.2013	7.83	6.00	9.77	2.73	65	0.00	-0.016
04.08.2013	9.07	6.20	13.13	3.60	294	1.00	-0.023
05.08.2013	9.57	7.61	12.23	3.50	253	0.00	-0.016

Date	Temp_Avg (2 m)	Temp_Min (2 m)	Temp_Max (2 m)	Wind speed (mean)	Wind dir (mean)	Rain_Tot	Snow height
	Deg C	Deg C	Deg C	m/s	m/s	Counts	m
06.08.2013	10.27	2.99	19.07	4.88	286	2.00	-0.012
07.08.2013	6.76	4.44	8.87	2.67	353	0.00	-0.016
08.08.2013	8.34	5.86	11.17	3.13	124	0.00	-0.025
09.08.2013	12.61	7.28	16.28	1.98	218	0.00	-0.019
10.08.2013	16.63	11.08	21.89	2.14	160	0.00	-0.019
11.08.2013	15.84	12.49	20.19	1.67	80	0.00	-0.020
12.08.2013	14.96	10.95	18.40	1.76	239	0.00	-0.015
13.08.2013	8.08	5.31	12.78	5.95	341	10.00	NaN
14.08.2013	5.28	4.66	6.03	5.14	358	10.00	NaN
15.08.2013	6.69	5.68	7.85	2.37	6	0.00	NaN
16.08.2013	7.60	5.93	9.22	2.39	320	0.00	-0.021
17.08.2013	6.89	6.20	7.66	2.09	335	28.00	NaN
18.08.2013	6.94	5.20	8.33	3.31	332	160.00	NaN
19.08.2013	6.62	5.05	7.88	3.91	64	26.00	NaN
20.08.2013	5.07	3.80	6.43	5.33	68	4.00	NaN
21.08.2013	4.08	3.47	4.90	4.61	73	0.00	-0.023
22.08.2013	4.65	3.91	5.50	4.29	104	0.00	NaN

Acknowledgments

First of all, I would like to thank Dr. Hanno Meyer for giving me the opportunitiy to write this thesis and giving my thoughts a direction and a structure during my work with a lot of dedication and effort. I also like to thank Prof. Dr. Hubberten for arousing my interest for stable isotope geochemstry in the first place and beeing my second supervisor. Furthermore I wold like to thank Dr. Steffen Frey for the help during the processing of the weather data of Samoylov Island. Special thanks to Clara Kleine for providing the first contact to the stable isotope laboratory of the AWI, teaching me the usage of the IRMS and helping me with the layout of my thesis.

I also like to provide special thanks to Juliane Leister and Stefan Klingler for making the working time easier through sharing fun and thoughts during sample preperation and writing.

Affidavit

Eidesstattliche Erklärung zur Bachelorarbeit

Ich versichere, die Bachelorarbeit selbständig und lediglich unter Benutzung der angegebenen Quellen und Hilfsmittel verfasst zu haben. Alle Stellen, die wörtlich oder sinngemäß aus veröffentlichten oder noch nicht veröffentlichten Quellen entnommen sind, sind als solche kenntlich gemacht. Die Zeichnungen oder Abbildungen in dieser Arbeit sind von mir selbst erstellt worden oder mit einem entsprechenden Quellennachweis versehen.
Ich erkläre weiterhin, dass die vorliegende Arbeit noch nicht im Rahmen eines anderen Prüfungsverfahrens eingereicht wurde.
Potsdam, den _____ _____